ISTANBUL TECHNICAL UNIVERSITY ★ GRADUATE SCHOOL OF SCIENCE ENGINEERING AND TECHNOLOGY

PREPARATION AND CHARACTERIZATION OF CARBON NANOFIBER ADDED MESOPHASE PITCH BASED CARBON FOAM

Ph.D. THESIS

Ayşenur GÜL

Department of Advanced Techonologies

Material Science and Engineering Programme

JUNE 2012

ISTANBUL TECHNICAL UNIVERSITY ★ GRADUATE SCHOOL OF SCIENCE ENGINEERING AND TECHNOLOGY

PREPARATION AND CHARACTERIZATION OF CARBON NANOFIBER ADDED MESOPHASE PITCH BASED CARBON FOAM

Ph.D. THESIS

Ayşenur GÜL
(521042012)

Department of Advanced Techonologies

Material Science and Engineering Programme

Thesis Advisor: Prof. Dr. M.Ferhat YARDIM

JUNE 2012

İSTANBUL TEKNİK ÜNİVERSİTESİ ★ FEN BİLİMLERİ ENSTİTÜSÜ

KARBON NANOFİBER İLAVE EDİLMİŞ MEZOFAZ ZİFT BAZLI KARBON KÖPÜĞÜN HAZIRLANMASI VE KARAKTERİZASYONU

DOKTORA TEZİ

Ayşenur GÜL
(521042012)

İleri Teknolojiler Anabilim Dalı

Malzeme Bilimi ve Mühendisliği Programı

Tez Danışmanı: Prof. Dr. M. Ferhat YARDIM

HAZİRAN 2012

Ayşenur Gül, a Ph.D. student of ITU **Graduate School of Science and Technology** student ID 521042012, successfully defended the **thesis/dissertation** entitled "**PREPARATION AND CHARACTERIZATION OF CARBON NANOFIBER ADDED MESOPHASE PITCH BASED CARBON FOAM**", which she prepared after fulfilling the requirements specified in the associated legislations, before the jury whose signatures are below.

Thesis Advisor :	**Prof. Dr. M.Ferhat YARDIM** İstanbul Technical University	.....
Jury Members :	**Prof. Dr. Mustafa ÜRGEN** İstanbul Technical University	.....
	Prof. Dr. A.Sezai SARAÇ İstanbul Technical University	.....
	Prof. Dr. Yuda YÜRÜM Sabancı University	.....
	Prof. Dr. Ersan PÜTÜN Anadolu University	.....

Date of Submission : 24 April 2012
Date of Defense : 29 June 2012

FOREWORD

To endure my difficulties of my thesis, it takes guidance and encouragement from the following people.

First of all, I would like to express my special thanks and gratitude to my supervisor and mentor, Prof. Dr. M. Ferhat YARDIM with whom I worked for many years and who helped me in countless ways to bring me up in the scientific and academic area, and supervised me to carry out this study. I would like to express my deep and sincere gratitude to Prof. Dr. Mustafa ÜRGEN, Prof. Dr. A. Sezai SARAÇ for their continual encouragement, support, advices, and extensive knowledge throughout the study. Without their support this thesis would not have been accomplished.

I am also very thankful to Prof. Dr. Ekrem EKİNCİ, who pays attention to students' academic growth, from which I benefit a lot, and for showing me understanding, giving me many valuable advices throughout my undergraduate and graduate studies.

I would also like to send my special thanks to Prof. Dr. Yüksel AVCIBAŞI GÜVENİLİR and Prof. Dr. Tuncer ERCİYES for providing me both guidance and moral support during my post graduate studies at here ITU.

I am grateful to Turkish State Planning Organization (SPO) for financial support during my PhD.

This thesis was a product of long and intensive study which, with regard to experimental investigation, was the partly realized in Kyushu University in Japan. The long journey set out with the 6 month scholarship that was awarded by Istanbul Technical University and Kyushu University. I would like to express my special thanks and sincere appreciation to Prof. Isao MOCHIDA and Prof. Seong-Ho YOON, who gave me a chance to work in Materials Science Laboratories in Kyushu University.

I would like to thank to Prof. Dr Birgül TANTEKİN ERSOLMAZ, Prof. Dr. F. Seniha GÜNER, Prof. Dr. Gültekin GÖLLER, Prof. Dr. Hüseyin ÇİMENOĞLU and Prof. Dr. Nusret BULUTÇU, from ITU Chemical and Metallurgical Engineering Department for providing the scanning electron microscopy (SEM), He-pycnometry, X-ray diffraction (XRD) and mechanical strength analyses and their technical help and support.

I would like to thank Hüseyin SEZER, Mehmet OKUR (M.Sc.), Dr. Özgür ÇELİK who are conducted SEM, He-pycnometer and mechanical strength analyses.

I would also like to thank Işık YAVUZ (M.Sc.) and Esra ENGİN (M.Sc.) for their help with the SEM and XRD analyses.

I would like to thank to the Chemical Engineering and Metallurgical Engineering departments of Istanbul Technical University for their encouragement and support they have provided.

I wish extend my thanks to many friends and colleagues who have been meaningful part of my life professionally and personally at ITU: Dr. Birgül ARSLANOĞLU, Dr. Yasin ARSLANOĞLU, Dr. İpek AKIN, Dr.Andelip AYDIN, Dr.Neslihan ALEMDAR, Dr. Hale DÜŞKÜNKORUR, Dr. Osman EKSİK, Dr.Çiğdem TAŞDELEN YÜCEDAĞ, Aylin KERTİK (M.Sc.), Gülçin UYGUR (M.Sc.), Taner BOSTANCI (M.Sc.), Esra IŞIKSAL (M.Sc.), Mesut KIRCA (M.Sc.), Pelin YAZGAN (M.Sc.), İlker DEMİRYOL (M.Sc.), Emre YÜZBAŞIOĞLU(M.Sc.).

I would like to express my special thanks to my sisters (Zeynep, Necla, Jale, and Nigar) and brothers (Barbaros and Cengiz) who supported me patiently during this long journey and give this thesis as a gift to my mother, my father and my grandmother, who passed away several years ago, who could be proud of me for releasing this study.

June 2012

Ayşenur Gül, M.Sc
(Chemical Engineer)

TABLE OF CONTENTS

Page

ABREVIATIONS

RVC : Reticulated vitreous carbon foam
CNF : Carbon nanofiber
HCNF : Herringbone type carbon nanofiber
SEM : Scanning Electron microscopy
TEM :Transmission Electron microscopy
XRD : X-Ray Diffraction
L_c : The crystal sizes in the c-direction
L_a : The crystal sizes in the a-direction
d_{002} : The interlayer spacings between the closed-packed hexagonal planes
U : Upper section
M : Middle section
B : Bottom section
CF1 : Carbon foam with 1% (w/w) CNF additive
CF3 : Carbon foam with 3% (w/w) CNF additive
CF5 : Carbon foam with 5% (w/w) CNF additive
CF7 : Carbon foam with 7 % (w/w) CNF additive
CF10 : Carbon foam with 10% (w/w) CNF additive
CF5-0 : Carbon foam produced at 5 atm (without additive)
CF5-1 : Carbon foam with 1% (w/w) CNF additive produced at 5 atm
CF5-3 : Carbon foam with 3% (w/w) CNF additive produced at 5 atm
CF5-5 : Carbon foam with 5% (w/w) CNF additive produced at 5 atm
CF5-7 : Carbon foam with 7 % (w/w) CNF additive produced at 5 atm
CF5-10 : Carbon foam with 10% (w/w) CNF additive produced at 5 atm
CF10-0 : Carbon foam produced at 10 atm (without additive)
CF10-1 : Carbon foam with 1% (w/w) CNF additive produced at 10 atm
CF10-3 : Carbon foam with 3% (w/w) CNF additive produced at 10 atm
CF10-5 : Carbon foam with 5% (w/w) CNF additive produced at 10 atm
CF10-7 : Carbon foam with 7% (w/w) CNF additive produced at 10 atm
CF10-10 : Carbon foam with 10% (w/w) CNF additive produced at 10 atm

LIST OF TABLES

Page

LIST OF FIGURES

PREPARATION AND CHARACTERIZATION OF CARBON NANOFIBER ADDED MESOPHASE PITCH BASED CARBON FOAM

SUMMARY

The recent development of new technology devices in industrial, commercial and military fields emerge the requirement of new material systems with the unique multi-functional characteristics. For instance, in thermal management applications such as heat exchangers, thermal conductivity is a critical property while strength and stiffness are also important. In biomedical orthopedic devices, the stiffness is critical and should be tailorable as the bone fracture heals. Carbon and graphite foams provide unique properties that meet these requirements and act as unique solutions for novel technologies.

Carbon foams are rigid, porous materials consisting of an interconnected network of ligaments with certain features such as low density (0.04-0.8 g/cm^3), high temperature tolerance (up to 3000 ^oC in inert atmosphere), high compressive strength (up to 20 MPa), large external surface area with interconnected structure and adjustable thermal and electrical properties. The potential applications of carbon foam include such diverse areas a high-temperature thermal insulation, high thermally conductive heat sinks, electrodes for energy storage, energy absorption material, catalyst support and filters, etc.

The first carbon foams were developed by Walter Ford in the 1960s as reticulated vitreous carbon foams by carbonizing thermosetting polymer foams. RVC foam is a low cost material system for thermal insulation, impact absorption, porous electrodes, filtration and scaffolding. A few decades later in the 1990's, the Air Force Research Laboratory (AFRL) discovered a new processing technique (thermodynamic flash) utilizing a mesophase pitch precursor and ignited a new wave of carbon foam research. More recently, Scientists at Oak Ridge National Laboratory developed an alternative process to manufacture graphitic carbon foams with good bulk thermal and electrical conductivity.

This dissertation is focused on interpreting the foaming mechanism, analyzing the preparation process of mesophase pitch based carbon foams with the addition of carbon nanofiber (CNF) and characterization of the properties of final products. In order to produce carbon foams, mesophase pitch was introduced into a cylindrical aluminum mold and then mold was placed in a stainless steel high temperature and pressure reactor. The reactor was purged with nitrogen to provide an inert atmosphere. Then pressure was applied and kept constant during heating. The samples were heated to 350^oC with a heating rate of 5^oC/min and after system was set at 350 ^oC for 2 hours, then heating was continued with a heating rate of 5^oC/min until 600^oC and again 30 min soak time was applied. Finally pressure was released rapidly and samples were cooled down to ambient temperature in order to obtain

green carbon foam samples. The green carbon foams were carbonized by heating up to 1000 ºC (1 hour) under nitrogen in a horizontal furnace.

Carbon foam produced with this technique was characterized with scanning electron microscopy (SEM), X-ray diffractometry, helium pycnometry and compressive strength test equipment. Also densities of the samples were measured.

The structures and properties of the produced carbon foams were obtained with respect to the parameters involved and further using the characterization results. The effects of foaming pressure and carbon nanofiber additives on the structure were investigated.

As a result of these experiments it is found that; more homogenous, better structured, higher density, higher compressive strength and lower porosity carbon foams were derived at the pressure of 10 atm. The bulk and skeletal density of carbon foams exhibited a decreasing trend with increasing amount of additive. The compressive strength of the carbon foams reduced with the addition of carbon nanofiber.

KARBON NANOFİBER İLAVE EDİLMİŞ MEZOFAZ ZİFT BAZLI KARBON KÖPÜĞÜN HAZIRLANMASI VE KARAKTERİZASYONU

ÖZET

Endüstriyel, ticari ve askeri alanlarda yeni teknoloji cihazlarının gelişmesi ile özgün ve çok fonksiyonlu yeni malzeme sistemlerinin gereksinimi ortaya çıkmaktadır. Örneğin, ısı yönetimi uygulamalarında kullanılan ısı değiştiricilerde ısıl iletkenliğin yanı sıra güç ve sertlik de önemli olan özelliklerdir. Biyomedikal ortopedik cihazlarda sertlik özelliği kemik kırıklarının iyileşmesinde kritik bir parametredir ve ihtiyacı karşılayacak şekilde uyarlanabilmelidir. Karbon ve grafit köpükler, özgün özellikleri ile bu ihtiyaçları karşılayabilmektedirler. Yeni teknolojiler için özgün çözümler sağlamaktadırlar.

Köpük kelimesi genellikle gözenekli ve düşük yoğunluğa sahip malzemeler için kullanılır. Köpükleşme olayı gaz baloncuklarının, katı veya sıvı maddeler içinde dağılımıyla oluşur. Bazı malzemelerin köpüklerinin elde edilmesiyle o malzemelere pek çok alanda uygulama imkânı sağlamaktadır. Bu malzemelerden biri de karbon köpüktür.

Karbon köpükler gözenek yapılarına göre kapalı hücreli veya açık hücreli olmak üzere iki gruba ayrılırlar. Açık hücreli köpüklerde, köpük hücrelerinin sahip oldukları gözenekler diğer komşu hücrelerle bağlantılı durumdadır ve bu hücrelerde gaz giriş-çıkışı olmaktadır. Kapalı hücreli köpüklerde ise hücreler komşu hücrelerle aradaki gözenekler yoluyla ilişkili olmayıp yalıtılmış odacık durumundadır ve herhangi bir gaz taneciği giriş-çıkış yapamamaktadır. Genellikle kapalı hücreli köpükler, açık hücreli köpüklere göre daha yüksek dayanıma sahiptirler.

Karbon köpükler poliakrilonitril (PAN), poliüretan, polivinilklorür, fenolik polimer, petrol ve katran zifti, kömür, piroliz edilebilir organik bileşikler ve sentetik mezofaz zift gibi çeşitli başlatıcı malzemeler kullanılarak üretilebilirler. Karbon köpüğünün fiziksel özellikleri üretim yöntemlerine ve seçilen ana malzemeye göre değişiklikler göstermektedir. Basınç ve sıcaklık karbon köpük üretiminde önemli birer parametredir. Üretim aşaması sırasında değişik basınç ve sıcaklıklar uygulandığında köpüğün hücre yapısı, yoğunluk, dayanım, ısıl iletkenlik gibi özelliklerin de değiştiği gözlenmektedir.

Karbon köpükler birbiri ile bağlantılı ligament örgü yapısına sahip katılardır. Aynı zamanda düşük yoğunluğa (0.04-0.8 g/cm^3), yüksek sıcaklığa karşı dirence (inert ortamda 3000 ^{o}C'ye kadar), yüksek dayanıma (20 MPa'a kadar), birbiriyle bağlantılı yüksek dış yüzey alanına ve uyarlanabilir ısıl ve elektriksel iletkenliğe sahiptirler. Karbon köpükler düşük sıcaklıklarda (1273 K'nin altında) üretildiğinde düşük ısıl iletkenliğe sahip iken yüksek sıcaklıklarda üretildiğinde (2773 K ve üzeri) yüksek ısıl iletkenliğe sahip olduğu görülmüştür.

Karbon köpüklerin geniş uygulama alanları vardır. Yüksek sıcaklıklarda ısı yalıtımında, yüksek ısıl iletkenlikli ısı kuyularında, enerji depolamak için elektrotlarda, enerji absorlayıcılarında, katalizör yataklarında, filtrelerde, kompozit yapımında, düşük ağırlıklı aynalarda, roket nozüllerinde, optik bençlerde, uydu uygulamalarında,katalitik konvörtörlerde, akustik uygulamalarda, fren balatalarında yangına dayanıklı bloklarda, aşındırıcı aletlerde ve benzeri pek çok alanda kullanılabilirler.

İlk karbon köpüğü 1960'lı yıllarda Walter Ford tarafından üretilmiştir. Ford termoset polimerlerin karbonizasyonu ile retiküle karbon köpük (RVC) elde etmiştir. RVC köpük, ısı yalıtımında, darbenin emilmesinde, gözenekli elektrotlarda, filtrelerde ve iskele yapımında kullanılan düşük maliyetli bir malzemedir. 1990'lı yıllarda ise Hava kuvvetleri Araştırma Laboratuvarı (AFRL), başlangıç malzemesi olarak mezofaz zifti kullanarak karbon köpük araştırmalarında yeni bir akım (termodinamik flaş tekniğini) geliştirmiştir. Daha sonraki yıllarda ise Oak Ridge Ulusal Laboratuvarındaki (ORNL) bilim adamları, iyi termal ve elektriksel iletkenliğe sahip grafit karbon köpükler üretimi için alternatif bir proses geliştirmişlerdir.

Bu çalışmada hammadde olarak Mitsubishi AR zifti kullanılmıştır. Bu zift sentetik naftalin türevli olup %100 anizotropik mezofazdır. Mezofaz zifti ilk olarak 1965 yılında keşfedilmiştir. Ziftin katılaşmadan önceki durumunda oluşan küreler ve mozaikler nedeniyle mezofaz terimi kullanılmıştır. Anizotropik mezofaz ısıl çözülmeden sonra belirli aromatik hidrokarbonlara dönüşen ara bir üründür.

Mezofaz zift yüksek ölçüde düzenli bir anizotropik sıvı-kristal sistemidir ve küresel formdadır. Mezofaz ziftin de elde edildiği ana malzemeye göre çeşitli tipleri mevcuttur.

Petrol, kömür katranı veya sentetik malzemeler mezofaz ziftin üretilmesinde kullanılmaktadır. Mitsubishi AR zifti gibi sentetik malzemelerden türetilmiş mezofaz ziftler kömür katranı veya petrol ziftinden türetilmiş mezofaz ziftlerine oranla daha homojen molekül dağılımına sahiptirler.

Karbon köpüğü üretmek için genellikle kendiliğinden köpürme tekniği kullanılır. Mezofaz zift önce basınç altında eritilir ve böylece düşük molekül ağırlıklı bileşikler oluşur. Zift içersinde polikondenzasyon ve bozunma reaksiyonları gerçekleşir ve düşük molekül ağırlıklı bileşikler buharlaşır. Düşük molekül ağırlıklı bileşiklerin buharlaşmasıyla hücreler, ligamentler ve hücreler arasındaki bağlantı noktaları oluşmaya başlar. Tüm bu değişimler birbiriyle bağlı karbon köpük yapısının oluşmasıyla sonuçlanır. Viskozite, sıcaklık ve basınç bu oluşum sırasında önemli bir role sahiptir. Bu süreçte ve daha sonraki ısıtma aşamalarında fiziksel ve kimyasal değişimler gerçekleşir. Karbon köpüğün özellikleri üretimde kullanılan başlangıç malzemesine, proses şartlarına (sıcaklık ve basınç) ve ısıl işlem koşullarına (ısıtma hızı, bekleme süresi vb) bağlıdır. Bu nedenle de istenilen özelliklere sahip karbon köpüğün üretilebilmesi için mezofaz zift bazlı karbon köpük oluşum mekanizması incelenmektedir.

Pek çok araştırmacı karbon köpüklerin üretim mekanizması üzerine araştırmalar yapmıştır. Yapılan çalışmalarda köpük yapısına proses parametrelerinin etkisi, hücre geometrisi ve köpüğün malzeme özellikleri modellenmiştir. Fakat bu modeller daha çok ideal köpük yapısı üzerinedir. Bu modellerin doğruluğunun artması için köpükleşme prosesi sırasında kabarcık yapısı ve değişimleri açığa kavuşturulmalıdır.

Bu nedenle köpükleşme mekanizmasını ve köpüğün özelliklerini kontrol etmek amacıyla mezofaz zift bazlı köpüğün oluşum sürecini daha iyi araştırmak gerekmektedir. Küresel olmayan kabarcıkların büyüme mekanizmasını incelemek ve kontrol etmek için parametrik araştırmalar yapılmıştır. Ayrıca köpükleşme sırasında küresel kabarcıkların hareketi ve büyümesini ele alan sayısal çalışmalar da mevcuttur. Sonuç olarak başlangıç viskozitesinin düşürülmesiyle kabarcık büyümesinin ve hareketinin arttığını gözlemlenmiştir. Tasarlanan bu modeller istenilen özelliklere sahip karbon köpüğü üretmek için yapılan çalışmalara ışık tutmuştur. Karbon köpük üretim sürecini ve bu süreçte oluşan kabarcık şeklinin büyümesini açığa kavuşturmak için çeşitli çalışmalar yapılmıştır. Mezofaz ziftin köpükleşmesi sırasında kabarcık büyümesini incelenmiş ve ilk oluşan kabarcıkların erimiş zift içersinde homojen olarak dağılmadığını tespit edilmiştir. Karbon köpük içersinde üst kısımdan alt kısımlara doğru yoğunluk farklılıklarının olduğu pek çok araştırmacı tarafından kanıtlanmıştır. Fakat köpüğün özelliklerinin araştırılmasıyla ilgili bu çalışmalar kısıtlıdır.

Karbon köpükler genellikle yüksek sıcaklık ve basınç altında üretilir. Dolayısıyla karbon köpük üretim prosesi boyunca enerji tüketimi fazladır. Bu nedenle de üretim prosesinin fizibilitesini arttırmak için enerji tüketimini kontrol altına almak gerekmektedir. Bu çalışmada düşük basınç altında ve çeşitli yoğunluklarda karbon köpükler üretilmiştir. Bu çalışmada üretilen düşük ağırlıklı karbon köpükler ileriki çalışmalarda pek çok uygulama alanı bulabileceklerdir.

Düşük yoğunluklu karbon köpükler anten sistemleri, radyatörler, yakıt hücreleri, filtreler, düşük ağırlıklı zırhlar, bağlantı panelleri ve diş implantları gibi pek çok hava-uzay ve endüstriyel alanında kullanım alanına sahiptirler.

Bu tezin amacı köpükleşme mekanizmasının yorumlanması, karbon nanofiber katkılı mezofaz zift bazlı karbon köpüklerin hazırlık aşamasının incelemesi ve elde edilen sonuç ürünlerin karakterizasyonudur. Karbon köpük üretimi için mezofaz zift silindirik alüminyum bir kalıbın içine koyularak yüksek sıcaklık ve basınç reaktörüne yerleştirilmiştir. Reaktör içersinde inert bir ortam sağlamak için sistem azot gazı ile süpürülmüştür. Sonra sisteme basınç uygulanmıştır ve basınç ısıtma işlemi boyunca sabit tutulmuştur. Numuneler 350 ^{o}C'ye 5^{o}C/dak ısıtma hızıyla ile ısıtılmış ve bu sıcaklıkta iki saat bekletilmiştir. Daha sonra sistem 600 ^{o}C 'ye 5^{o}C/dak ısıtma hızıyla ısıtılmış ve bu sıcaklıkta 30 dakika bekletilmiştir. Reaktör içersindeki gaz hızlıca boşaltılmıştır ve sonra sistem soğumaya bırakılmıştır. Elde edilen karbon köpükler 1000 ^{o}C de azot ortamında 1 saat süre ile karbonize edilmiştir.

Bu teknik ile üretilen karbon köpükler taramalı elektron mikroskobu (SEM), X-ışını difraktometresi, helyum piknometresi ve basma dayanımı ölçüm cihazı ile karakterize edilmiştir. Ayrıca numunelerin yoğunluğu ölçülmüştür.

Üretilen karbon köpüklerin yapıları ve özellikleri ilgili parametreler ile ve karakterizasyon sonuçları kullanılarak elde edilmiştir. Proses basıncının ve karbon nanofiber katkısının karbon köpüğü yapısı üzerine etkisi araştırılmıştır.

Yapılan deneylerin sonucunda, 10 atm basınçta daha homojen, daha yoğun ve daha dayanıklı karbon köpükler elde edilmiştir. Ayrıca 10 atm basınçta elde edilen karbon köpükler daha az gözeneklidir. Karbon köpüklerin iskelet ve yığın yoğunluğu katkı maddesi ilavesi ile azalan bir eğilimi göstermiştir. Karbon köpüklerin dayanımı karbon nanofiber ilavesi ile azalmıştır.

1. INTRODUCTION

Mesophase pitch-based carbon foams possess low bulk density, open cell structure, moisture insensitivity, high mechanical strength, high thermal stability and low coefficient of thermal expansion. Beside these properties thermal and electrical conductivity and porosity can be tailored. Depending on its tailored properties carbon foams can be used in high impact energy and acoustic absorption as well as electromagnetic shielding material. Carbon foams have excellent potential for various applications such as rocket nozzles, engine components, high thermally conductive heat sinks, electrodes for energy storage and catalyst supports, etc [1–7].

Generally, self–bubbling technique is used for the production of carbon foams. A mesophase pitch precursor is firstly melted under pressure and sequentially the low molecular weight compounds are evolved. Polycondensation and decomposition of the pitch is occurred and low molecular weight compounds begin to vaporize. The evaporation of light components initiates formation of cells, junctions and ligaments between the cells. All these changes end up with an interconnected foam structure. [8-10]. Viscosity, temperature, and pressure play an important role during this phenomenon. Physical and chemical changes take plays at this and in the subsequent further heat treatment stages. The properties of carbon foam depends precursor used in the manufacturing process, the process conditions (temperature and pressure) and the heat treatment. Thus, it is significant to further understand the formation mechanism of carbon foams derived from mesophase pitch, for adjustment of the properties of carbon foams [11, 12].

Substantial research has been carried out on growth mechanism of carbon foams by several researchers. Foam structure with processing parameters, microstructural geometry, and material properties of the foam are predicted in many model studied. However these models are much based on the ideal structures of the foam. The bubble structure and their changes during the foaming process must be completely understood in order to increase the accuracy of these models [12-17]. Beechem et al. predicted a growth mechanism of a non-spherical bubble assisted for a carbon foam

fabrication and obtained a greater qualitative understanding of bubble shape during growth [15]. A parametric study highlighting the effect of the non-spherical growth of the bubble was performed in order to indicate how controllable bubble growth could be achieved. Rosebrock et al. carried out a numerical study to explore growth and movement of spherical bubbles during foaming [16]. It was found that decreasing the initial viscosity produced an increase in both the bubble growth and movement. The predicted results shed light on the carbon foam formation, which helped to achieve the adjustment of carbon foams. Klett et al. demonstrated that the aromatic units rearranged parallel to the axis of ligaments under a certain stress [12]. Wang et al. studied the bubble growth during mesophase pitch foaming. They observed that the initial foam bubbles were not uniformly dispersed in the molten pitch. The phenomenon of bulk density gradient of carbon foam was proved by some researcher [17- 19]. However, investigation related in sections from top to bottom of the foams is not discovered. Limited studies about addition of various additives including carbon nanofiber (CNF) can be found in the literature [20-27] but the effect of carbon nanofiber addition on density gradient is not well understood and beside this there are more rooms to understand the effect of CNF addition to final properties of carbon foams. Therefore, it is necessary to study further the evolution process of mesophase pitch derived carbon foams in order to control the foaming mechanism of pitch, and thus to adjust their properties.

Carbon foam production requires high energy consumption due to high pressure and high temperature in the process therefore it is very important to diminish the energy consumption for the feasibility of the process. In this study, carbon foams were obtained by low pressure with various density and further studies will reveal the application of area of these foams on the designated areas.

The application of carbon foams varies depending to the properties of the carbon foams. Light weight carbon foams are widely used in many industrial and aerospace applications such as antennae systems, radiators, fuel cell, filter, light armor, joiner panels, and tooth implants.

In this work, mesophase pitch derived carbon foams are studied by scanning electron microscopy (SEM), X-ray Diffractometry (XRD), He-pycnometry, and compressive strength measuring instrument. Effects of the carbon nanofiber addition on pitch including examination of final product properties are discussed in detail.

2. GENERAL INFORMATION ABOUT CARBON AND CARBON FOAM

2.1 Carbon

Carbon is the most important element for all living organism on the Earth, because all organic compounds are composed from carbon networks. Carbon materials, which consist of mainly carbon atoms, have been used since prehistoric times in the form of charcoal [28].

Carbon has an atomic weight of 12 and it is the sixth element in the periodic table. Three isotopes are mostly known: ^{12}C, ^{13}C, ^{14}C. Carbon-12 and carbon-13 are stable isotopes. They do not spontaneously change their structure and disintegrate.^{12}C accounts for around 99% of the naturally occurring carbon and is used as reference definition of atomic mass. ^{13}C is used as probe in nuclear magnetic resonance because of its magnetic moment (spin=1/2). ^{14}C is radioactive and generated in the earth's upper atmosphere by the interaction of neutrons with nitrogen. Also, it has very long half-life of 5730 years and is used extensively in the dating of archaeological artifacts and as a 'label' in the study of organic reaction mechanisms [28,29].

$$N^{14}+n \rightarrow C^{14}+H^{1} \qquad \textbf{(2.1)}$$

The properties of carbon based materials depend upon its electronic configuration (Figure 2.1). Carbon has four electrons in its valance shell (outer shell). Since the energy shell can hold eight electrons, each carbon atom can share electrons with up to four different atoms. Carbon displays"catenation" (bonding to itself) to such a degree that the number of resulting chains, rings, and networks are almost limitless. It makes advantages to combine with different kind of atoms [29].

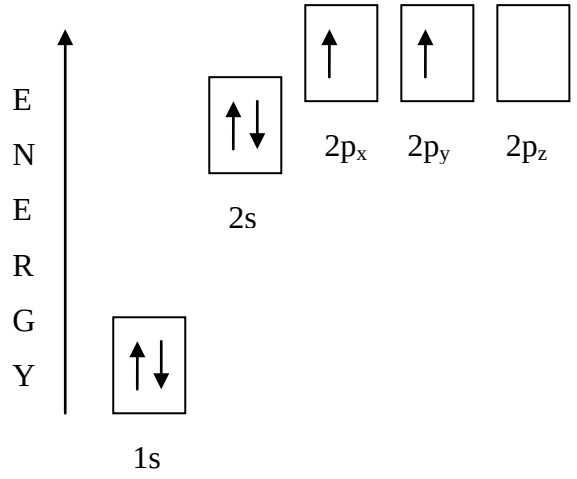

Figure 2.1 : Energy levels graph of carbon atom [30].

2.2 Bonding in Carbon Material

Bonding in carbon compounds is explained by two principle regimes as described below:

σ–bonds: diamond or aliphatic type. This result in chain of carbon atoms such as polyolefine's, or three dimensional structures which are rigid and isotropic.

A mixture of σ and π bonds: graphite aromatic type. This results in predominantly layered structures with high degree of anisotropy.

The majority of carbonaceous materials contain examples of both bonding regimes with an immense range of complexity [29].

2.3 Crystal Structures of Carbon

Carbon atoms can have three different hybrid orbital, sp^3, sp^2, and sp. This variety makes carbon atom to have different forms therefore there are many kinds of carbon allotropes. Diamond, graphite and fullerene are mostly known. C-C bonds using sp^3 and sp^2 hybrid orbital was known in the construction of diamond and graphite respectively. Fullerene is constructed by combining sp and sp^2 hybrid orbital [31].

Diamond is the one of the hardest material and has no color. Its structure consists of regular three dimensional networks of sp^3 σ bonds with long range periodical repetition. Most diamond crystal (Figure 2.2) belongs to cubic system. Diamond is

used as an electrical insulator because of its fixed bonding electron within the diamond lattice. It is used as industrial cutting tools due to its hardness [31,32].

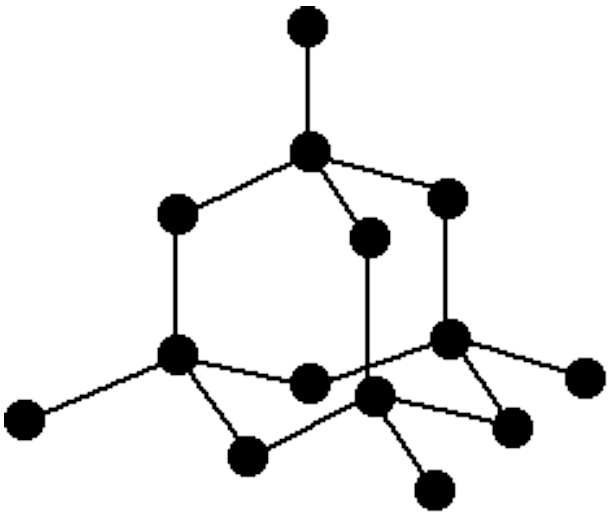

Figure 2.2 : Structure of diamond [33].

Graphite structure (Figure 2.3) has sp^2 σ and π bonds. It represents the hexagonal crystal system with the regularity of ABAB. There is a σ bond between the layers and the π bonds between the stack. The small amount of material is stacked according to the ABCABC which is known as rhombohedral form. This material accounts for less than 10% of the graphite. Graphite is a good conductor of heat and electricity. Since the energy for sliding layers over one another is low, graphite is very soft material. Thus, it used as a lubricant [29].

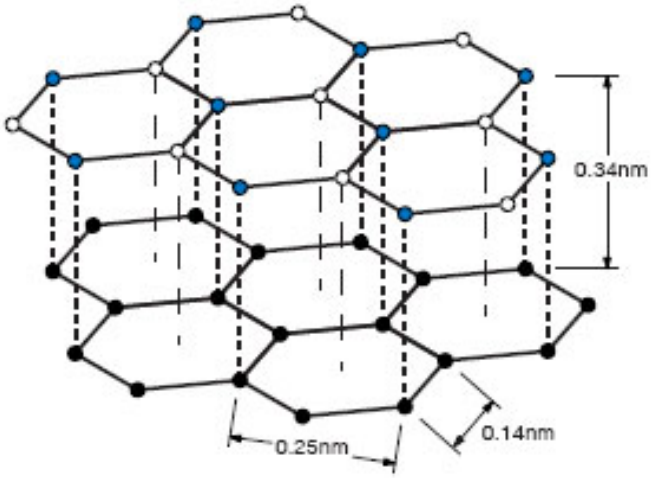

Figure 2.3 : Graphite structure [34].

Fullerene (Figure 2.4) was discovered in 1985. It is the cage molecule of carbon. The nature of bonding close to the sp^2 bond but it isn't clear. The hybridization is modification of the sp^3 hybridization and sp^2 hybridization. It means the sigma (σ) orbital don't display σ character, and the pi (π) orbital don't display π character purely. Fullerene is the one of the well known superconductive material [31]

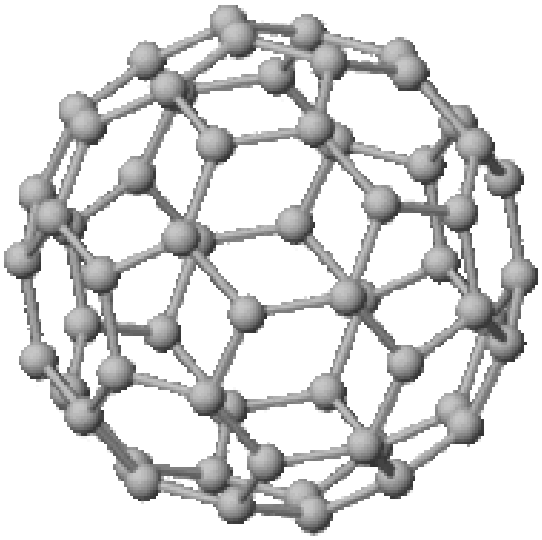

Figure 2.4 : Fullerene Molecule [35].

2.4 Historical Overview of Carbon Materials

Carbon, in the form of charcoal, is an element of prehistoric discovery and was familiar to many ancient civilizations. A historical perspective of carbon and its allotropes are shown in Figure 2.5 [28].

Pre-1880

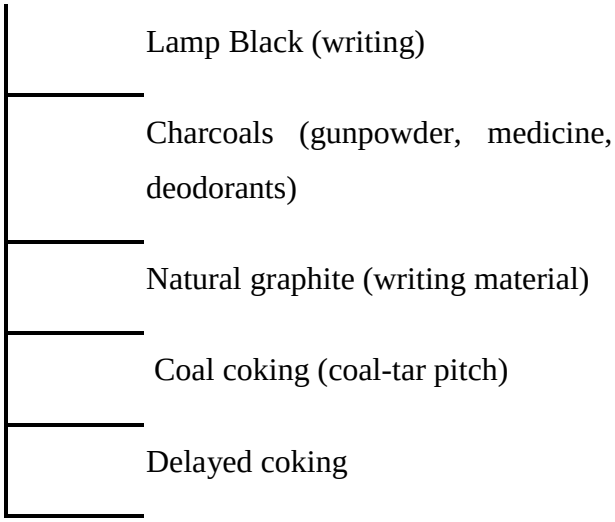

1940-1999

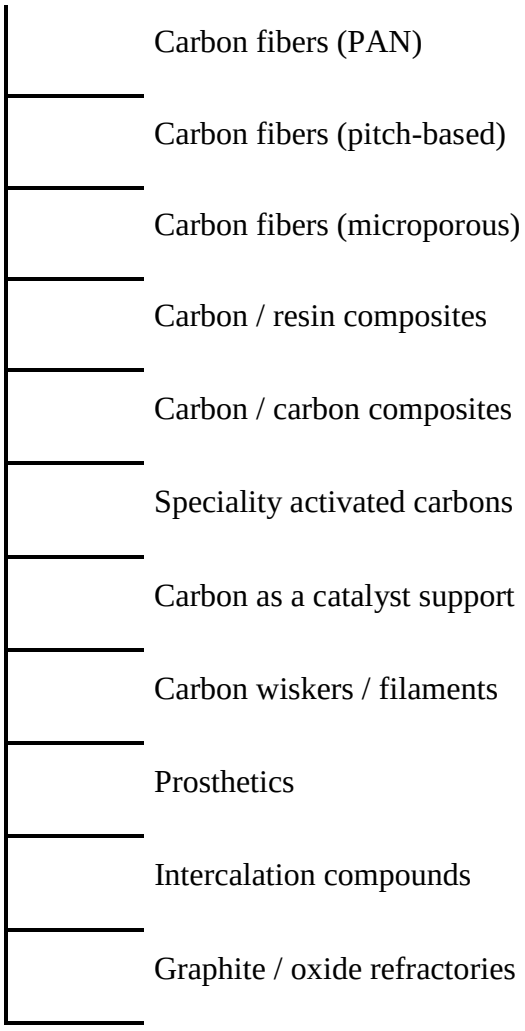

Figure 2.5 : A diagram indicating the growth of carbon materials.

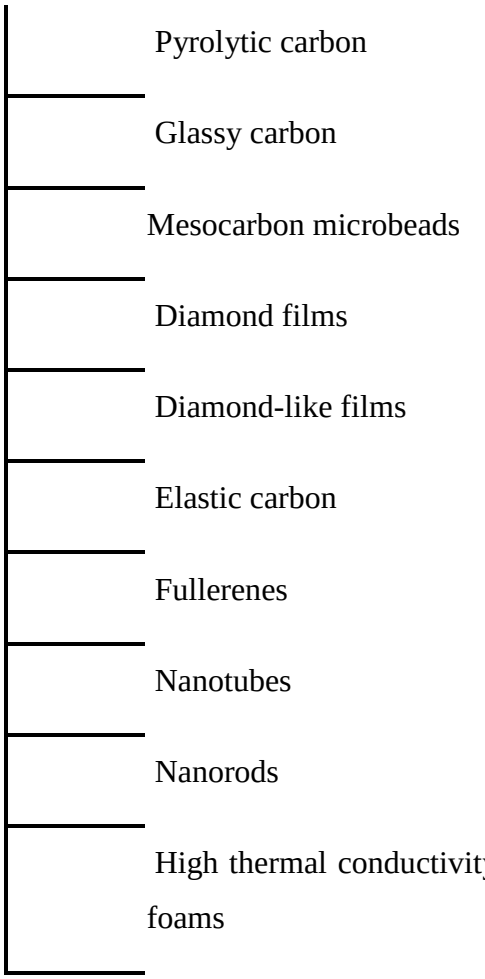

Figure 2.5 (continued) : A diagram indicating the growth of carbon materials.

2.5 Order and Disorder in Carbon Materials

Carbon material can be classified with respect to the proportion of the ordered and disordered structure. The proportions of them are related with the properties of the material.

2.5.1 More ordered structures

Ordered structure can be imagining by graphite lattice. Small volumes exhibit perfect graphite crystal structure. As volume increases, the presence of defects, distortions and heteroatom destroy the regularity and produce disordered material. Layers can be slide over another layer by little amount of energy. Also twisting makes the structure parallel and equidistant layers, but with random orientation. These are called ‘turbostratic’ carbons [29,36].

The diamonds like parts of the most carbon materials have shorter range order than graphitic regions, although large proportions of the disordered parts are aliphatic order. Defects and irregularities can be observed in the long range orders [29].

2.5.2 Less ordered structures

Carbon materials can be classified by the isotropy and anisotropy. Anisotropic carbons have ordered and graphitic structure. Isotropic carbons have randomly arranged materials. The order can be increased by further heat treatment. The crystal structure changing by heat treatment is shown in Figure 2.6 [29].

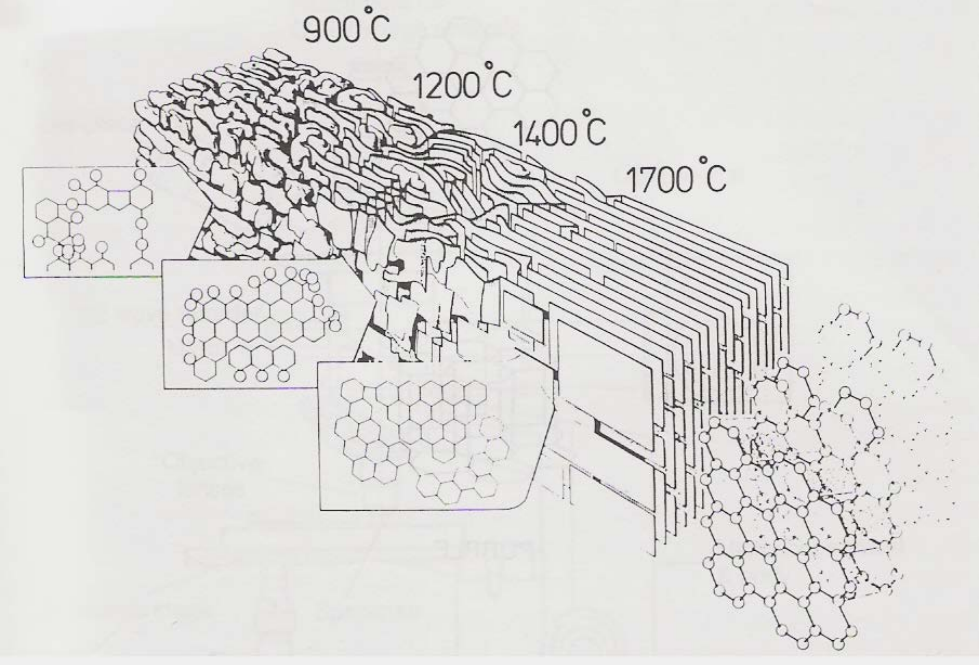

Figure 2.6 : Marsh-Griffiths model of carbonization/graphitization process [29].

2.6 Carbon Forms

2.6.1 Graphitic and non-graphitic carbons

Graphitic carbons are all varieties of material consisting of the element carbon in the allotropic form of graphite, irrespective of the presence of structural defects. Natural graphite is a mineral consisting of carbon regardless of crystalline perfection. Some natural graphite's show a high degree of perfection but most are mined in the form of flake graphite's containing other mineral matter [37].

Synthetic graphite is defined as a material consisting mainly of graphitic carbon, which has been obtained by means of a graphitization heat treatment of a non graphitic carbon or by chemical vapor deposition (CVD) from hydrocarbons at temperatures above 1800ºC [37].

Non-graphitic carbons are all varieties of substances consisting mainly of the element carbon with two-dimensional long range order of the carbon atoms in planar hexagonal networks, but without any measurable crystallographic order in the c-direction. Many non-graphitic carbons can be converted to graphite by graphitization heat treatment to above 2200 ºC.

2.6.2 Graphitizable and non graphitizable carbons

Non-graphitizable carbons (Figure 2.7) can not be transformed into graphitic carbon solely by heat treatment at temperatures of 3000ºC or above under atmospheric or lower pressures. Non Graphitizable carbons are produced from wood, nutshells and non fusing coals. During heat treatment, their macromolecular structure does not change. Fusion can not take place only small molecules leave from the structures, and at the same time more cross linking structure occurs [37].

Graphitizable carbons can pass fluid stage during the heat treatment. Molecules can grow and large aromatic molecules can be formed. Thus they align with each other so graphitic structure can be developed [37].

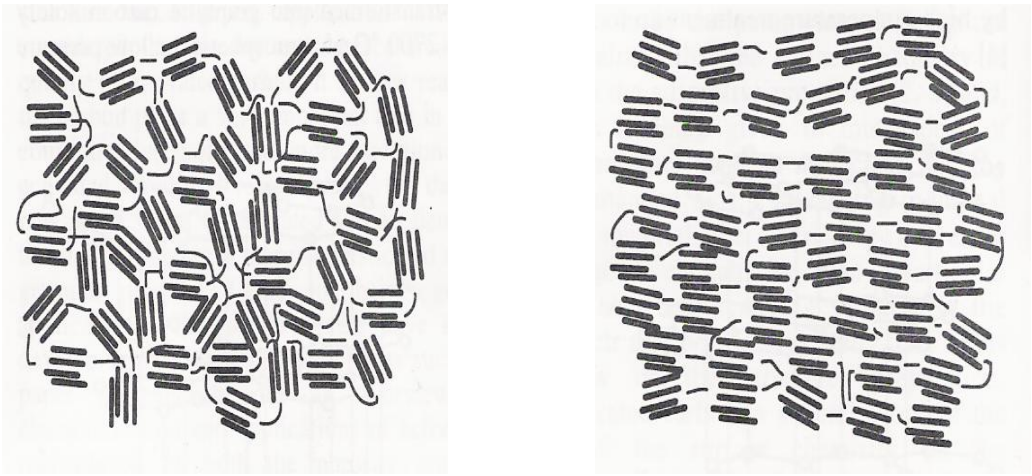

Figure 2.7 : Schematic representation of nongraphitizable (left) and graphitizable carbon (right) [37].

2.7 Carbon Foam

2.7.1 History of carbon foam

Walter Ford first developed carbon foam in the late 1960's. This initial carbon foam was produced by carbonizing thermosetting polymer foams to obtain reticulated vitreous (glassy) carbon foam which is shown Figure 2.8. This initial carbon foam was obtained by the carbonization of foams of plastic materials, such as phenolic resins and polyurethanes [5, 38].

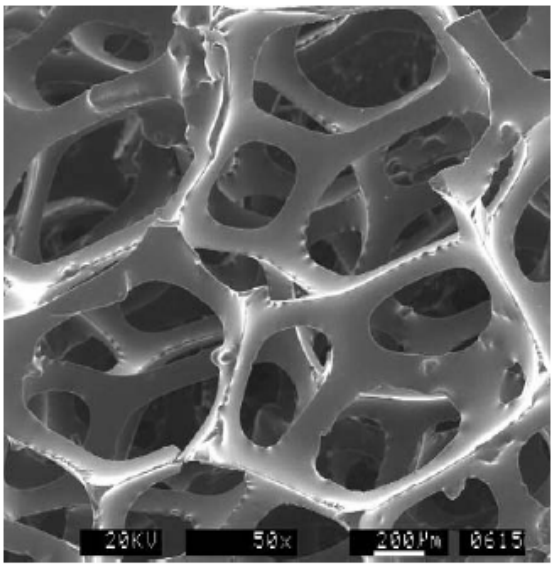

Figure 2.8 : A Typical RVC foam [12].

Googin et al. produced carbon foam by polymerization of furfuryl alcohol and urethane to get partially cured urethane foam in 1967. It was the first process to controlling the structure and material properties of carbon foam [39].

Researches focused on variety of applications of carbon foam. Carbon foam was used as electrode, insulator, filter, catalyst bed and catalyst support. In addition, carbon foam was used as the template for many of the metal. In 1970's and 1980's, alternative precursors and processing conditions were explored for producing carbon foam and modifying its properties [40-43].

In the 1970's, researches focused primarily on producing carbon foams from alternative precursors, various processing and precursor changes in an attempt to modify properties and reduce cost.

In 1976, Raley et. al. used vinylidine chloride polymers with ammonia to derive carbon foam. This carbon foam had been used as a catalyst support and filter material for gases, such as cigarette smoke and liquids [41].

In 1981, Bonzom et. al. developed carbon foam from petroleum and coal tar pitch. The carbon foam was used for thermal and sound insulating [1].

In 1988, Hopper dissolved pulverized sodium chloride particles and phenolic polymeric resin into tetrahydrofuran (THF) as a precursor of carbon foam [44]

Mesophase pitch derived carbon foam was discovered in the early 1990's. This work was focused on the developing a highly structural lightweight material which exhibits very high specific thermal conductivity [2].

In 1997, Klett, J. at the Oak Ridge National Laboratory (ORNL) reported the first graphitic foams with bulk thermal conductivities up to 180 W/m.K. They used naphthalene derived mesophase pitch as a precursor. Due to high bulk thermal conductivity, the graphitic carbon foam is a potential material as thermal management materials [7, 8, 45,46].

2.7.2 Carbon foam precursors

Carbon foam has been produced from different kind of precursors since 1960's such as polyacrylonitrile (PAN) [47-50], polyurethane [40,48], polyvinylchloride [51-54], phenolic polymer [55], coal tar [56,57] and petroleum pitch [1,58], coal [59], synthetic mesophase pitches [3, 51-55, 57,58,60,61].

- **Polyacrylonitrile**

Polyacrylonitrile in a heated alkali metal halide solution was used for producing carbon foam. PAN (polyacrylonitrile) was inserted in containment then sufficiently cooled the heated solution to form a liquid gel of the polyacrylonitrile by phase inversion. Removing the dissolved alkali metal halide from the gel provided porous foam consisting essentially of polyacrylonitrile. Cross-linking the polyacrylonitrile foam was obtained by removing residual traces of solvent under vacuum. Porous foam was oxidized at an elevated temperature in an oxygen-containing environment (e.g., air). Finally porous foam was heated in an inert atmosphere to a temperature sufficient to carbonize the polyacrylonitrile to provide a microcellular carbon foam product. Carbon foam produced with this method has uniform distribution of cell size

and open porosity. It is used as catalyst support, absorbents, filters and electrodes [47]. A SEM micrograph of Polyacrylonitrile derived carbon foam is shown in Figure 2.9 [62].

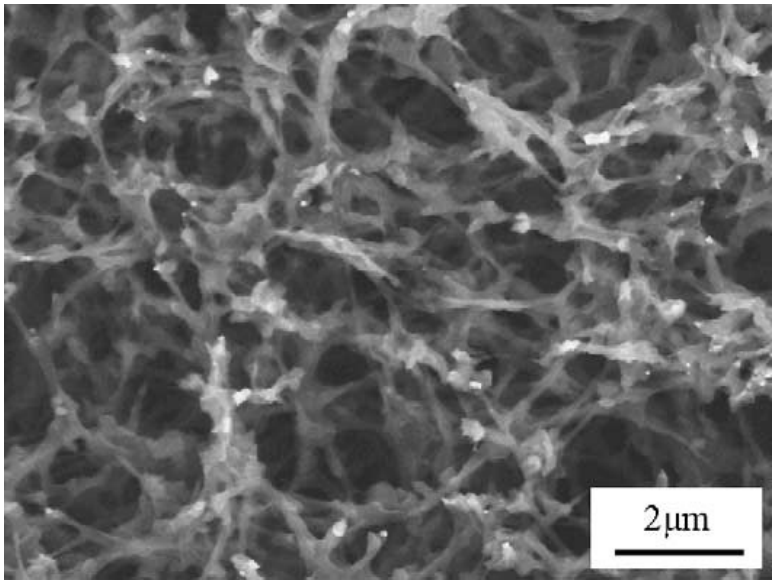

Figure 2.9 : Polyacrylonitrile derived carbon foam.

- **Thermosetting polymer**

"Glassy" or reticulated vitreous carbon (RVC) (Figure 2.8) foams are formed by curing and carbonization process of thermosetting resin-based precursors such as polyurethane, polyamide, polycarbodiimide, epoxy, phenol [40, 63-65]. Most thermosetting foams are prepared by simultaneous occurrence of polymer formation and gas generation. Principle of preparation of thermosetting foams is shown in Figure 2.10 [65].

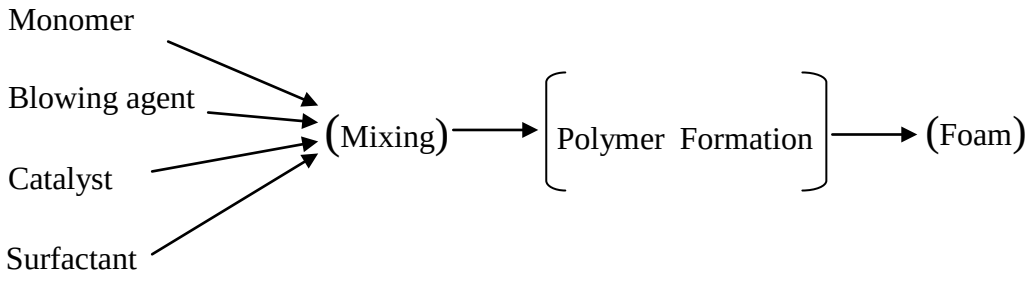

Figure 2.10 : Mechanism of thermosetting foam preparation.

They are used for many aerospace and industrial applications such as thermal insulation, impact absorption, acoustic control, catalyst support, and metal and gas filtration. Reticulated carbon foam is poor in oxidation resistance at high temperatures and corrosion resistance in a chemical reaction and is insufficient in thermal conductivity because of their amorphous carbon morphology [56, 60]. However they are thermally stable, low in weight and density, and chemically pure. They resist thermal stress and shock, and are relatively inexpensive [66].

Phenolic resin based carbon foam can be used for high-strength thermal insulation material and has been prepared by using various methods. Union Carbide and Ultramet have carried out studies on carbon foam since 1960. Union Carbide employed the methods of pyrolysis of phenolic foam and carbonization of phenolic microsphere mixture with phenolic resin to produce carbon foams with various pore sizes and densities (pore size of 25–150 μm at the density of 0.05–0.25 g/cm^3) [38, 67-71]. Ultramet prepared the carbon foam by impregnating polyurethane foam template with phenolic resin then carbonizing [71-73]. Shiwen et.al tried to achieve phenolic-based carbon foams with controllable pore structure and high compressive strength. Average pore size of carbon foam was controlled by changing the resin concentration. Carbon foam with bulk density of 0.73 g/cm^3, average pore size of 20 nm, compressive strength of 98.3 MPa and thermal conductivity of 0.24 W/mK was obtained [74].

- **Coal tar or petroleum pitch**

The coal tar or petroleum pitch based carbon foam is used as thermal insulation, as catalyst supports or as filters for corrosive products [64]. Although Mitsubishi mesophase AR pitch can be foamed directly without pretreatment, most coal and petroleum-derived pitches need to be treated before foaming can be achieved. Plastic properties of coal and petroleum-derived pitches are not enough for foaming. The properties and composition (viscosity and degree of anisotropy) of coal–tar pitches can be controlled by the temperature of thermo-oxidation treatment, amount of added acid and conditions of heat treatment. Commercially available pitches, such as Ashland A240 petroleum and Koppers coal tar pitch are not suitable for making carbon foam directly. Viscosity of these precursors is too low to hold the foam cell shape. Therefore, the pitch properties of these materials were tailored by heat treated in an autoclave between 200 ^{o}C and 400 ^{o}C under N_2 atmosphere [11]. B. Tsyntsarski

et.al are used H_2SO_4 and HNO_3 as a chemical agent to modify the commercial coal–tar pitch. Carbon foams with an anisotropic texture and high mechanical strength were produced using precursors obtained after thermo-oxidation treatment of commercial coal–tar pitch with H_2SO_4 and HNO_3 [75]. Figure 2.11 shows the SEM images of carbon foams derived from the petroleum pitch and coal tar pitch [11].

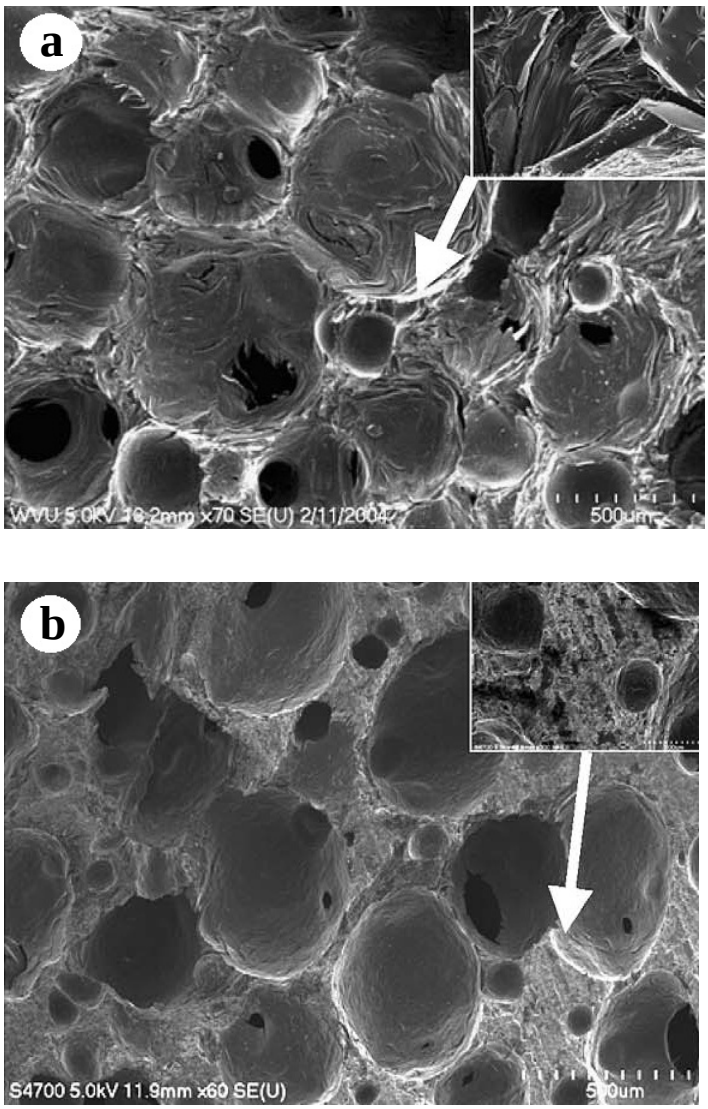

Figure 2.11 : SEM images of carbon foam derived from different precursors (a) petroleum pitch (b) coal tar pitch [11].

- **Coal**

The properties of coal vary widely, and thus some coals are suitable as foaming precursors and others are not. The foaming behavior of coal precursors is strongly related to their plastic properties, which are dependent on the maceral composition of the coal. Liptinite exhibits strong dilatation power but inertinite does not, while

vitrinite is intermediate. Therefore, the selection of the appropriate coal precursor is important [11, 76]. The coal-based carbon foam with open cell and interconnected pores is shown in Figure 2.12 [77].

Figure 2.12 : Coal-based carbon foam microstructure.

While using a raw coal or hydrogenated coal, as a precursor, it is de-ashed and its asphaltene fraction is separated by a solvent treatment. The coking of the asphaltene fraction under controlled conditions of temperature and pressure results in the formation of a carbon foam, which can be subsequently graphitized [69]. The production method, developed by a research group at West Virginia University in USA, was licensed to Touchstone Research Group under the trade name CFOAM™ [77]. Touchstone Research Laboratory, Ltd. (Touchstone) has developed a tooling system using a coal-based carbon foam (CFOAM®) that obviates many of the concerns associated with alloy-based tools (Figure 2.13) [78].

Figure 2.13 : Coal derived carbon foam tooling.

Coal based carbon foams have lightweight and their costs are relatively low. It can be used for efficient conductor of heat and electricity. Also, depending upon the end use, the degree of thermal conductivity can be altered. In general, the isotropic foam is not a high thermal conductor and the non-graphitized foam is poor thermal conductor. Coal based carbon foam have numerous usage area such as separator for ions in membranes, substrates for integrated circuits or aerospace applications, high temperature filters, a substitute for wood and steel beams in building and structural members, automotive parts (pistons, vehicle frames, impact absorbers for doors and connecting rods exist), aerospace and airplane parts (wings, brakes, satellite and space station structure) [59,79,80].

- **Mesophase pitch**

The mesophase phenomenon is discovered in 1965 by Brooks and Taylor [81]. Mesophase means sphere and mosaic substances that form before the solidification. When hydrocarbon is heated under inert atmosphere, it condenses to large planar molecules. As the molecules grow, they nucleate and grow a liquid crystal phase, called the mesophase. The liquid crystal phase consists of stacking planar molecules that are footprint of the graphitic pellets [54-55].

The mesophase pitch based carbon foam was produced at the Wright Patterson Air Force Base Materials Lab in 1990’s [2]. It is a synthetic naphthalene derived pitch, which is 100% anisotropic mesophase.

Mesophase pitch is derived from various precursors such as petroleum and coal tar and other synthetic precursors. Mesophase pitches derived from synthetic precursors, such as Mitsubishi AR pitch which is prepared by the catalytic polymerization of naphthalene using HF-BF_3 catalyst have more homogeneous compositions compared to mesophase pitch derived from petroleum and coal tar pitch [82-84]. Figure 2.14 schematically shows the presentation of the structures of Mitsubishi AR and typical petroleum mesophase pitches [12].

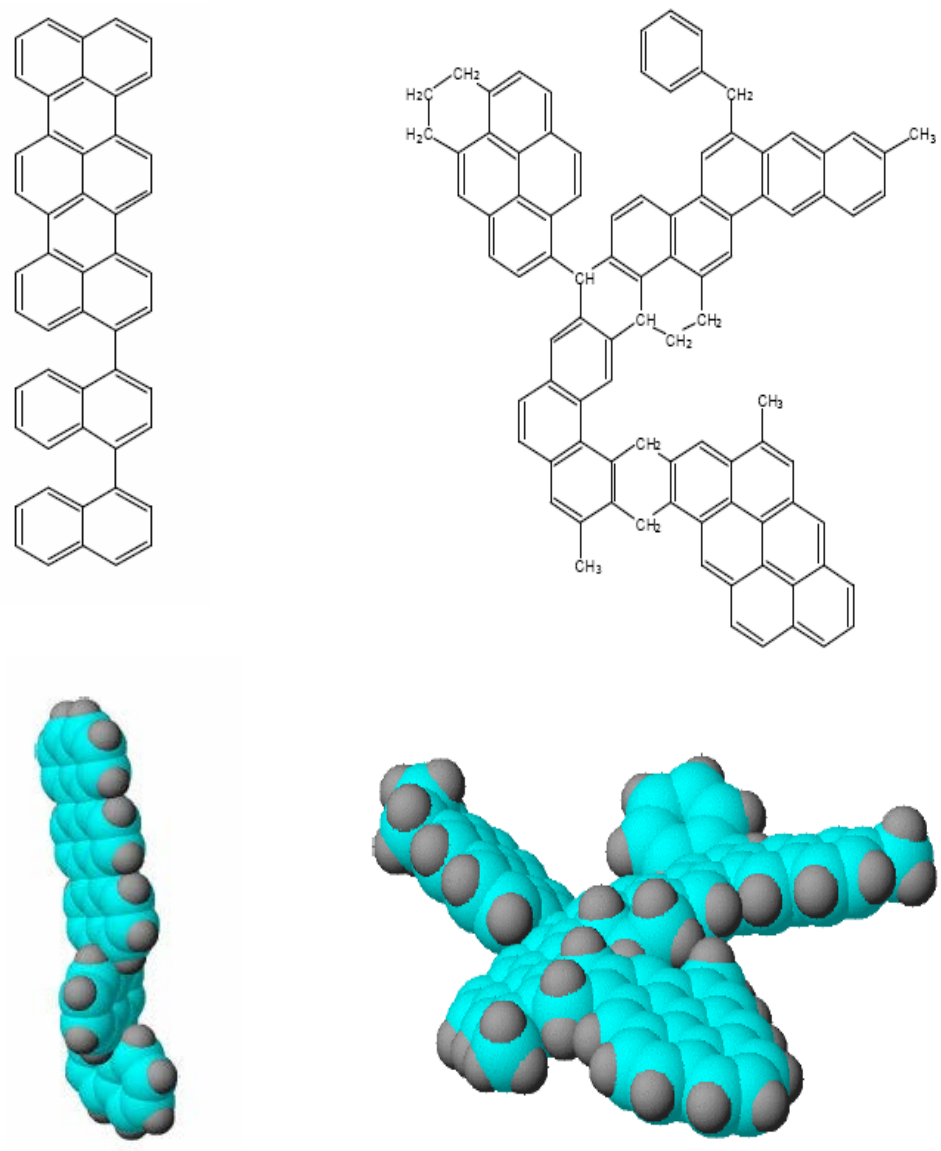

(a) (b)

Figure 2.14 : Structure of mesophase pitch (a) AR mesophase pitch (b) A typical petroleum mesophase.

Figure 2.15 shows a simplified bloc and process flow diagram of the naphthalene derived mesophase pitch.

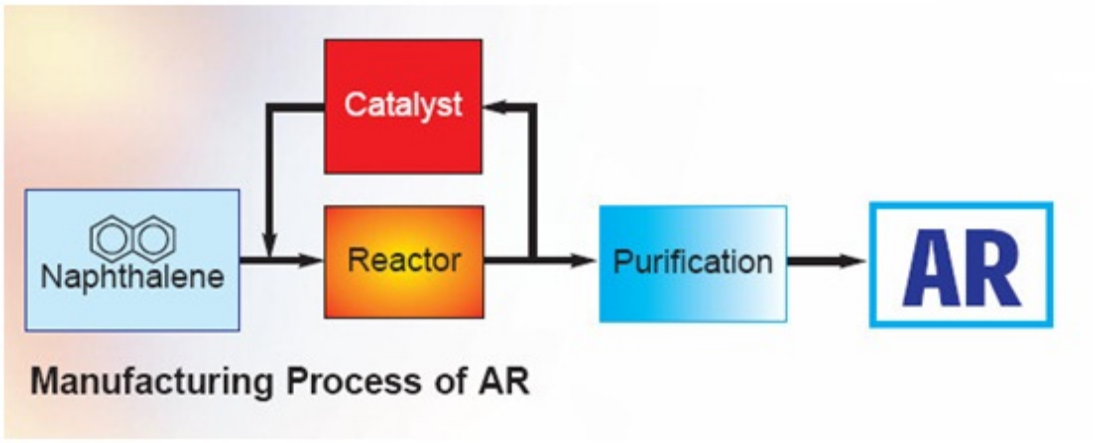

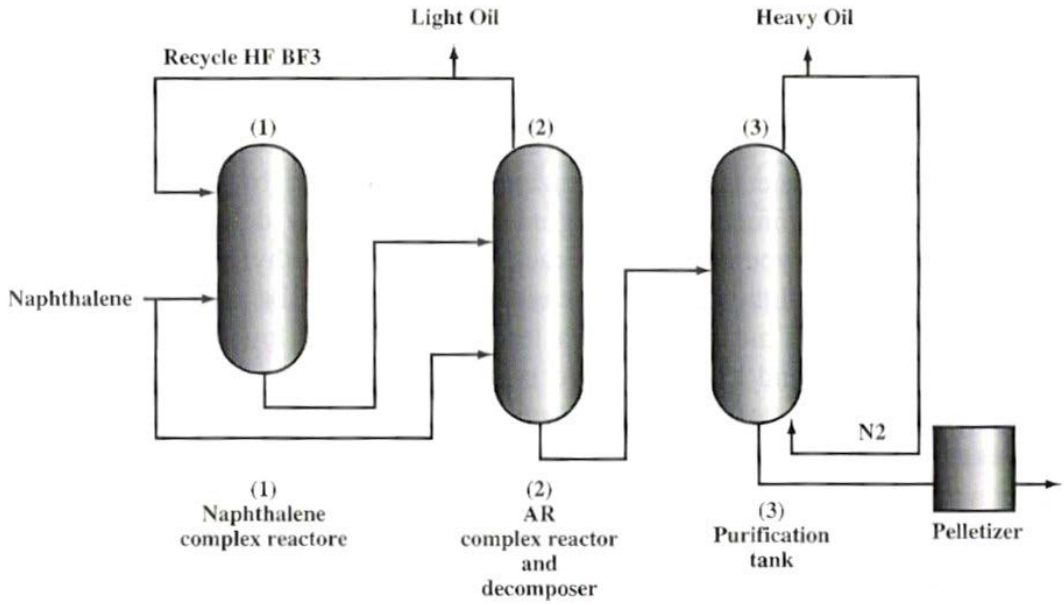

Figure 2.15 : Block and process flow diagram of the naphthalene derived mesophase pitch [85].

Naphthalene and HF and BF_3 are mixed in a stirred tank reactor to form the naphthalene HF–BF_3 complex. The AR complex section is where the naphthalene complex is further reacted with naphthalene to form the AR/ HF–BF_3 in a stirred tank reactor. After the polymerization reaction, the AR/HF–heating in the stirred tank reactor decompose BF_3.HF and BF_3 are recovered and recycled to the naphthalene complex section. At the same time, the light oil is recovered to assure 100 % anisotropy [85].

The purification section is where nitrogen is blown into the purification tank to remove the low-boiling products, so adjusting the volatile contaminants in the AR resin. Solid contaminants are removed by filtration. Very pure AR resin melt is extruded into strands and cut into pellets [85].

Synthetic mesophase pitch is the preferred precursor for high thermal conductivity carbon materials because it is graphitizable [3,45] . When a synthetic mesophase pitch is used, the domains are stretched along the cell walls of the foam structure and thereby produce a highly aligned graphitic structure parallel to the cell walls [3]. This implies that the internal structure of a carbon materials produced from mesophase pitch is similar to that of graphite [45].

2.7.3 Properties of carbon foams

Carbon foam is complex cellular structures. The word cell is derived from the latin word "cella," which is a small compartment. A cluster of cells is a cellular solid. Honeycomb materials would be the simplest of cellular structures. They used for industrial, architectural and transportation application such as sandwich panels, molded parts, wind tunnels etc. A cellular solid consists of an interconnecting network of struts or plates forming the edges and faces of the cells. Foam consists principally of packed polyhedral structures, which can either be open or closed cell [81]. If the pores of the foam are connected to one another, the foam is defined as open cell foams. If the pores of the foam are isolated within the mass, the foam is defined as closed cell foams [86] (Figure 2.16).

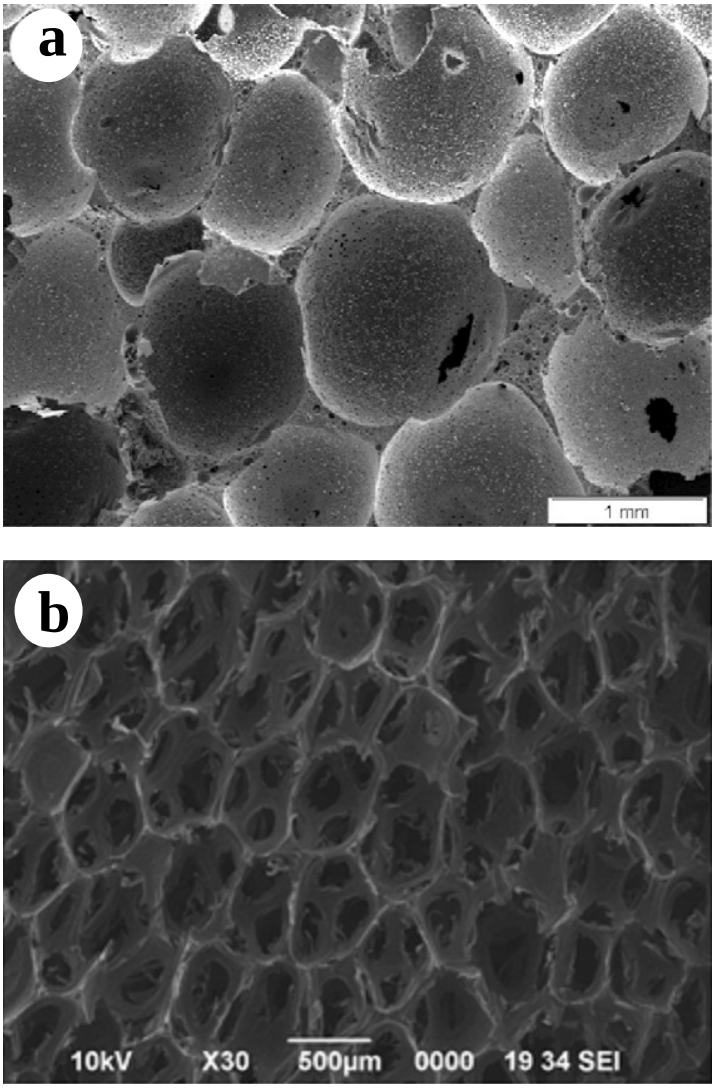

Figure 2.16 : a) phenolic resole resin derived closed cell foam [87] b) mesophase pitch derived open cell foam.

Carbon foam can be made from a variety of precursors. The precursor and the process conditions determine the properties of the foam; therefore carbon foam is a tailorable material [59]. It is denoted in the literature that, the size of the bubbles formed during the foaming can be changed by varying the operating conditions. Moreover other foam properties (density, porosity, strength and conductivity) can be affected. Higher density, increased compressive strength and a more interconnected open celled porous structure are obtained at higher pressures [88,89]. Pressure release time also affected the formation of porous structure. A more interconnected open-celled porous structure is formed for shorter pressure release times [89]. Solvents treatment (tetrahydrofuran (THF), toluene, and xylene,) and additive additions (graphite powder, H_2O_2 treated isotropic Bulgarian pitch,

Polymethylmethacrylate (PMMA) and Polystyrene (PS)) to the mesophase pitch decreased quality of foam, in terms of density, compressive strength, porosity and structure [88,90].

Carbon foam is an attractive alternative material to traditional materials in many applications due to its unique properties such as lightweight, high compressive strength, high or low thermal conductivity that depends on temperature while it is processing [56]. Carbon foams have nearly 90 % open pore structure. The density of carbon foam is ranging from 0.04 g/cm^3 to 0.6 g/cm^3. Carbon foam has high porous structure and uniform pore size distribution (average between 10 and 500 microns) [59]. Properties of various kinds of carbon foams from manufacturers are listed in Table 2.1 [91].

Table 2.1 : Properties of several kinds of carbon foams.

Property	Density (g/cm^3)	CTE (ppm/C^o)	Compressive Strength (MPa)	Thermal Conductivity (W/mK)
Ultramet's RVC	0.042	1.15 – 1.65	0.763	0.085
ERG's RVC	N/a	1.2 – 1.8	0.28 – 0.48	N/a
Touchstone	0.16 – 0.5	6.2	15.2 – 20.7	0.4 – 17.5
MER	0.016 – 0.62	N/a	1.7 - 7	0.05 - 210
PocoFoam	0.2 – 0.6	2	3.4	100 - 150

Carbon foams can be used as a thermal insulator or conductor. Carbon foams produced below the temperature of 1200 ^{o}C have low thermal conductivity. In contrast, carbon foams produced above the temperature of 2500 ^{o}C have high thermal conductivity [79,92]. The carbon foam developed at Oak Ridge National Laboratory (ORNL) are four times more conductive than copper and six times more conductive than aluminum (approximately 1500W/m.K compared to 400 W/m.K for copper and 250 W/m.K for aluminum) [93-95].

Carbon foam shows highly ordered graphite properties when it is graphitized. It exhibits average interlayer spacing close to perfect graphite [12]. Carbon foams produced by Klett et al. has a 0.336 nm inter layer spacing and 203.3 nm coherent length (L_a) and 442 nm stacking height (L_c) [7].

2.8 Preparation and Characteristic of Mesophase Pitch Derived Graphitized Carbon Foam

2.8.1 An overview of carbon foam technology

Typical processes utilize a blowing technique is to produce carbon foam from the pitch precursor in which the pitch is melted and passed from a high-pressure region to a low-pressure region. Thermodynamically, this produces a "Flash" thereby causing the low molecular weight compounds in the pitch to vaporize (the pitch boils), resulting in a pitch foam. Then, the pitch foam must be oxidatively stabilized by heating in air (or oxygen) for many hours, thereby, cross-linking the structure and "setting" the pitch so it does not melt during carbonization. This is a time consuming step (up to 100 hours) and can be an expensive step depending on the particle size and equipment required. Without this oxidative stabilization step, the pitch may melt during further heat treatment [96,97].

The "set" or oxidized pitch is then carbonized in an inert atmosphere to temperatures as high as 1100ºC. Then, graphitization is performed at temperatures as high as 3000ºC to produce a high thermal conductivity graphitic structure (Figure 2.17).

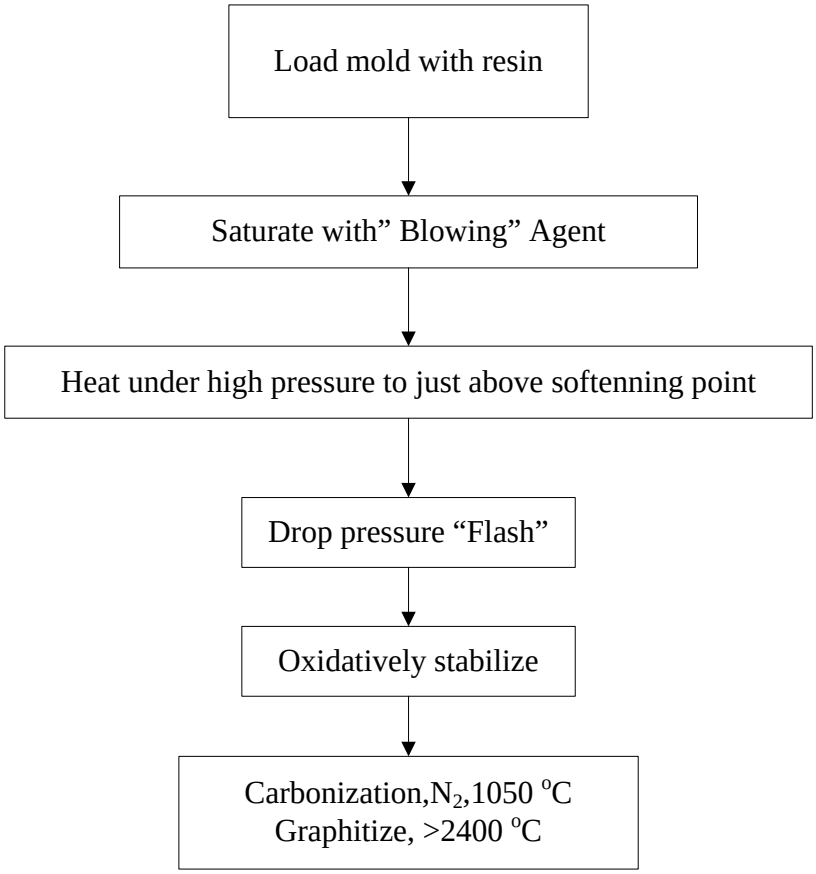

Figure 2.17 : Traditional "Blowing" technique [98].

Related process was developed and patented by the researchers from US Air Force Materials Laboratory. Carbon and graphite foams produced according to the related process can be used for many applications, including core material to replace aluminum in honeycomb panels, composite mandrels or tooling, sound insulation around engine cars and support structure for satellite antennas [98].

Other techniques utilize a polymeric precursor, such as phenolic, urethane, or blends of these with pitch. High pressure is applied and the sample heated. At the specified temperature, the pressure is released, thus causing the liquid to foam as volatile compounds are released. The polymeric precursor are cured and then carbonized without a stabilization step. However, these precursors produce a "glassy" or vitreous carbon which does not exhibit graphitic structure and, thus, has low thermal conductivity and low stiffness [97].

More recently, a breakthrough has come out about carbon foam, which would totally change the physical characteristics and application areas of the material. A process that does not require the "blowing" and "stabilization" steps was developed at Oak

Ridge National Laboratory (ORNL) as shown in Figure 2.18. The process is said to be less time consuming, and easier to fabricate. As shown in Figure 2.19, the foam obtained with this process has an open porosity with highly aligned more ordered graphitic structure compared to traditionally produced carbon foams. The process was licensed to Poco Graphite under the trade name PocoFoam™ [99-101].

In order to produce open pores and high conductivity carbon foams, a pitch made from coal, petroleum or synthetic molecules must be used as the precursor. Carbon foam, derived from a pitch precursor can be considered to be an interconnected network of graphitic ligaments or struts with fiber like properties [56].

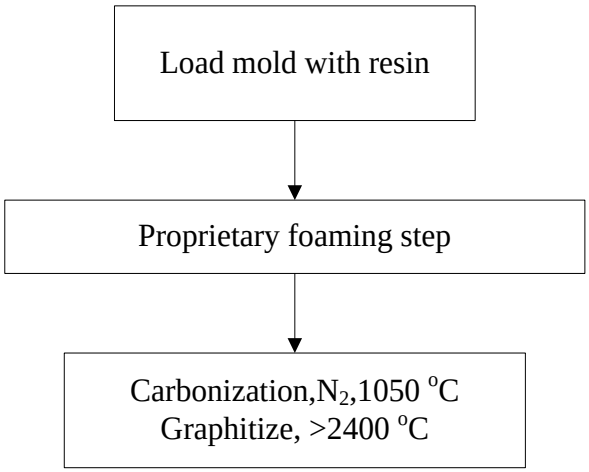

Figure 2.18 : Novel production method of ORNL [98].

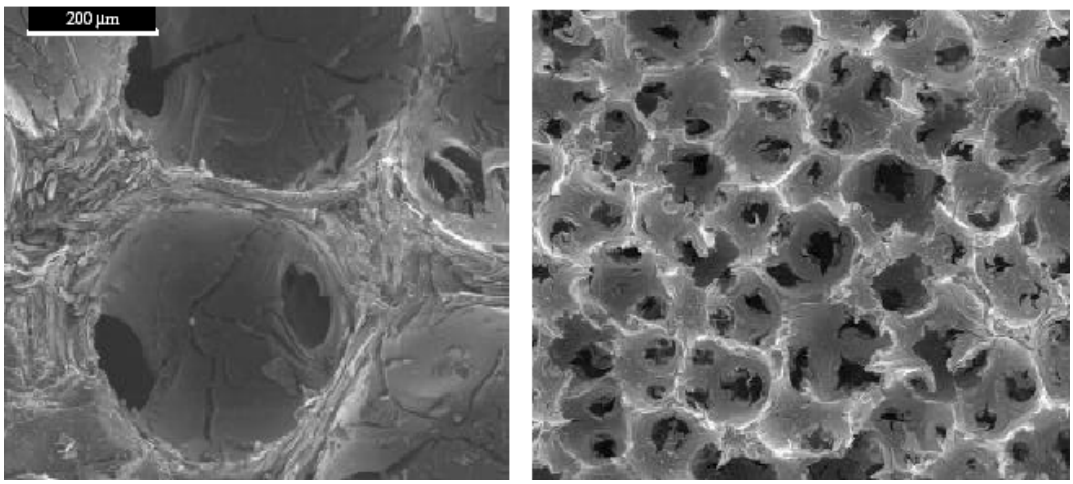

Figure 2.19 : Photomicrographs of high thermal conductivity graphite foam [100].

Pitch precursors undergo liquid-crystal (mesophase) formation during pyrolysis and result in a carbon with crystalline order. Currently, mesophase pitches are available that already have liquid crystal properties and provide an ideal precursor for foams [50].

2.8.2 Carbonization of carbon foam

Carbonization is a pyrolysis process to increase content of the element carbon at inert atmosphere. The precursor is heated slowly to a range of temperature, which depends on the nature of precursor and may be as high as 1300°C until the hydrogen and oxygen in the molecular structure has been driven off. The organic material is decomposed into a carbon residue. Volatile compounds diffuse out structure. Weight loss occurs during the carbonization stage [102,103]. Several reactions such as dehydrogenation, condensation and isomerization take place at the same time in the carbonization process. Inert gases such as nitrogen, helium or argon may be used, preferably in the form of a stream of gas. It is important to accurately control the rise in temperature, to avoid thermal stresses, which could cause cracks in the foam. Accordingly, the heating rate should be about 1°C/minute to 5°C/minute. The resulting porous carbon foam should be held at the final temperature for at least 1 hour and the cooled down slowly [104]. Lower heating rates and longer soaking times reduce carbonization yield during carbonization [102-105].

2.8.3 Graphitization of carbon foam

Graphitization is the transformation of non graphitic carbon into graphitic carbon by means of heat treatment at temperatures between 1700 ^{o}C and 3000 ^{o}C under an inert atmosphere [106]. During graphitization, crystal size increases from 50 A^{o} to 1000 A^{o} and interlayer spacing decreases from 3.44 A^{o} (amorphous carbon interlayer spacing) to the 3.35 A^{o} (graphitic carbon interlayer spacing). Graphitization involves displacement and rearrangement of planes and small groups of planes to achieve three dimensional ordering [107].

The mechanism is schematically explained in Figure 2.20 [5]. Basic structural unit (BSU), is a parallel stack of two or four layer planes each containing less than 10-20 aromatic rings. At stage 1, up to 1000 ^{o}C heat treatment temperature (HTT), the carbon contains flat BSU with a high degree of disorientation. Between 1000 and 1500 ^{o}C (stage 2), the BSU grow thicker and columnar arrays look like stuck of

coins. In stage 3, around HTT= 1500-2000 ^{o}C, the disorientation between the columns of BSU decreases, carbon layers planes can form by coalescence of adjacent BSU. At the final stage, above 2000 ^{o}C, perfect carbon layer planes are produced. Formation and growth of graphite crystallites occur.

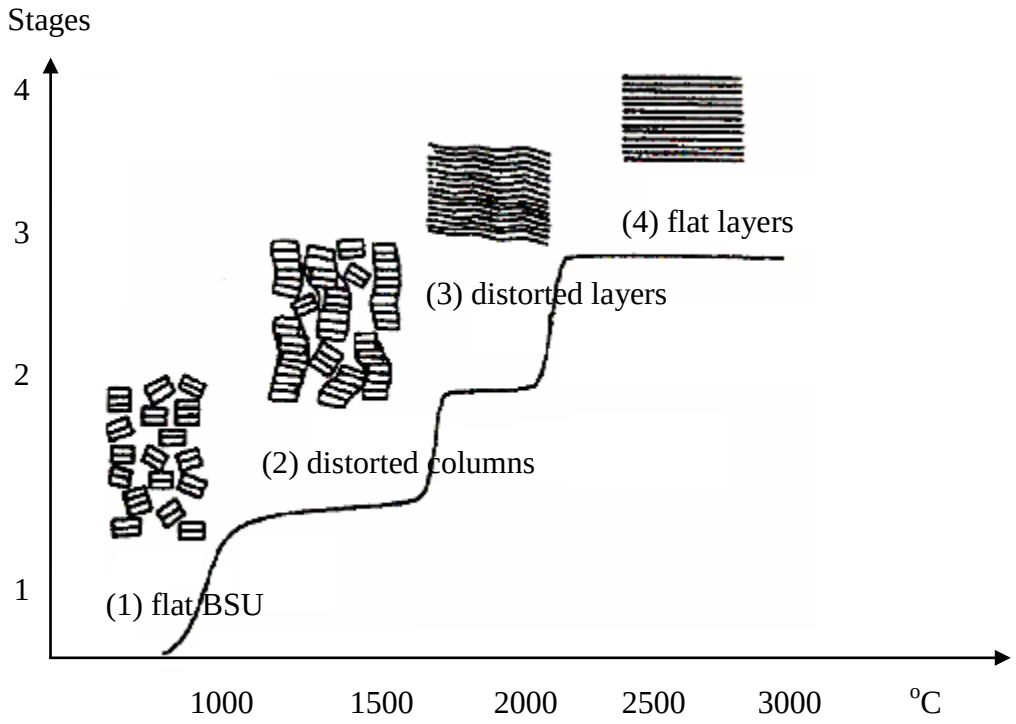

Figure 2.20 : The mechanism of graphitization.

2.9 Carbon Nanofiber

Carbon nanofibers (CNF) are graphitic filament with diameters ranged from 0.4 to 500 nm and lengths in the range of several micrometers to millimeters. Carbon nanofibers are grown by the diffusion carbon (via catalytic decomposition of carbon containing gases or vaporized carbon from arc discharge or laser ablation) through a metal catalyst and its subsequent precipitation as graphitic filaments [108,109]. Three distinct structural types of filament have been identified based on the graphene layers with respect to the filament axis namely platelet tubular herringbone [108-110]. As shown in Figure 2.21.

- Parallel-tubular Type: alignment parallel to the axis
- Platelet type: alignment perpendicular to the fiber axis

- Herringbone (Fishbone) type: planes have an angle in the range 0^o to 90^o with axis of carbon nanofiber

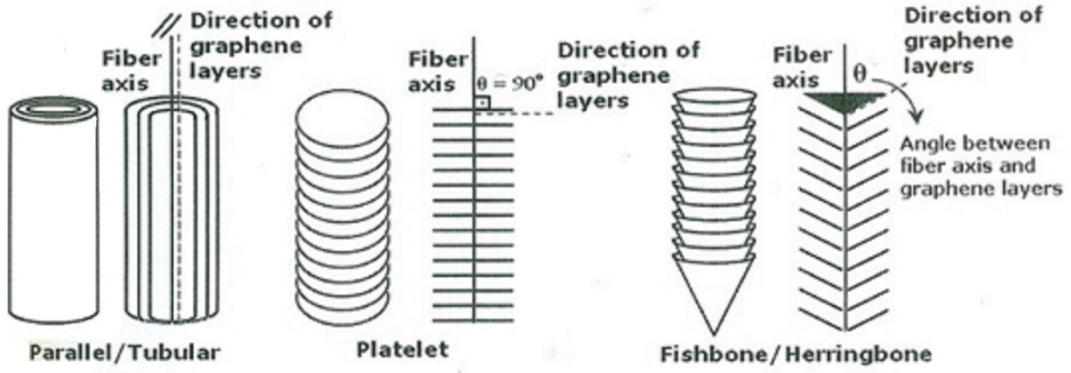

Figure 2.21 : Carbon nanofiber structures according to the angle between fiber axis and graphitic layers [111].

Figure 2.22 shows the electron microscopic images of three kinds of CNFs [110]. Synthesis of CNFs has been studied over various catalyst forms from carbonmonoxide, methane, ethylene or hydrocarbons at temperatures ranging from 400-800 ^oC. The most important metals to catalyze the growth of CNFs are cobalt, nickel, iron, magnesium. Copper, molybdenum, and several ceramic compounds such as silica, alumina, and zeolite have been generally used for supports platinum as a single metal also have shown the catalytic activity for CNFs growth [112-119].

Figure 2.23 shows a schematic representation of the different steps in the metal catalyst catalyzed growth of a CNF. First, the carbonaceous gasses absorb and decompose on the free metal surface. Some of the formed carbon atoms dissolve into the metal particle and diffuse to the bottom of the metal particle. At the bottom of the metal particle the dissolved carbon precipitates in the form of a graphene layer. By continuous precipitation of these graphene layers the CNF is formed [120,121]. In Figure 2.24, critical factors and expected effects for control of CNF growth and tailoring of its structure/properties are schematically summarized.

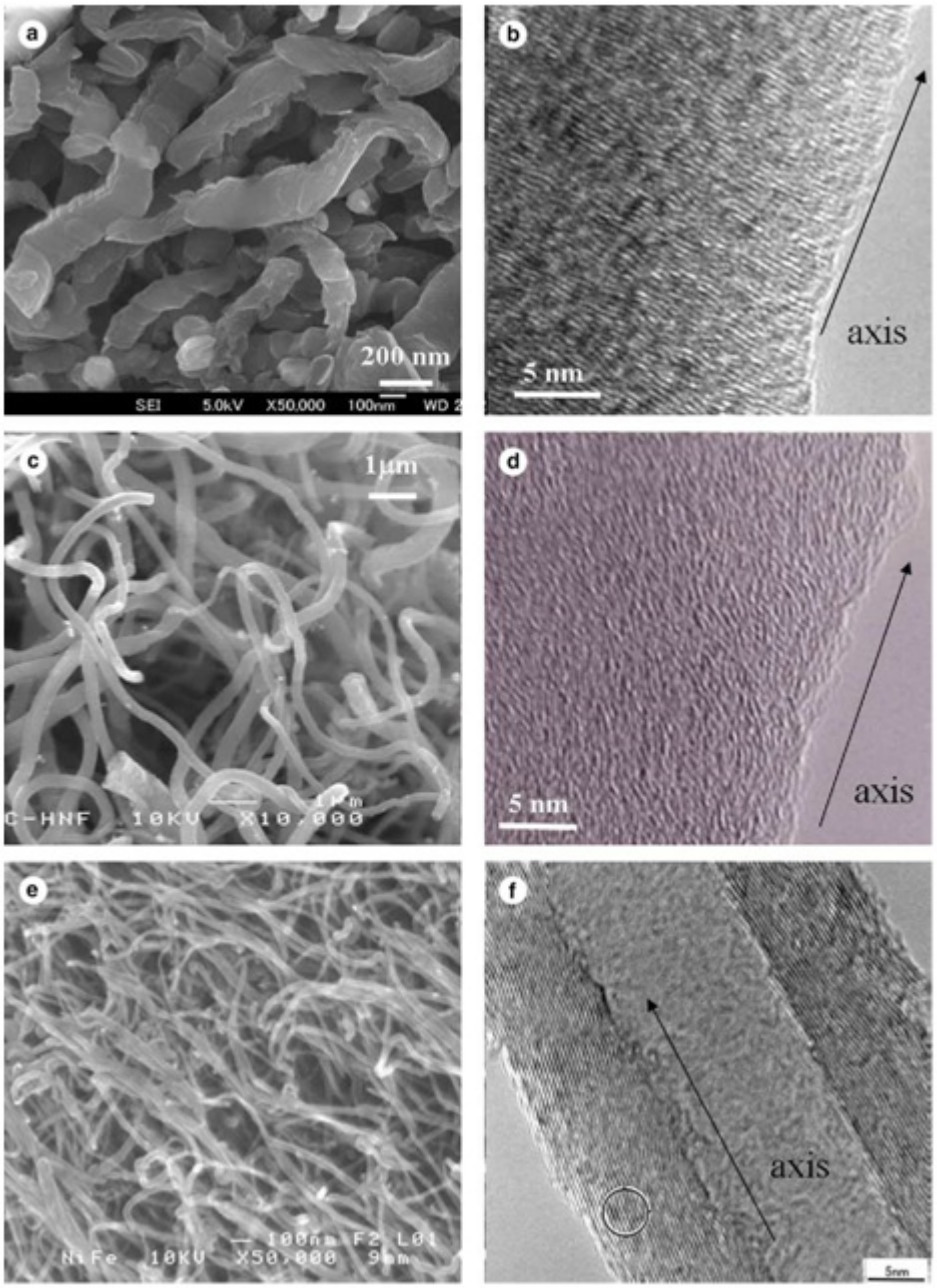

Figure 2.22 : SEM and TEM pictures of platelet (a, b), herringbone (c, d), and tubular (e, f).

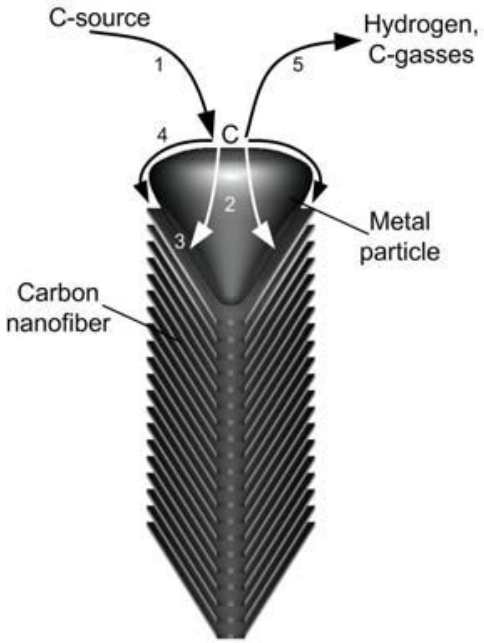

Figure 2.23 : Schematic representation of the growth mechanism of carbon nanofibers. 1) Absorption and decomposition of carbonaceous gasses on the surface of the catalytic metal particle; 2) dissolution of the carbon in the metal particle and subsequent diffusion of the dissolved carbon through the metal particle; 3) precipitation of the dissolved carbon into graphene sheets; 4) surface diffusion of the dissociated carbon; 5) desorption of hydrogen and other gasses.

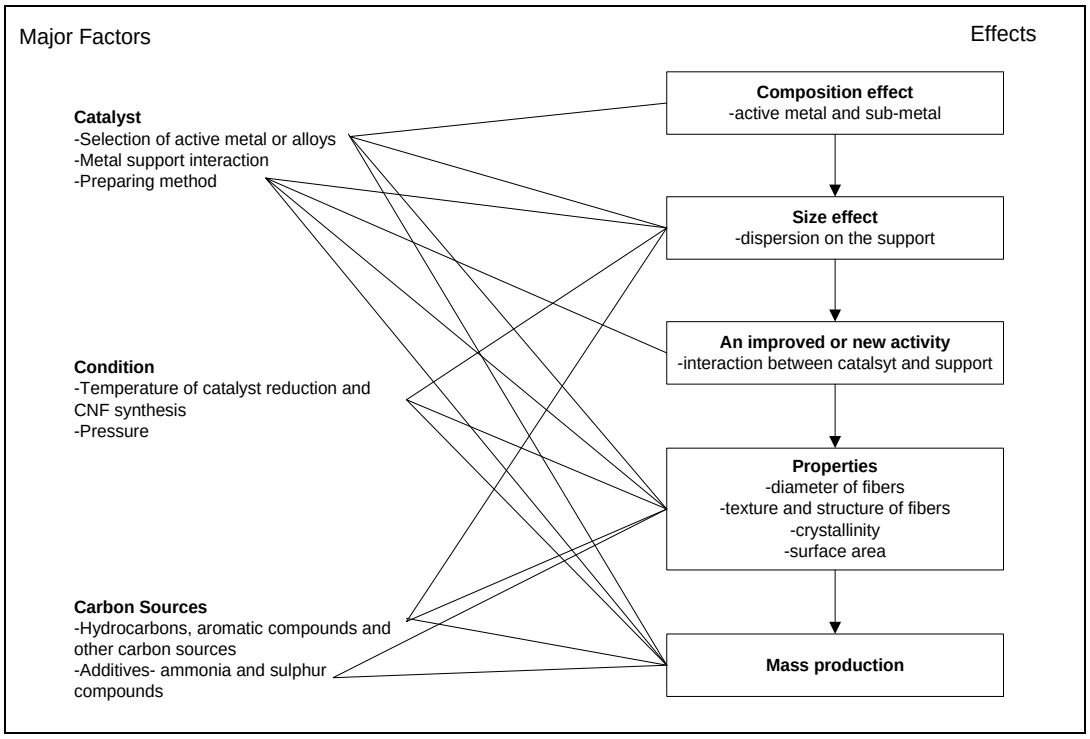

Figure 2.24 : Critical factors in catalytic synthesis of CNF and their effects.

Platelet CNF, which is characterized by a high graphitization degree and highly exposed edge sites, can be an anode material of Li secondary battery [115-119]; herringbone CNF, which is characterized by high surface areas and highly exposed edge sites, has been attempted for a hydrogen adsorbent and a catalyst support of DMFC (direct methanol fuel cell) [110-113]; while tubular CNF, which is characterized by longitudinal conductivity and promising electronic properties, has been expected for a conductive polymer filler, an electron emitter, a thermally super-conductive material and a novel semi conductive material [109-113].

In this study, herringbone CNFs were synthesized from ethylene (C_2H_4) over Fe-Ni/MgO catalyst in Kyushu University Laboratory, Japan. The preparation procedure for herringbone type carbon nanofiber is described in detail by Yoon et. al. [108,110,112-118]. The process used to manufacture CNF is mentioned in Section 4.

2.10 Application Areas of Carbon Foam

The carbon foams can be easily machined and have large surface area for bonding. The versatility of carbon foam eliminates the limitations of conventional materials. These can be listed as;

- **Product forms;** it can be manufactured both as panels of various thicknesses and as foamed-to-shape parts as shown in Figure 2.25 [122].

Figure 2.25 : Machined carbon foam disk and machined joint.

- **Fire resistance;** after heat treatment, the foam generally does not contain a sufficient amount of volatile material to support combustion. Three different CFOAM-based composite panel structures that provide alternatives for fire-resistant walls or barriers is shown in Figure 2.26. CFOAM appears as the blackened strip in the panel [123].

Figure 2.26 : Carbon foam composite panel.

- **Joining;** the foam can be joined by means of pitch bonding and heat treatment or, more simply, using low-temperature cure graphite-phenolic adhesives, allowing the use of carbon-foam building blocks to create larger or more intricate structures, as well as repair to damaged structures.

  Several foam core sandwich panels were fabricated by laminating the foam with aluminum and copper facesheets (0.5-mm thick). The isotropic thermal conductivity of these foam-core composites (Figure 2.27)should provide thermal management characteristics comparable to existing materials. This should lead to more efficient thermal management materials and, possibly, a new approach to thermal management. Also, successful densification with aluminum, carbon, epoxy, and thermoplastic resins has been accomplished, demonstrating the use of foam as the reinforcement in a composite structure where high thermal conductivity is required, but at a lower cost than traditional high conductivity carbon fibers [12].

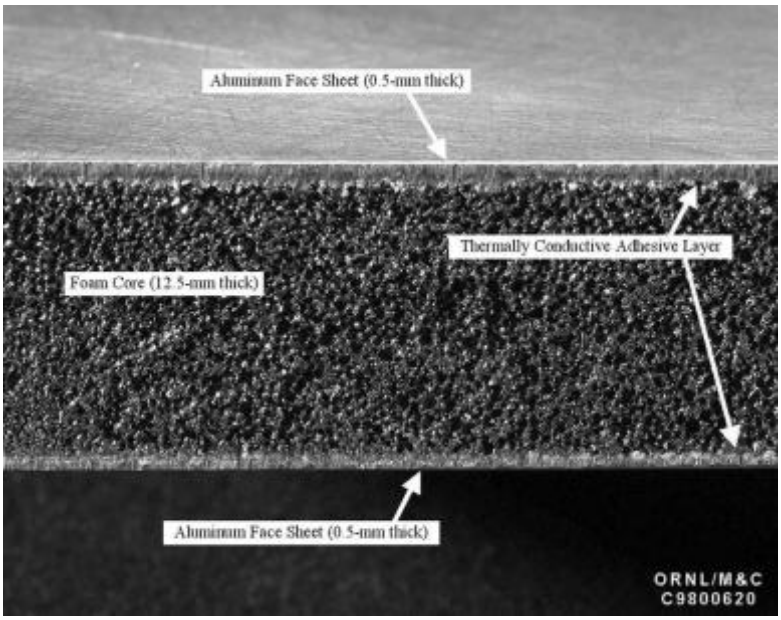

Figure 2.27 : High thermal conductivity foam-core composite with aluminium face sheets.

- **Design flexibility;** properties such as density, cell size and cell connectivity can be readily engineered to meet different requirements.
- **Impact absorption;** the foam outperforms conventional polymer foams in mechanical properties and impact resistance.
- **Machinability;** the foam is easily worked with most woodworking tools or machining equipment (Figure 2.28) [124].

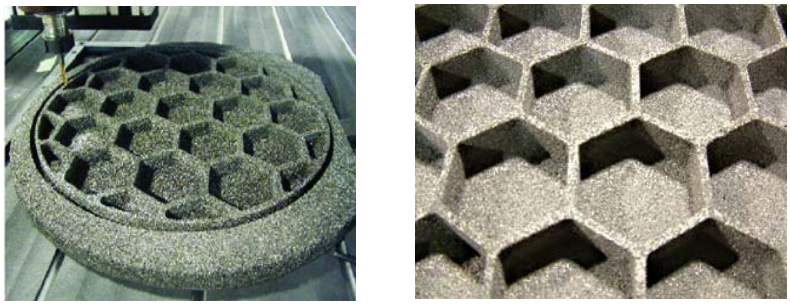

Figure 2.28 : Lightweight space mirrors support being machined on Touchstone's 5 ft by 9 ft three-dimensional router.

- **Finishing;** the material can be integrated with other materials, such as lamination with fiber reinforced face sheets, impregnation with resins or metals and thermal spraying with metals or ceramics and aluminum coatings. A kind of a typical lamination is shown in Figure 2.29 [125].

Figure 2.29 : Lamination with reinforced vinyl ester face sheets.

- **Coatings;** Nickel and copper have been successfully deposited on foam artifacts by conventional electro plating and electroless plating.

As a result of these unique properties carbon foam is used in many application areas by itself or as a combination with other engineering materials. Some of the application areas are listed below:

- AEOROSPACE
  - Antennae systems
  - Composite tooling
  - Lightweight mirrors
  - Rocket nozzles
  - Optical benches
  - Thermal protection
  - Satellite application

- AUTOMOTIVE
    - Bumpers
    - Radiators
    - Catalytic Converters
    - Cooling device for hybrid electric vehicle
- ENERGY
    - Battery electrodes
    - Fuel cells
    - Nuclear shielding
- COMMERCIAL
    - Abrasives
    - Acoustic Tile
    - Filters
    - Fire Blocks
    - Insulation
    - Prefab Walls
    - Safe Rooms
    - EMI shielding
- MILITARY
    - Insensitive munitions
    - Lightweight armors
    - Stealth materials
    - Thruster nozzle
- SHIPBUILDING
    - Low RSC structures
    - Joiner panels
    - Smokestack
- THERMAL APPLICATIONS
    - Power electronics cooling
    - Cross flow heat exchangers
- MEDICAL
    - Tooth implant
    - Artificial bone

2.10.1 Thermal management applications

Heat exchangers and heat sinks are used for thermal management. Heat exchangers transfer heat energy from one area to another, and heat sinks dissipate heat into the air. Conventionally, aluminum and copper heat exchangers and heat sinks are superior for most of the areas. Carbon foam are the alternative of them by the having light weight and high thermal conductivity. Effective heat transfer coefficient of heat sinks is over 40 times greater with carbon foam than traditional materials [71-73]. The foam's graphitic ligament has high thermal conductivity. Open cellular structure of foam allows for fluid flow that draws thermal energy from the graphitic ligaments to the fluid extremely efficiently [126,127]. Carbon foam has been used as an evaporator in a thermosyphon [128]. For the purpose of graphite foam thermosyphon design in electronics cooling, various effects such as graphite foam geometry, sub-cooling, working fluid effect, and liquid level were investigated. The best thermal performance was achieved with the large graphite foam, working fluid with the lowest boiling point, a liquid level with the exact height of the graphite foam, and at the lowest sub-cooling temperature [129] The graphite foam as the evaporator in a thermosyphon enables the transfer of large amounts of energy with relatively low temperature difference and without the need for external pumping [129,130]

Performance of the system with FC-72 and FC-87 was examined, and the effects of liquid fill level, condenser temperature, and foam height, width, and density were studied. Performance with FC-72 and FC-87 was found to be similar, while the liquid fill level, condenser temperature, geometry, and density of the graphite foam were found to significantly affect the thermal performance. The boiling was found to be surface tension dominated, and a simple model based on heat transfer from the outer surface is proposed. As much as 149 W were dissipated from a 1 cm^2 heated area [130]

High-conductivity graphite foam is investigated for use as a surface enhancement for improved thermal performance in both pool boiling and an FC-72 thermosyphon. The influences of heat load and fluid level on the overall system thermal performance including surface superheat, effective heat transfer coefficient, and thermal resistance were examined. The thermal resistance of the foam heat sink was found to be extremely low at a minimum of 0.024 K/W, well below that of many

other methods. The featured low thermal resistance was the primary benefit of this system. The thermal resistance was found to rise with increasing heat flux, but still remains advantageously low and exhibits excellent potential for high heat flux dissipation with low surface superheat, making it suitable for thermal management of advanced electronics [131].

Aluminum heat sinks use to cool the electronics processors with increased processing capability currently. Graphitic foam, with forced air flowing through, has been used as an alternative heat sink to cool a high performance Pentium 133 microprocessor (Figure 2.30). The foam is more efficient because the exposed surface area (due to the structure of the porosity) is larger than the aluminum heat sink. After this, the fins were machined off the finned foam heat sink and the test repeated. Remarkably, the temperature of the aluminum plate equilibrated at 39°C. The carbon foam outperformed the standard aluminum at a reduced weight of 10% [132].

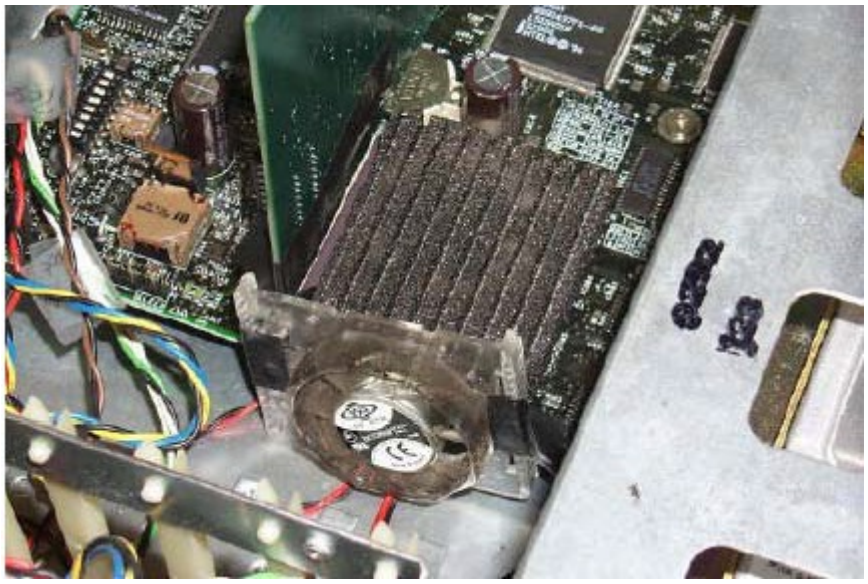

Figure 2.30 : Foam heat sink in Pentium 133 microprocessor [133].

The combination of open porosity that results in large specific surface area and high thermal conductivity achieved with the graphite foam allows for the improvement of heat exchangers. The use of graphite foam may lead to extremely efficient and lightweight heat exchangers in high performance aircraft, rocket nozzles, and aircraft brakes [79,134].

2.10.2 Energy storage

Graphite foams in conjunction with phase change materials (PCM) have been investigated for use as advanced energy storage systems for space and terrestrial applications. Because of the high thermal conductivity of graphite foams, the PCM-foam system thermal performance has been improved significantly. Tremendous amounts of thermal energy are stored and emitted very rapidly. a phase change material (PCM) filled with porous foam was conduct heat to the phase change material such that the temperature of the phase change material remain close to the operating temperature of the device. As heat is added to the surface, from a heat source such as a computer chip, friction due to re-entry through the atmosphere, or radiation such as sunlight, it is transmitted rapidly and uniformly throughout the foam and then to the phase change material. As the material changes phase, it absorbs orders of magnitude more energy than non-PCM material due to transfer of the latent heat of fusion or vaporization. Conversely, the filled foam can be utilized to emit energy rapidly when placed in contact with a cold object.

For space applications, the average value of the output power of the new energy storage system has been increased by more than eight times. While for terrestrial applications, the average output power using carbon foam of porosity 97% is about five times greater than that for using pure PCM [134,136].

Mesophase pitch based graphite foams (GFs) with different thermal properties and pore-size were used to increase the thermal diffusivity of phase change material (PCM), paraffin wax, for latent heat thermal energy storage application. Thermal diffusivity of the Paraffin-GF can be enhanced 190, 270, 500, and 570 times as compared with that of pure paraffin wax. Latent heat of Paraffin-GF systems increased with the increasing of the mass ratio of the paraffin wax in the composite. Moreover, pore-size and thickness of ligaments of the foam played a key role in improving the thermal diffusivity and the storage capacity of the Paraffin-GF system: small pore-size (less paraffin wax were filled) and thicker ligament in GF resulted in a higher thermal diffusivity; large pore-size (less paraffin wax were filled) and thinner ligament in GF resulted in a larger latent heat [137].

2.10.3 Acoustic and electromagnetic absorption

Sound absorbers reduce reflected sound energy in spaces and so reduce the reverberance and the sound level. Most materials that are thermally conductive are poor absorbers of sound. However, Graphite foam has excellent acoustic absorption and can be used in the shipbuilding, aerospace, and automotive industries. Graphite foams performed up to 20% better than open cell Pyrell Foam (typically used in anechoic chambers) at all frequencies tested. In addition, graphite foam is an excellent electromagnetic shield due to the foam's high electrical conductivity [101, 138,139].

Electrically conductive carbon foams are effective in blocking high frequency electromagnetic interference (EMI) such as that generated by microwave emitters, including radar sources. Typically, such electrically conductive carbon foams have an electrical resistivity of less than about 1 ohm-cm and in some instances less than about 0.1 ohm-cm. Such electrically conductive carbon foams may be used on structures such as walls, enclosures, or shelters, to shield an interior volume from EMI. The interior volumes of these enclosures provide areas in which personnel, electronic equipment, and/or items and materials may be sheltered and function without the negative effects that may result from exposure to such interference. Additionally, due to the inherent strength of carbon foam, the carbon foam may be used to form such structures. Further, other embodiments may include rigid porous electrically conductive carbon [140].

Coal derived carbon foam is under development for numerous EMI shielding applications including ships, tactical shelters, fixed site shelters, and other electronic enclosures. Carbon foam can be easily joined together with electrically conductive adhesives to form a non-metallic "Faraday cage" enclosure [141].

Carbon foam enclosures can provide greater than 60 dB of RF shielding from 100MHz to 20 GHz with no metallic components. The advantage of using carbon foam in an electronic enclosure is that it serves as a multifunctional material by providing both EMI shielding and structure as a composite core material for the enclosure (Figure 2.31). Multifunctional carbon foam electronic enclosures will provide fire protection, reduce weight by eliminating metallic components, eliminate corrosion issues, and provide longer service life in harsh environments [141]

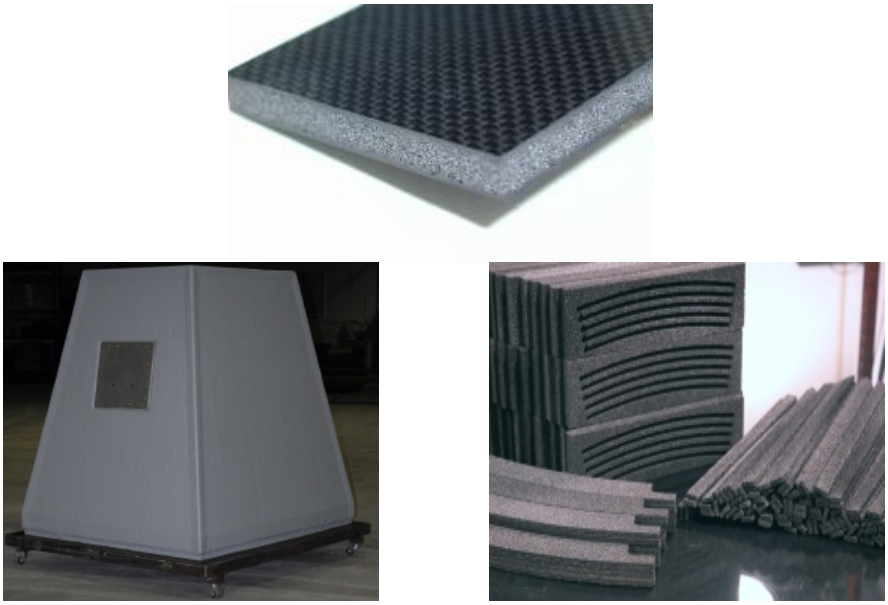

Figure 2.31 : EMI sheltered composite structures.

2.10.4 Batteries

Carbon Foam with inherently large surface area, high electrical conductivity, and chemically inert state is an ideal material for the construction of advanced electrodes. Carbon Foam can be readily coated to form either an anode or cathode with a number of active materials.

- Cyclic voltammetry and galvanostatic charge–discharge experiments were performed on the material to evaluate its electrochemical properties. Initial charge–discharge characterization of the carbon foam coated with lead oxide pastes shows that the carbon foam is suitable for use as negative current collectors of lead acid batteries [142].
- Lead electrodeposited pitch based carbon foam (LCF), was investigated as possible positive current collectors for lead acid batteries. Comparative charge–discharge tests show that a battery equipped with a LCF collector exhibits higher PAM utilization efficiency and longer cycle life, for LCF can provide large specific surface area which is beneficial to electrochemical reactions and PAM adhesion [143].

Benefits of foam for batteries are:

- reduces the weight of the battery.
- excellent discharge performance at low ambient temperatures due to the very high available surface area of the graphite foam.
- Performance at high temperatures is also improved due to the high thermal conductivity of the graphite.
- a longer battery life: The graphite foam electrodes transfer heat out of the battery quickly enabling an overall "cool" operation compared to conventional lead-acid batteries.
- reduces heat signature and reduces the likelihood of infrared detection (for military operations) [144,145].
- higher power, greater energy delivery, and faster recharge capabilities relative to conventional lead-acid batteries.

Currently, Touchstone has developed a working fuel cell and batteries, and is in the process of creating lightweight mirrors and thermal protection panels with CFoam technology. Firefly Corporation is to replace the solid lead grids in lead-acid batteries with high porosity graphite foam. The foam is the electrode and is impregnated with a slurry of lead oxides and sulphuric acid as the electrolyte. Due to the high porosity the battery consists of thousands of micro-cells. The primary advantage of this new structure is that it in conventional lead-acid batteries liquid diffusion occurs in a single direction along direct pathways on the order of millimeters. Within the discrete microcells that collectively make up a new type of electrode structure liquid diffusion occurs in all directions along direct pathways on the order of microns.

2.10.5 Composite tooling

Conventional tooling has used Invar®, aluminum, and steel for the fabrication of large composite components such as aircraft wing skins and fuselage structures. Carbon foam composite tooling offers an alternative to these conventional materials by simplifying tool design and reducing the time to build a tool.

Touchstone performed Carbon foam has been used for large scale composite tooling. Carbon foam would be a suitable alternative to the current method and would provide the following advantages:

- Low CTE for composite tooling, more closely matching the composite part
- Lower fabrication costs
- Lighter weight tools
- Tooling easier to modify or repair
- Improved performance durability
- Increased autoclave part throughput due to low mass tooling

The use of coal-based carbon foam in tooling for carbon composites is advantageous because of its low cost, light weight, machinability, vacuum integrity, and compatibility with a wide range of curing processes. Large-scale tooling case studies will be presented detailing carbon foam's potential for tooling applications [146].

2.10.6 Structural applications

Fabrication of metallic tooling requires many expensive stages of long duration with a large infrastructure investment [146].Carbon foam has been considered for several replacement metallic honeycombs and as a core material for interior panels, sandwich structures, non-structural bulkheads, space borne mirrors supporter, sound absorption panels, electromagnetic radiation shield [147,148]. Specific modulus of Carbon foam is higher than conventional aluminium and Kevlar honeycomb core materials. They are used typically in aerospace applications for low weight stiff structures. Therefore carbon foam in structural applications where reduced weight is critical [149].

The foam-structured photo reactor benefits from a strong gain of exposed surface leading to an increased surface to reactor volume ratio with a large increase in the TiO_2 amount inside the reactor resulting from a high porosity and large cell size morphology. Further, the improved air-to-surface contact probability ratio induced by the static mixer effect of the foam resulted in a high methanol conversion obtained at a given TiO_2 amount in the reactor[150]. Graphite foam, developed and

produced at Oak Ridge National Laboratory, is being evaluated as a candidate material for the core of basic heat source modules in solid state reactor [151]. The capacity of microcellular carbon foam / epoxy resin composite electrode was two orders of magnitude greater than that expected for carbon are compared to those of both a glassy carbon electrode and microelectrode array [152].

3. EXPERIMENTAL PROCEDURE

In this section, experimental techniques for making carbon foam, its further processing and characterization stages will be discussed. Carbon foam is produced in a high-pressure/temperature reactor using a pitch precursor. The produced carbon foams are carbonized in a temperature programmed furnace. A basic flow diagram of the process is shown in Figure 3.1. Finally, carbon foams produced with this technique are examined with scanning electron microscopy (SEM), He pycnometry, X-ray diffractometry (XRD), In addition, compressive strength values of the carbon foams are measured.

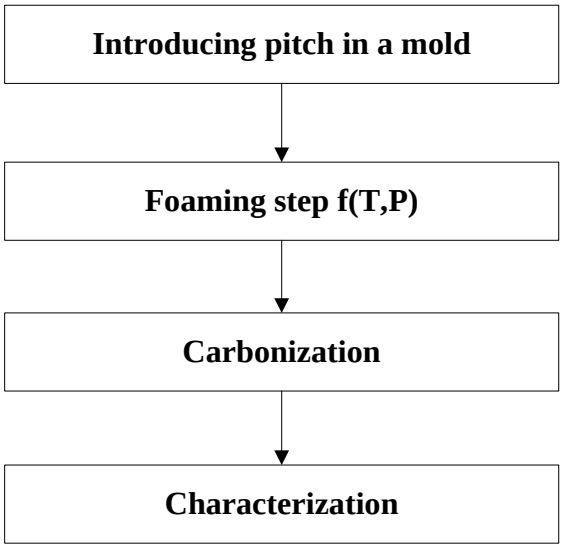

Figure 3.1 : Flow diagram of the process for making carbon foam.

3.1 Raw Material

3.1.1 Mesophase pitch

Mesophase pitch (Figure 3.2) was provided by Mitsubishi Gas Chemical Corp., Tokyo, Japan. The pitch; namely Mitsubishi AR mesophase pitch is produced by catalytic polymerization of naphthalene with the aid of HF-BF_3 catalyst. Naphthalene is aromatic hydrocarbon, so it is called as a synthetic mesophase pitch. Properties of AR mesophase pitch are given in Table 3.1.

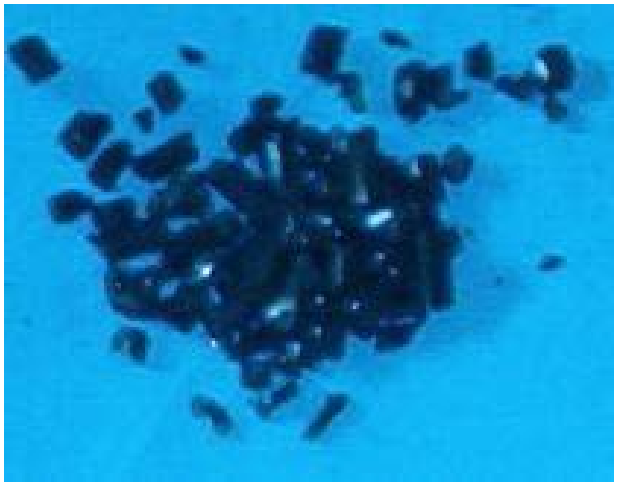

Figure 3.2 : Mesophase Pitch.

Properties of AR mesophase pitch are presented in Table 3.1. The production process is explained in section of 2.7.2 and structure of the AR mesophase pitch is given in Figure 2.14.

Table 3.1 : Typical properties of mesophase pitch [153].

Physical Properties	
Appearance	Black pellets (25ºC)
Bulk Density (g/cm³)	0.70 ± 0.3 ; pass: 0.69
Specific Gravity (25ºC)	1.23
Specific Heat (cal/g ·ºC)	0.65
Softening Point (ºC)	285 ± 5 ; pass: 282.9
Mesophase Content (%)	100
Hydrogen/Carbon (atom/atom)	0.58-0.64
Flash Point (ºC)	> 300
Ash (ppm)	< 20
Solubility (%)	
Water Soluble	0
Benzene Soluble	35-44
Pyridine Insoluble	40-50
Coking Value (%) at 1 hr, 600ºC	
1 atm	80-85
30 atm	90-95
Toxicological Information	
Acute Oral LD60 (rat)	> 5000 mg/kg
Skin Irritation	slightly irritating
Mutagenicity (Salmonella)	negative
Mutagenicity (E.coli)	negative

3.1.2 Carbon nanofiber production

Carbon nanofibers have been widely used in literature for improving some properties of carbon materials [154-157]. Herringbone CNFs are added into mesophase pitch with various proportions in order to investigate the effects on the interconnected pore structure and cell formation of carbon foams.

Herringbone CNFs (H-CNF) were synthesized from ethylene/hydrogen gas mixture over Fe-Ni/MgO alloy catalyst and were mixed with hand to mesophase pitch before the samples put into the reactor. CNFs were added to mesophase pitch in five different weight ratios; 1 %, 3%, 5%, 7%, 10 %.

3.1.2.1 Catalyst Preparation

Chemicals

Reagent grade iron nitrate (Fe $(NO_3)_3.9H_2O$), nickel nitrate ($Ni(NO_3)_2.6H_2O$), magnesium nitrate ($Mg(NO_3)_26H_2O$), and citric acid ($C_6H_8O_7$) were obtained from Wako chemical Inc (Japan). Hydrogen (>99.9999%), Helium (>99.9999%), Oxygen (>99.9999%), Nitrogen (>99.9999%), Ethylene (C_2H_4) (>99.9999%) were used without further purification.

Fe-Ni/MgO Catalyst

To prepare Fe-Ni/MgO catalyst (4:1:5 metal mole ratio), iron (12.12 g iron nitrate nanohydrate) was solved in water (300 ml). Nickel (34.75 g. nickel nitrate hexahydrate), citric acid (30.44 g) and magnesium (38.44 g magnesium nitrate hexahydrate) were added respectively. The mixture was mixed thoroughly (~ 30 minutes) and then heated at 100 ^oC for nearly 3 hours. The amount of liquid in the solution was kept constant with adding water during this period. Then the aqueous solution was boiled and solid was obtained. This product was dried in an oven at 120 ^oC overnight. The dried lump was ground to powder. The raw product was oxidized at 400 ^oC for 3 h under oxygen flow. The oxidized catalyst was reduced in 20% H_2/He mixture for 20 h at 500 ^oC. The reduced catalyst was subsequently cooled to ambient temperature in a helium atmosphere and passivated in a 10% Air/He mixture for 1 h at room temperature.

3.1.2.2 Herringbone carbon nanofiber production

Herringbone CNFs were synthesized in a fixed reactor. Powdered catalyst was placed quartz boat at the centre of reactor. The reactor was heated up to 590 ^{o}C under 20% H_2/N_2 mixture flow in 3 h and then N_2 gas was flushed for 30 min. The reactant gas 50% ethylene/hydrogen mixture was then allowed to flow for 1 h at 590 ^{o}C. Later, 10% H_2/N_2 mixture flow was applied for 30 min at 590 ^{o}C. Finally reactor was cooled down to room temperature under N_2 flow. The total flow rate was 3 L/min through the whole process. The summary of the heating regime is shown Figure 3.3. The synthesis CNFs were treated in 10 wt % HCl until the metal content was less than 0.2 wt %. The HCl treated CNFs were used in subsequent steps. The structure and morphology of the CNF observed by electron microscopy is shown in Appendix A.

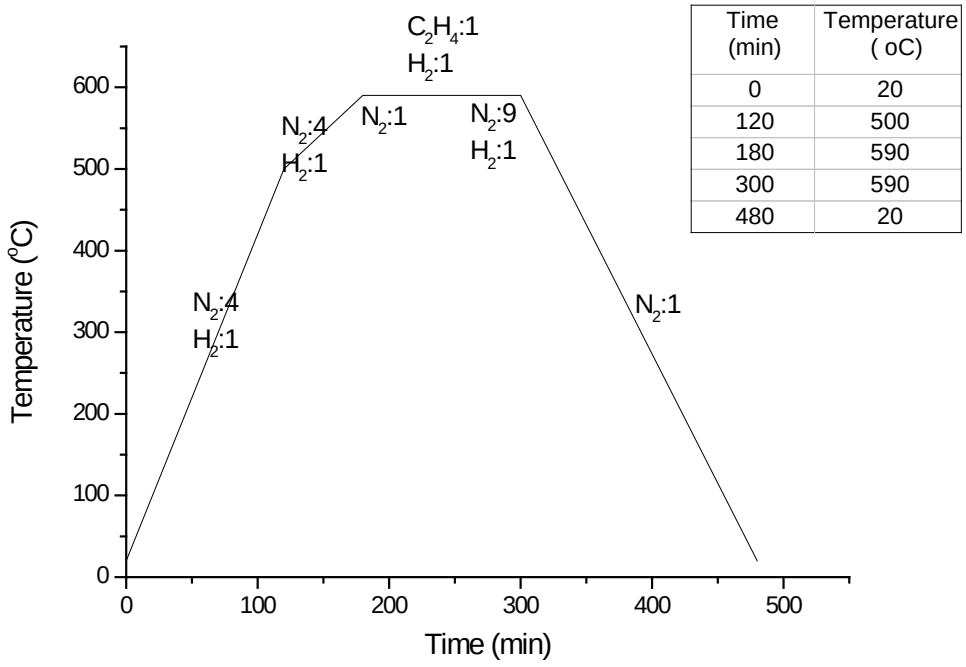

Time (min)	Temperature (oC)
0	20
120	500
180	590
300	590
480	20

Figure 3.3 : Heating regime during CNF synthesis process.

3.2 Carbon Foam Production

3.2.1 Experimental setup

In order to produce carbon foam, mesophase pitch was introduced into an aluminum mold. The mold has cylindrical shape made from aluminum with dimensions of 2 cm diameter and 10 cm length. The photograph of the aluminum mold is given in Figure 3.4.

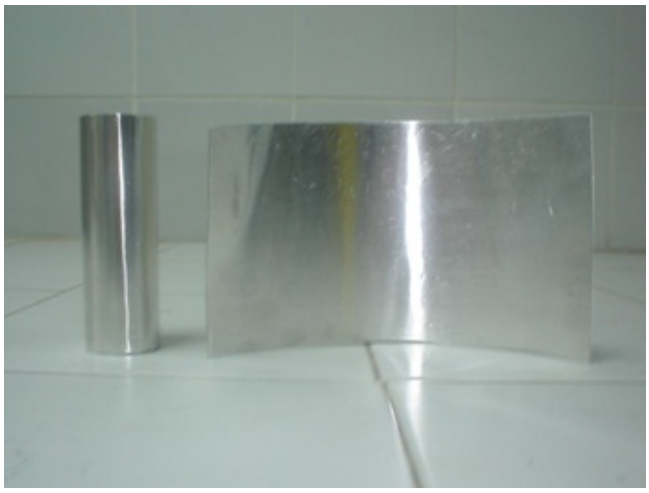

Figure 3.4 : Aluminum mold.

The mold is introduced in a stainless steel high temperature and pressure reactor. Maximum allowable working temperature and pressure are 600°C and 300 bars respectively. The photograph of reactor is shown in Figure 3.5.

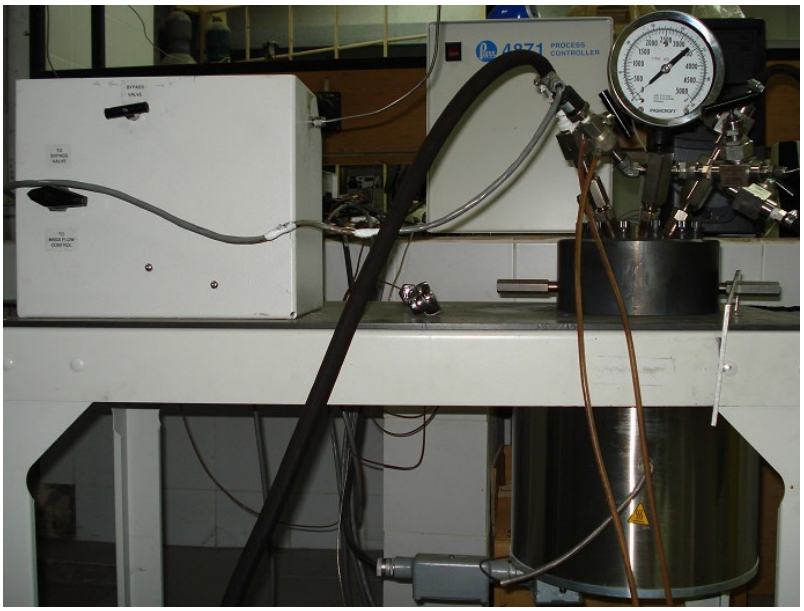

Figure 3.5 : Reactor.

Reactor is managed by a multifunctional computer program called cascade control system. The reactor temperature, pressure, heating rate, and standby temperature can be adjusted by this system. Figure 3.6 the cascade control menu is shown.

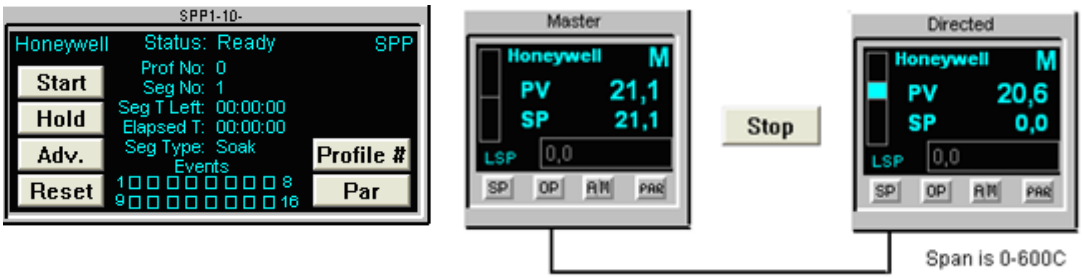

Figure 3.6 : Computer software menu to control reactor temperature and pressure.

Process of carbon foam production from mesophase pitch is summarized briefly as follows; firstly, air in the system is purged out with nitrogen and then this sweeping process is repeated at least three times to ensure the removal of air from the reactor. After sweeping is completed, system is vacuumed [88-90]. Then vacuum is released and the pressure is increased to preferred value with an inert gas (nitrogen, argon, helium etc) [48, 88-90, 158-160]. The sample is heated to a temperature sufficient to coalesce the pitch into a liquid which preferably maintained for is of about to 50 ^{o}C to 100°C above the softening point of the pitch. The system is maintained in this state. Then temperature of system is raised to about 500 ^{o}C to about 1000 ^{o}C. This is performed at a rate of no greater than about 5^{o}C/min. The temperature is held for at least 15 minutes to achieve assured soak and then pressure is released to atmospheric pressure rapidly at about 3-5 seconds or longer. The reactor power is turned off and cook to room temperature [160-164].

In this study; all experiments were performed at constant pressure in order to determine the effect of operating pressure on the carbon foam properties. The reactor was pressurized to 5 and 10 atm and then heated up to 350 ^{o}C with a heating rate of 5 ^{o}C/min. The soak time 2 hours was applied at this temperature. At the second step the reactor was continued to heat up to 600 ^{o}C with a heating rate of 5 ^{o}C/min and finally 30 min soak time was applied at this temperature. After that the pressure was released rapidly and reactor was allowed to cool down to the ambient temperature.

The green foam samples obtained were carbonized up to 1000 ^{o}C for 1 hour under nitrogen flow in a horizontal tube furnace with a heating rate of 5 ^{o}C/min. The carbonization furnace is shown in Figure 3.7.

Figure 3.7 : Carbonization furnace.

3.3 The process for the manufacture of carbon foam

While the foam synthesis process is rather simple, the morphological changes occurred during processing are complex. Balance and relationship between the viscosity-temperature behavior, melting temperature, and pyrolysis temperature of the mesophase pitch is very subtle. The average pore size, orientation, and distribution are determined primarily by the pitch viscosity and processing pressure during foaming. This process includes the following steps:

Step 1 – When a mesophase pitch precursor is heated to about 50°C -100 ^{o}C above its softening point in a oxygen free environment under specific pressure, the aromatic hydro-carbons through the process of dehydrogenation initiate free radical molecules and condense to form larger weight hydro-carbons. These large hydro-carbons coalesce into stacked mesophase crystals which increase the viscosity of the pitch [165-166].

Step 2 - After the mesophase pitch softens and then expands because of gas evolved from the pyrolysis of the pitch, but the initial foam bubbles are not uniformly dispersed in the molten pitch. They start to grow at the upper section of the pitch and then the whole molten pitch is foamed [167].

Viscosity of the pitch plays a key role in the ability to foam the mesophase pitch. When the pitch is in a molten form and the foaming process initiates, crystallites or mesophase domains orient in response to the stresses resulting from extension in the walls of the foam. The crystallites or mesophase domains orient parallel to the surface of the bubbles. As the bubbles join and openings between the bubbles develop, a strut-like morphology develops with the orientation in the surface of the bubbles translating to the ligaments, yielding highly aligned mesophase domains along the axis of the ligament. During this development, a lower viscosity will result in better re-orientation due to extension, thus resulting in enhanced alignment of the mesophase domains parallel to the axis of the ligaments [12].

Step 3- When the temperature continues to increase, as a result of the buoyancy force of the vapor phase, the bubble shape of the foams become from spherical to elliptical, which can be illustrated in Figure 3.8 . It should be noted that the as-prepared bulk foams always show bulk gradient between the liquid and the vapor phase in bottoms section, which is smaller than the upper section of the foams because of the gravitational force [167].

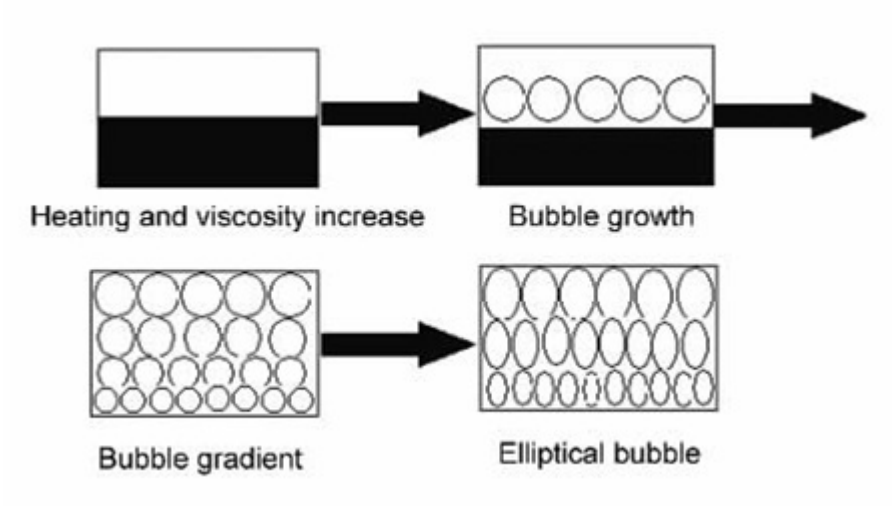

Figure 3.8 : Schematic illustration of bubble growth process.

At higher temperatures, the mesophase begins to pyrolyze (polymerize) and produce additional volatile species. The pyrolysis leads to weight loss, which can be very rapid and is dependent on the precursor, and is accompanied by an increase in the molecular weight of the precursor which, in turn, increases the viscosity of the liquid mesophase [167].

The pyrolysis of pure AR mesophase produced significantly lower amounts of toluene, but also produced $C_{4–6}$, C_{16} and C_{24} paraffins, alkyl-substituted one- and two-ring aromatics, and partially saturated naphthalene [168].

Step 4- As the temperature of the furnace is further increases (about 500 ^{o}C to 600 ^{o}C) , the foamed mesophase pitch continues to pyrolyze, further increasing the viscosity of the material until it has sufficiently cross linked and is rendered infusible or cannot be melted [58,161].

Step 5- After that the pressure is released rapidly and reactor is cooled down to the ambient temperature. When the pressure is rapidly decreased, the gas expands to form bubbles, and further expands to break these bubbles thus forming an open cell structure. This extension causes mesophase molecules to orient parallel to the surface of the bubbles as shown in Figure 3.9 [101].

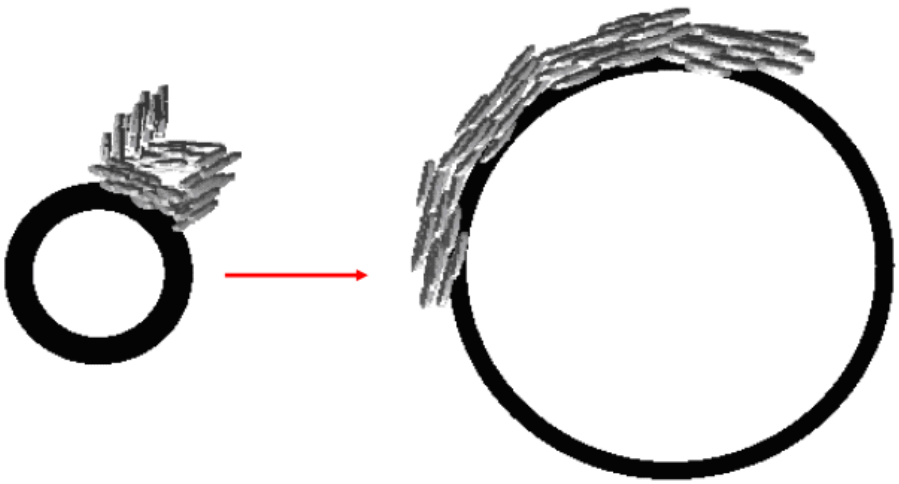

Figure 3.9 : Bubbles growth under applied pressure.

Step 6 - After the foaming process, the next stage is the carbonization. The foam is carbonized to obtain relatively pure carbon foam. In this state, the foam is an excellent thermal insulator. Following carbonization the carbon foam is graphitized at temperatures above 1700 ^{o}C. At this stage the carbon foam is more thermally conductive.

The related terminology is indicated in the Figure 3.10 for a better understanding of the evaluation of foam. As it can be seen from the figure, cell has a spherical geometry with open pores. The number of the pores generally varies between one and four. These pores are interconnected to other cells. Interlayer between the cells is

defined as ligaments. This is the part where rod-like mesophase molecules aligned and layered which causes graphitic structure at the further step of heat treatment. Junctions are located between three or more cells. Non uniform elongated region inside the cell are defined as cracks. The cracks affect the strength of the material [88].

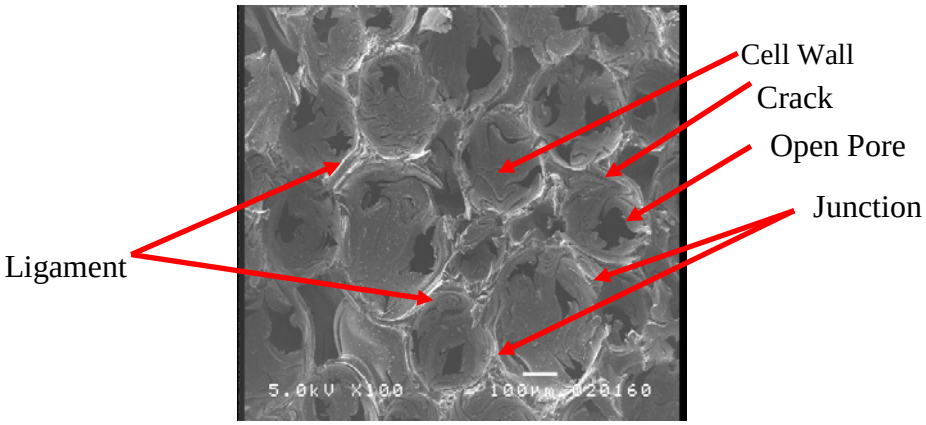

Figure 3.10 : The terminology used for SEM photographs of carbon foam.

Some of the key control mechanisms are as follows [169-173]:

1. Initially, the volatile gases must develop at a temperature such that the viscosity is sufficient to result in stable foam.
2. Premature gas evolution causes the pitch to froth, resulting in foam with a significant density gradient.
3. If the gases are produced too late in the process when the pitch viscosity is high, the bubbles will not be uniform, and cracking can occur due to thermal stresses.
4. If the pyrolysis gases are evolved very slowly, as for certain high melting point pitches, the pores will tend to be smaller.
5. Bubble formation is closely related to the operating pressure as well as temperature.
6. Depending on the unique rheological properties of the starting pitch, the cell walls have different thicknesses, the bubble sizes can be dramatically different, and the mechanical and thermal properties can be affected.

3.4 Characterization of Carbon Foam

Characterization of the structure and texture of carbon materials are essential and important for assigning proper utilization and understanding their structures. Before discussing foam material, fundamental techniques for the characterization of the structure and texture of carbon foam are explained below.

3.4.1 X-ray diffractometry

X-ray diffraction is one of the fundamental techniques to characterize crystal structure. The technique provides a measure of the amount of ordered materials and give an indication of the size of crystallites which make up the ordered structure.

When a beam of chromatic x-radiation is directed at a crystalline material, diffraction of the x-rays is observed at various angles with respect to primary beam. The relationship between the wave length of the X-ray beam (λ), the angle of diffraction (2θ), and the distance between each set of atomic planes of the crystal lattice (d), is given by the Bragg equation [174,175]

$$n.\lambda=2.d.\sin\theta \qquad \textbf{(3.1)}$$

In equation 3.3, n denotes the order of diffraction. Using this equation, the interplanar distances of crystalline material under study can be calculated. The interplanar spacing depends on the arrangement of atoms in the crystal unit cell. The intensities of the diffracted rays are function of both the diffraction power and the placement of the atoms within the unit cell [174,175].

The broadening of the diffraction peaks allows an estimation of the mean particle size. The approximate crystallite size (t) can be calculated from the amount of broadening (β), using Scherrer equation:

$$t= c.\lambda /\beta.\cos\theta \qquad \textbf{(3.2)}$$

Where c is the cell dimension, λ is the X-ray wavelength and 2θ the scattering angle and β is the amount of broadening due to sample [175,176]. The carbon foam samples were characterized with X'pert Pro PAN analytical X-ray Diffractometer.

3.4.2 Scanning electron microscopy

Scanning electron microscope (SEM) has been commonly used to observe the morphology and surface of the materials. SEM operates by focusing an electron beam passing through an evacuated column on the specimen surface using electromagnetic lenses. The beam is raster scanned over the surface of the specimen in synchronism with the beam of a cathode ray tube (CRT) display screen. Inelastically scattered secondary electrons emitted from the sample surface are collected by scintillator-counter and the signal form this used to modulate the brightness of the image on the CRT. Differences in secondary emission result from changes in surface topography. If the elastically (backscattered) electrons are collected, an image can be formed from the contrast resulting from compositional differences across the surface of the specimen [176].

The carbon foam samples were characterized with JEOL JSM-6390 LV Scanning Electron Microscope (Figure 3.11) .

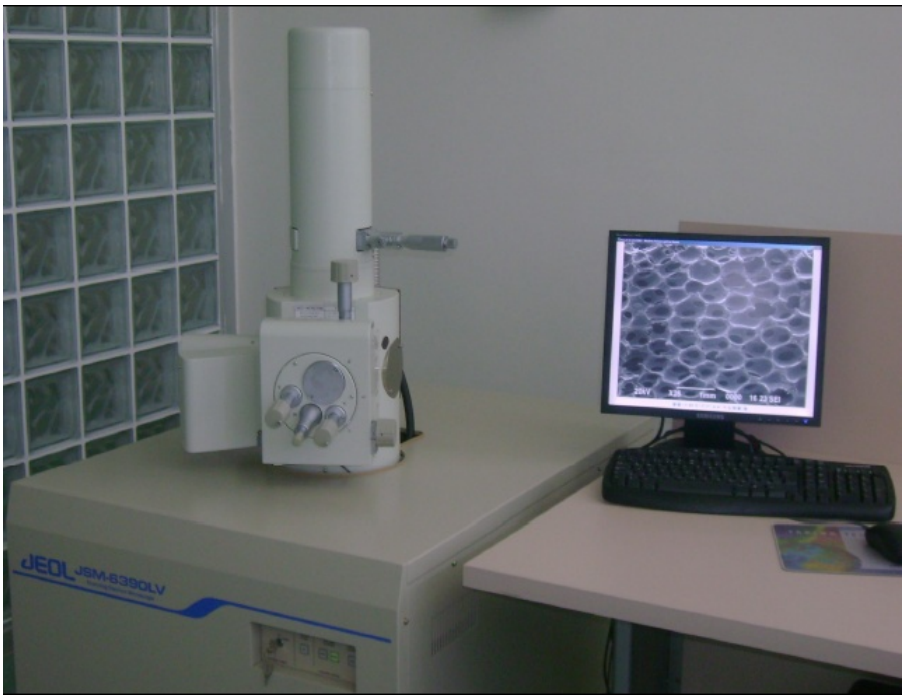

Figure 3.11 : Scanning Electron Microscope.

3.4.3 Density

Density, or as it is known bulk density, is obtained by measuring the volume and mass of samples. To calculate volumes, the samples are shaped like cylindrical or rectangular prism, and all sides are measured. After all, the rectangular/cylindrical shaped samples are weighed. In order to reach the density measurements M/V ratio is used [75,89,90,163].

3.4.4 Helium pycnometry

The skeleton density, which is defined as the structural or solid density, is determined with helium pycnometry. In this method, it is assumed that helium enters the smallest pores present, without being adsorbed. The porosity of the foam samples are calculated by the equation shown below [48]: d; bulk density, Dr; density measured using helium. In this study, Quantachrome Ultrapycnometer1000 is used.

$$P = (1-d/Dr).100 \quad \textbf{(3.3)}$$

3.4.5 Compressive strength

In order to get compressive strength of the samples analyses are conducted on Autograph-AGS-J SHIMAOZU Tension/Compression equipment (Figure 3.12). The instrument has ability to supply pressures up to 10 tons for compression of metals, paper, plastics, and fabrics, wire of all gauges, rubber, or any other specialized materials.

Figure 3.12 : Compressive Strength Test Equipment.

4. RESULTS AND DISCUSSIONS

This dissertation is focused on interpreting the foaming mechanism, analyzing the preparation process of mesophase pitch based carbon foams with the addition of carbon nanofiber and characterization of the properties of final products.

4.1 Structure of Mesophase Pitch based Carbon Foams Produced at Low Pressures

4.1.1 Properties of the carbon foam produced at 5 atm

In this set of experiment, green carbon foam was produced at a pressure of 5 atm and constant temperature of 600^{o}C and rapid pressure release time of 5 sec (Figure 4.1). Further, this green carbon foam was carbonized and then divided into three sections as upper, middle and bottom. Each section was analyzed separately.

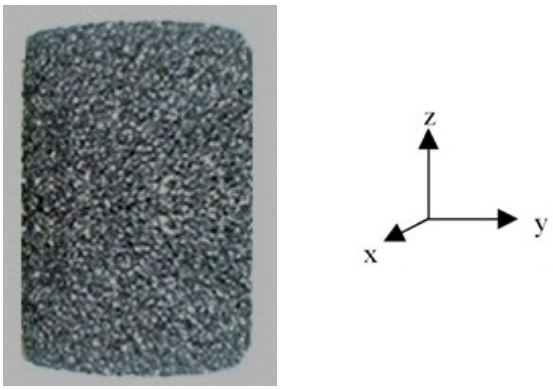

Figure 4.1 : A cylindrical shape of carbon foam sample.

The scanning electron microscopy (SEM) images of the carbon foam produced for two different magnifications in the z-direction are given in Figure 4.2. Porous structure of upper, middle and bottom sections of the carbon foam produced are shown in this figure. In the figure; L represents the ligaments (structure between two neighbor cells), J represents the junctions (structure occurred in the middle of more than two cells), and C represents the cracks in the carbon foam structure. In Figure 4.2; a, b, and c represent the SEM images of upper, middle, and bottom sections for the carbon foam produced, respectively.

The SEM images in Figure 4.2c showed that the formation of the cells was not well developed for the bottom section and non-spherical cell formation was observed. Cells contained fewer pores at various sizes which were not well distributed compared to the other sections. The non-uniform and less ordered cell structure was obvious. As it can be seen from Figure 4.2b, at the middle section, the number of the cells and pores increased and their geometries became more spherical compared to the bottom section. The SEM images in Figure 4.2a showed that more spherical cells with interconnected pores were obtained at the upper section. The number of the cells as well as the pores increased compared to the middle and bottom sections.

Z-axis point of view

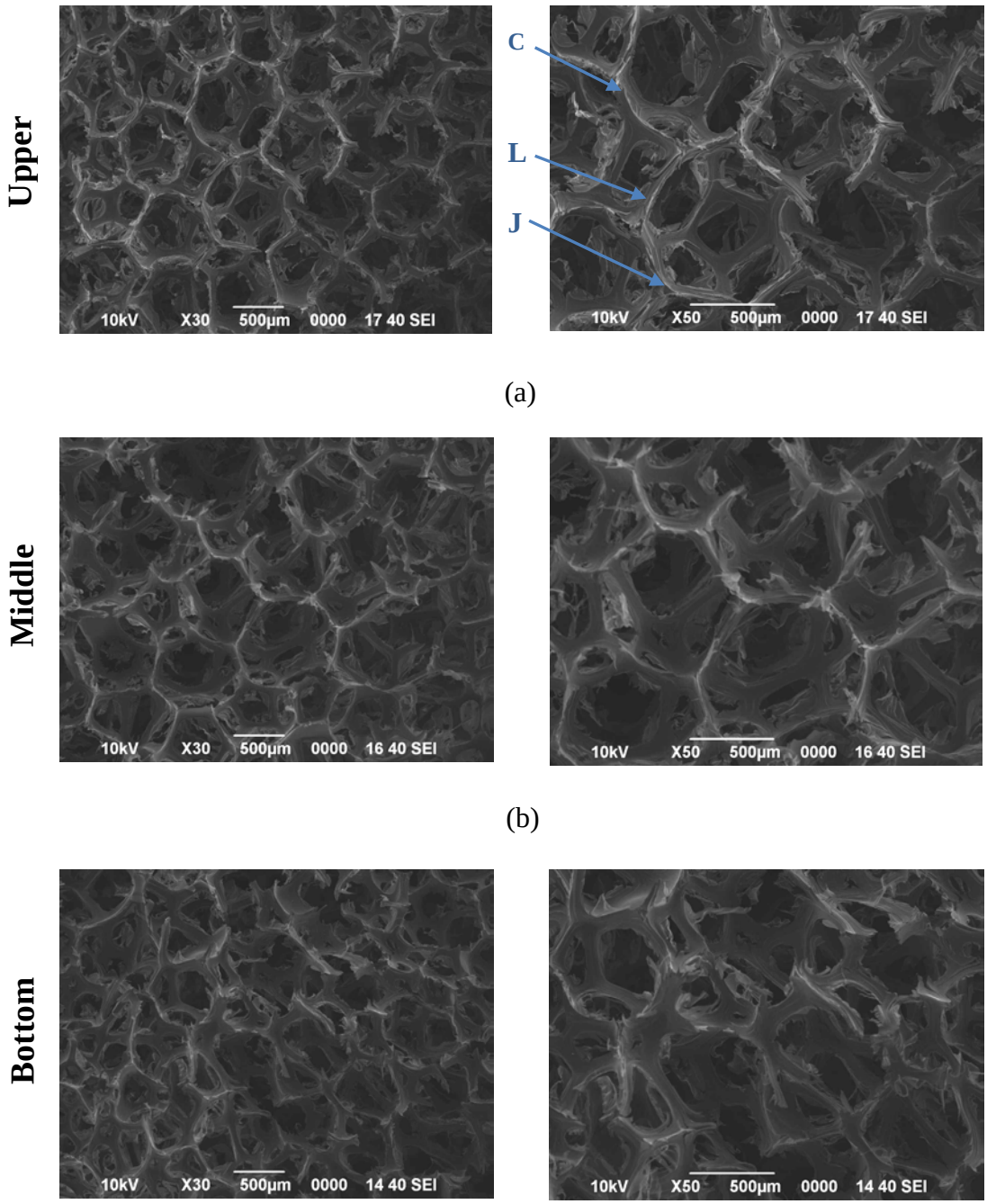

Figure 4.2 : SEM images of upper, middle, and bottom sections for the carbon foam produced at 5 atm in the z-direction.

The analysis of morphology for the carbon foam produced in the x-direction is illustrated in Figure 4.3. In this figure; upper, middle and bottom sections for the carbon foam produced are represented by a, b, and c, respectively. The SEM images of the carbon foam produced were taken for two different magnifications.

X-axis point of view

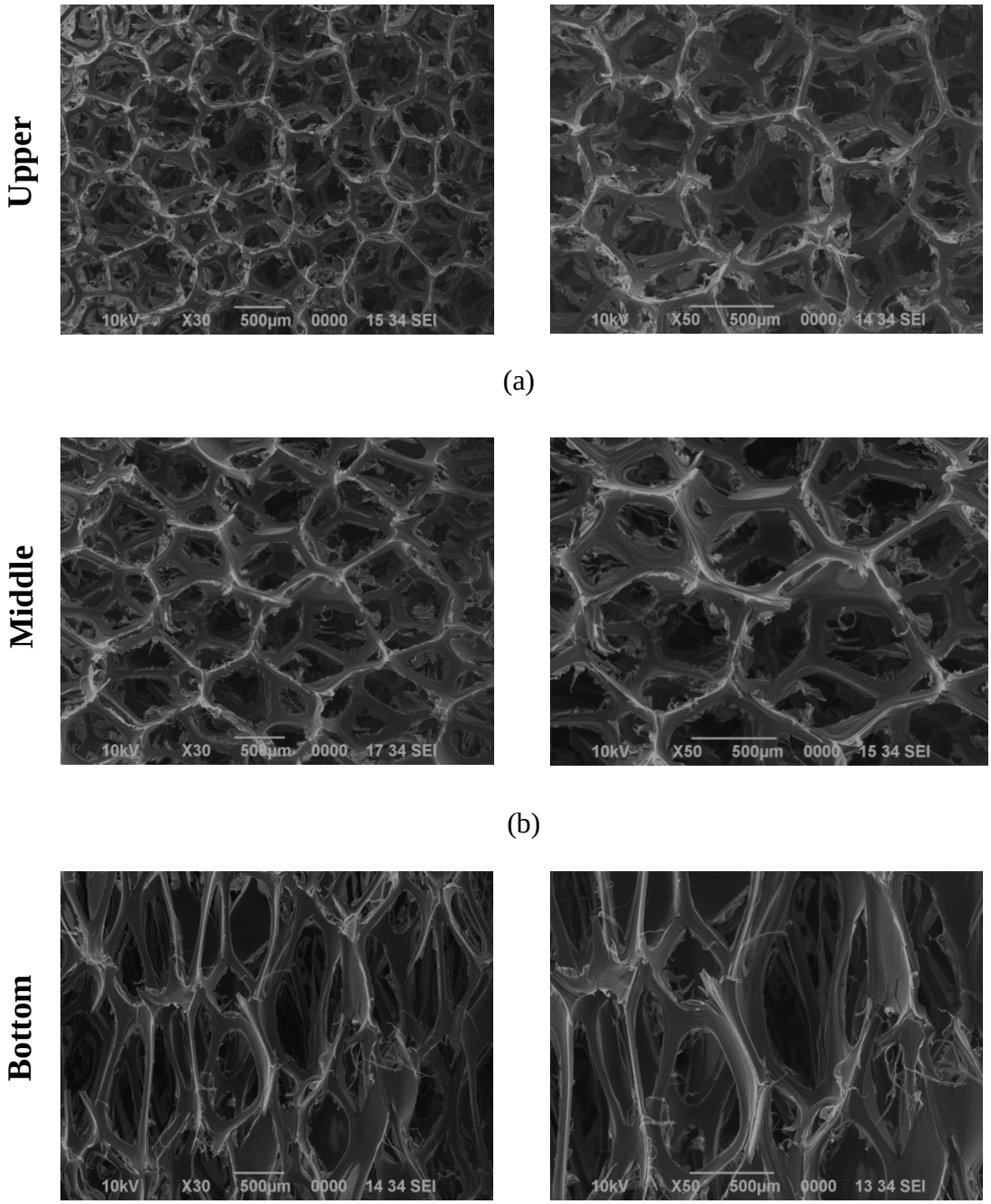

Figure 4.3 : SEM images of upper, middle, and bottom sections for the carbon foam produced at 5 atm in the x-direction.

As it can be seen from Figure 4.3c, the boundaries were not clear between the cells and also the formation of ligaments and junctions were not completed. In addition, structure similar to reticulated vitreous carbon foam (RVC) was formed and spherical cell formation was not observed. At the upper and middle sections of the carbon

foam produced, the cell boundaries were clear. This behavior reduced in the bottom section. It was evident from SEM investigation in the x-direction that the number of pores in a cell was relatively low at the bottom section compared to the upper and middle sections (parallel to z-direction view).

To sum up, it was observed from the SEM images that a more open-celled interconnected porous structure and enhanced alignment occurred at the upper section.

Figure 4.4 shows the X-ray diffraction (XRD) patterns of upper, middle and bottom sections for the carbon foam produced. The (002) peak (which are characteristic of interlayer spacing) of the upper section was narrower and more intense than the other sections. The high intensity (002) peak in the upper section could be explained by the compaction due to better alignment of pitch molecules at the cell walls, ligaments and junctions in the upper section.

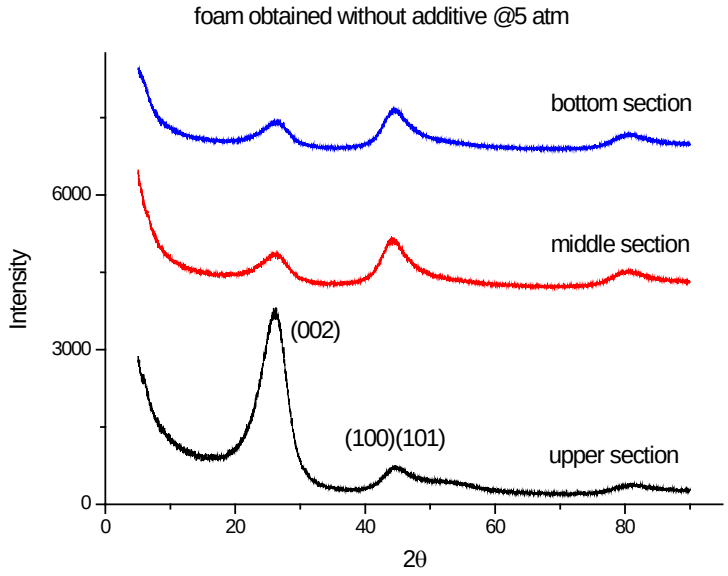

Figure 4.4 : X-ray diffraction patterns of the carbon foam produced at 5 atm.

Table 4.1 lists characteristic properties of the carbon foam produced at 5 atm (CF5-0). Skeletal density, sometimes called true density, is used to determine the volume of the sample under test. It does not include the internal voids of the material, which means that the skeletal density is usually higher than the bulk density since the latter includes the voids. The skeletal densities of the carbon foam sections were between 1.6812 g/cm^3 and 1.7735 g/cm^3. The bulk densities of the carbon foam sections were found in the range of 0.052 - 0.062 g/cm^3. According to the Equation

3.3, the total porosities were determined to be 96.91%, 96.51% and 96.75% for the upper, middle and bottom sections, respectively. The compressive strength of the carbon foam produced was 0.18 MPa.

Table 4.1 : Properties of the carbon foam produced at 5 atm.

Sample	**CF5-0**		
	Upper (U)	**Middle (M)**	**Bottom (B)**
CNF content (%)	0		
Skeletal density (g/cm^3)	1.6812	1.7735	1.7254
Bulk density (g/cm^3)	0.052	0.062	0.056
Porosity (%)	96.91	96.51	96.75
Compressive strength (MPa)	0.18		

The variation in density and porosity of carbon foams depends on the foaming mechanism. As the pitch is heated above its softening point, the releasing of volatile matter takes place. Volatile matter evaluation, viscosity and surface tension play an important role on this mechanism. Density variations in currently produced products are thought to occur between the foaming and solidification steps of the process while the foamed pitch is still in the liquid state. The liquid pitch tends to migrate due to gravity, thereby making the bottom of the foam denser than the top portion of the foam [161]. The volatile is believed to concentrate on upper section compared to bottom section which enhances the more uniform cell structures and formation of identifiable junctions and ligaments [167].

Carbon foams of higher density present much higher compressive strength. The compressive strength measured in literature are: Ultramet RVC (density 0.04 g/cm^3): 0.16– 0.763 MPa; ERG Corporation RVC of unknown (probably low) density: 0.10–0.48 MPa., Touchstone foam (density 0.16–0.50 g/cm^3): 15.2– 20.7 MPa; MER foam (density 0.016–0.62 g/cm^3): 1.7–7.0 MPa; ORNL foam (density 0.25– 0.65 g/cm^3): 1.0–3.5 MPa; Various carbon foams (density 0.25 to 0.67 g/cm^3): 2.5–18.7 MPa. [11, 98, 177-185].

The XRD results of upper, middle and bottom sections for the carbon foam produced were compiled in Figure 4.4 and Table 4.1. The (002) and (100) diffraction peak

breadths are analyzed to determine crystalline dimensions in the c- and a-directions. The sharp (100) peak can be observed in the XRD pattern when foam is graphitized [12, 161,170]. However, graphitization was not carried out in this study, therefore, the (100) peak did not appear clearly for the carbon foam produced (see Figure 4.4). The L_a values of upper, middle and bottom sections for the carbon foam produced couldn't be calculated. The interlayer spacings were calculated with Bragg Equation (Equation 3.1). The crystal sizes in c-direction were calculated by Scherer Equation (Equation 3.2). d_{002} is the distance between layers in graphite structure and is defined to be 0.3354 nm for a perfect graphite structure. The interlayer spacing (d_{002}) of carbon is traditionally used to estimate graphitization degree of carbon and in growing disorder in materials is reflected in increased values of d_{002} [111].

The interlayer spacings (d_{002}) were 0.3368, 0.3427, and 0.3434 nm for the upper, middle and bottom sections, respectively. The crystal sizes in c-direction (L_c) were found in the range of 1.4355 to 1.5910 nm for the carbon foam produced.

The interlayer spacings (d_{002}) of carbon foams were reported ranged from 0.3362 to 0.3497 nm and the crystal sizes in c-direction (L_c) of carbon foams were reported ranged from 1.2 to 20.3 nm in literature [185-189]

The general properties of various carbon foams are shown in Table D.1. The density of carbon foams produced from different precursor reported in literature are [21, 22, 25, 74, 75, 161, 166, 167, 188-191]: AR pitch 0.22-0.57 g/cm^3, coal derived pitch 0,52-0.59 g/cm^3,phenolic 0.24-0.73 g/cm^3, coal tar/carbon nanofiber 0.39-0.47 g/cm^3, mesophase-fluorine 0.51-0.55 g/cm^3, coal tar-clay 0.61-0.73 g/cm^3, mesophase pitch/carbon fiber 0.75-0.81 g/cm^3, mesophase pitch/natural graphite 0.12-0.20 g/cm^3.

4.1.2 Properties of the carbon foam produced at 10 atm

In this section the characterization results of the carbon foam produced at a pressure of 10 atm and constant temperature (600^{o}C) and rapid pressure release time of 5 sec were examined. The carbon foam was carbonized and then split into upper, middle and bottom sections. Each section was analyzed separately.

The SEM images of the carbon foam produced were taken for two different magnifications in the z- and x-directions. In these images; a, b, and c represents the upper, middle, and bottom sections for the carbon foam produced, respectively.

The SEM images for the carbon foam produced in the z-direction are shown in Figure 4.5. From the SEM images, it was clear that well formed cell structures with evenly distributed rather uniform circular pores interlinking the adjacent cells were observed at the upper section. The ligaments, junctions and walls were well developed and the cells were rather uniform in the upper section. At the middle section, the boundaries between cells became unclear compared to the upper section. The orientation and arrangement of the cells did not complete. The formation of non-spherical irregular structure increased. At the bottom section, the cell structures deteriorated such that the cells were distorted from spherical geometry. The formation of ligaments, junctions and cell walls weakened. The interconnected pores were reduced in number, and increased in size.

The SEM images of the carbon foam produced in the x-direction are shown in Figure 4.6. As seen in the SEM images, the number of pores in a cell was relatively low at the bottom section compared to the upper and middle sections. At the middle section, these textures seemed to be modified towards a comparatively more regular surface. The cell structures were formed more uniformly at the upper section compared to the middle and bottom sections.

Z-axis point of view

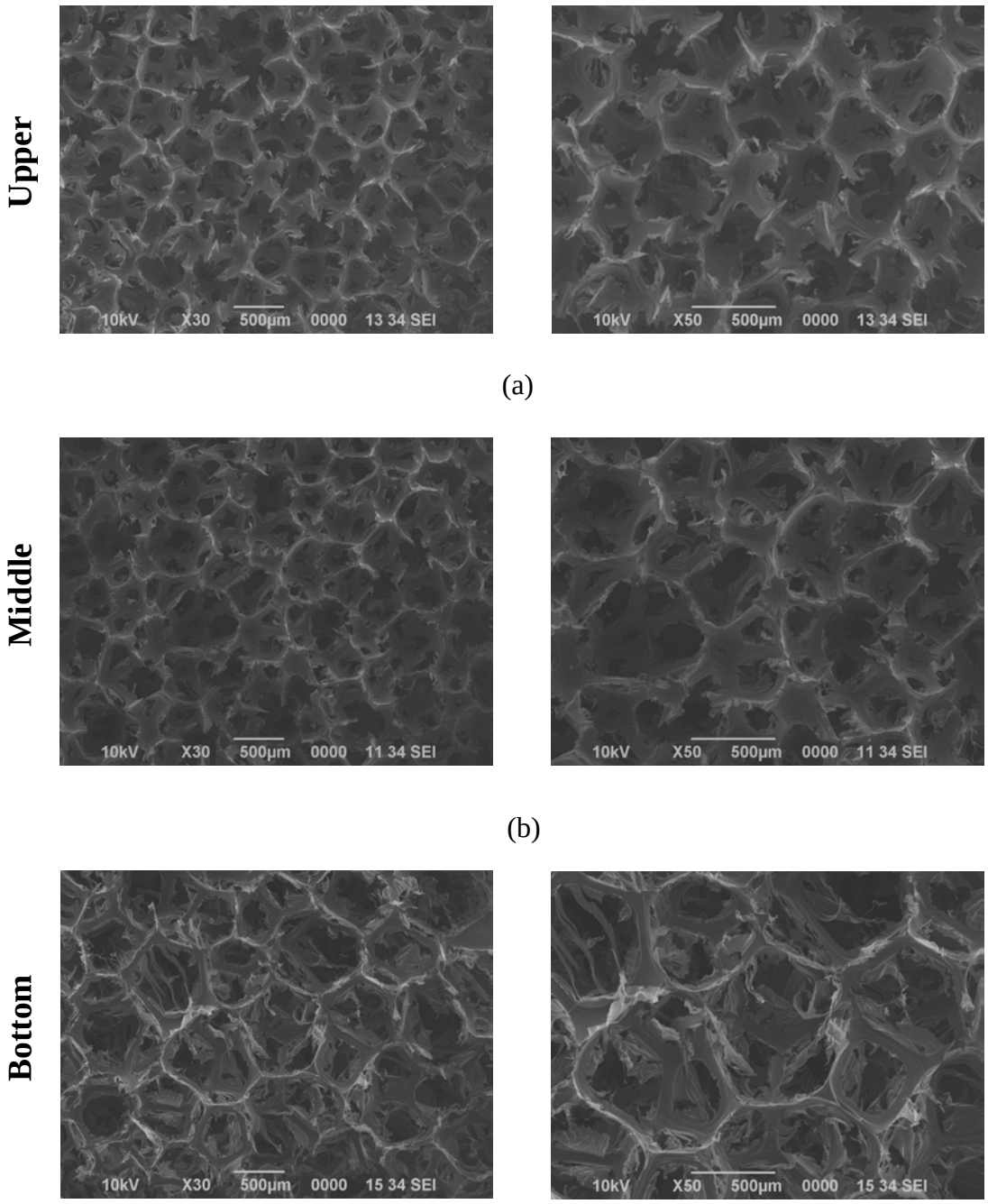

Figure 4.5 : SEM images of upper, middle, and bottom sections for the carbon foam produced at 10 atm in the z-direction.

X-axis point of view

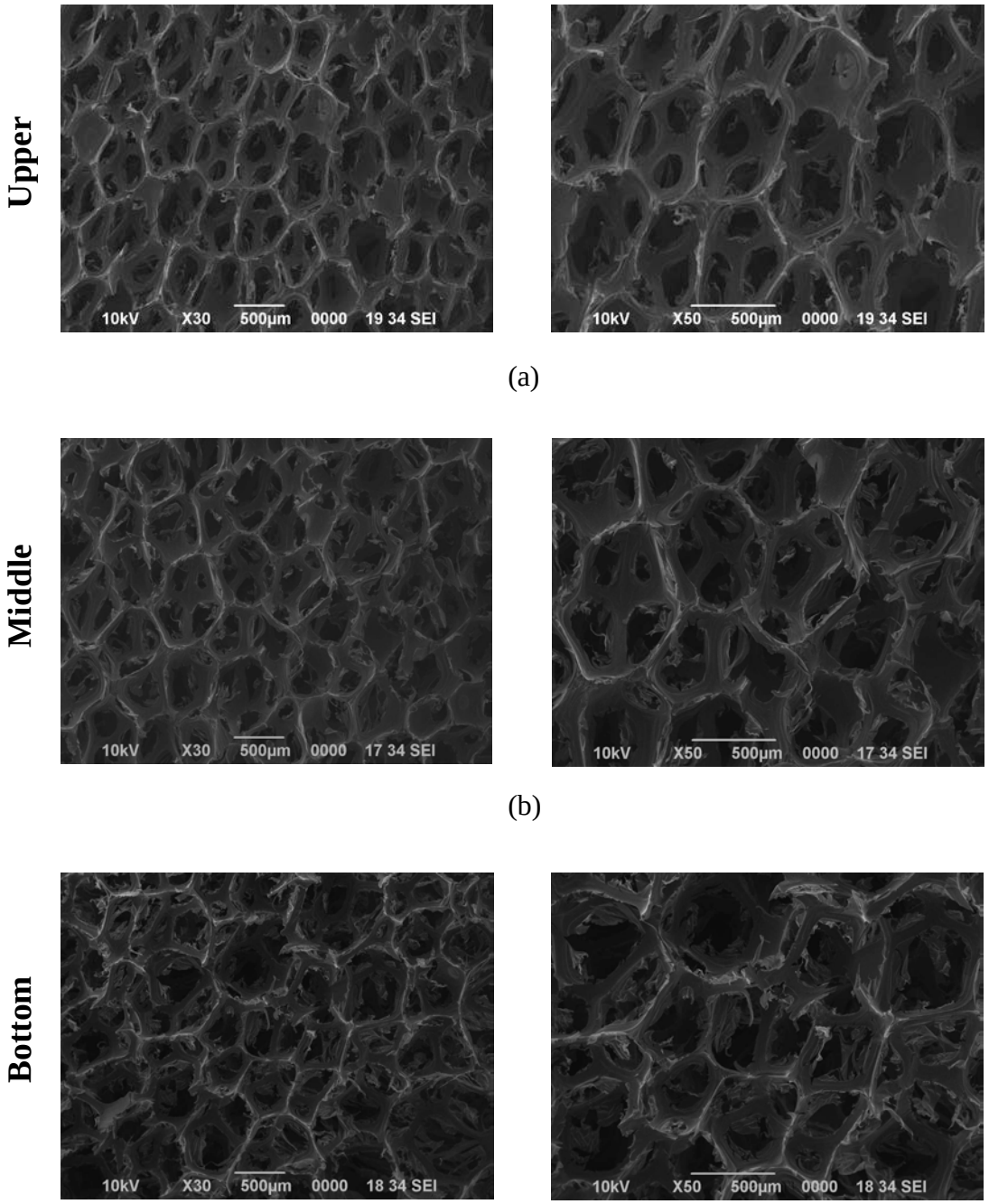

Figure 4.6 : SEM images of upper, middle, and bottom sections for the carbon foam produced at 10 atm in the x-direction.

Figure 4.7 shows XRD patterns of upper, middle and bottom sections for the carbon foam produced. At the upper section, the (002) peak was narrower. This is indicative of more ordered structure in the upper section compared to the other sections.

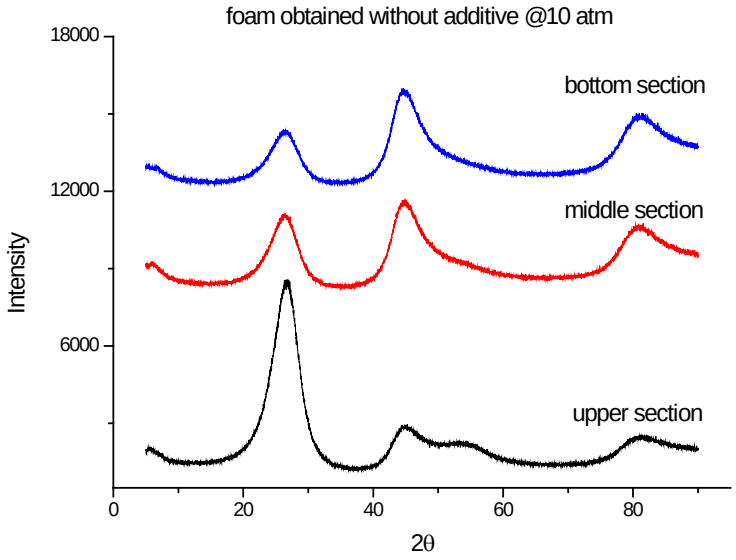

Figure 4.7 : X-ray diffraction patterns of the carbon foam produced at 10 atm.

Table 4.2 summarizes the general properties of the carbon foam produced at 10 atm (CF10-0). The skeletal densities were measured as 1.9848, 2.3660, 2.2498 g/cm^3 ; the bulk densities were determined to be 0.071, 0.112, and 0.095 g/cm^3 and the total porosities were calculated to be 96.42%, 95.27% and 95.78% for the upper, middle and bottom sections, respectively. The compressive strength of the carbon foam produced was 0.69 MPa. The values of skeletal and bulk densities were the lowest for the upper section and they were the highest for the middle section. This behavior was also obtained for the carbon foam produced at 5 atm. From this result, it may be concluded that the middle section was denser than the other sections; moreover, the upper section was the least dense for the carbon foams produced at 5 and 10 atm.

The interlayer spacings between the closed-packed hexagonal planes, d_{002}, of the carbon foam sections were between 0.3358 nm and 0.3378 nm. The crystal sizes in the c-direction (L_c) of the carbon foam sections were found in the range of 1.5893 - 1.7709 nm. The value of d_{002} of the upper section was lower due to more developed foam structure compared to the middle and bottom sections (as seen in SEM images). The crystal thickness in the c-direction (L_c) of the upper section was higher than the other sections in consistent with the formation of cell structure. The values of d_{002} increased from top to bottom; however, the values of L_c decreased from top to bottom. This trend in crystal parameters were also in accord with the carbon foam produced at 5 atm.

Table 4.2 : Properties of the carbon foam produced at 10 atm.

Sample	**CF10-0**		
	U	**M**	**B**
CNF content (%)	0		
Skeletal density (g/cm^3)	1.9848	2.3660	2.2498
Bulk density (g/cm^3)	0.071	0.112	0.095
Porosity (%)	96.42	95.27	95.78
Interlayer spacing of d_{002} (nm)	0.3358	0.3372	0.3378
L_c (nm)	1.7709	1.6760	1.5893
Compressive strength (MPa)	0.69		

The carbon foams produced at 5 and 10 atm were compared in Table 4.3. It is clearly observed that density and strength of the carbon foams increased with the increasing operating pressure. For the case of 10 atm pressure the stress created on the bubbles was higher than 5 atm pressure; therefore, mesophase molecules were more effectively aligned and oriented to form cell walls, ligaments and junctions. The porosity of the carbon foams exhibited a decreasing trend with increasing operating pressure. This is similar trend to the data reported in literature [2, 8, 12, 99, 192].

Low density foams exhibit less ordered structure in accordance with lower L_c and higher d_{002}. When carbon foams are denser, the alignment of mesophase molecules in junction becomes more oriented parallel to the surface of the bubbles [2, 8, 99, 12, 192]. The stack heights (L_c) of the carbon foam produced at 5 atm were lower than that of the carbon foam produced at 10 atm. The interlayer spacings (d_{002}) of the carbon foam produced at 5 atm were higher compared to the carbon foam produced at 10 atm. This can be explained by the less dense structure resulted weak alignment of mesophase molecules at the ligaments due to low pressure.

Table 4.3 : Comparison of properties of the carbon foams produced at 5 and 10 atm.

		Skeletal density (g/cm^3)	Bulk density (g/cm^3)	Porosity (%)	Interlayer spacing d_{002} (nm)	L_c (nm)	Compressive strength (MPa)
5 atm	Upper	1.6812	0.052	96.91	0.3368	1.5910	0.18
	Middle	1.7735	0.062	96.51	0.3427	1.4458	
	Bottom	1.7254	0.056	96.75	0.3434	1.4355	
10 atm	Upper	1.9848	0.071	96.42	0.3358	1.7709	0.69
	Middle	2.3660	0.112	95.27	0.3372	1.6760	
	Bottom	2.2498	0.095	95.78	0.3378	1.5893	

As a conclusion; the carbon foam prepared at 5 atm showed:

- lower skeletal and bulk density
- higher porosity
- higher interlayer spacing (d_{002})
- lower stack heights (L_c)
- lower compressive strength

4.2 Effect of Carbon Nanofiber Additive on the Properties of Carbon Foam

4.2.1 Properties of the carbon foam with the addition of CNF produced at 5 atm

Herringbone type carbon nanofiber was used as an additive at various weight ratios (1%, 3%, 5%, 7%, and 10 %) in order to investigate the effect of additives on the carbon foam structure and properties. A property of CNF is explained in section 2.9. Carbon foam samples were produced at a pressure of 5 atm and constant temperature of 600^{o}C and rapid pressure release time of 5 sec. The carbon foams were carbonized and then split into three sections as upper, middle and bottom. Each section was characterized separately.

The carbon foams produced were firstly characterized by taking the SEM images of the structure. The SEM images of the carbon foams produced were taken for two different magnifications. In these images; a, b, and c represents upper, middle, and bottom sections for the carbon foams produced, respectively.

The SEM images of the carbon foam with 1% CNF additive are illustrated in Figure 4.8. In this figure; the carbon foam produced was investigated in the z-direction. As can be seen from Figure 4.8, the boundaries between the cells were not clear indicating that the formation of ligaments and junctions did not complete for the middle and bottom sections. The pore and cell sizes showed a distinct difference among each other at the upper section. The formations of spherical cells did not complete in each section.

Z-axis point of view

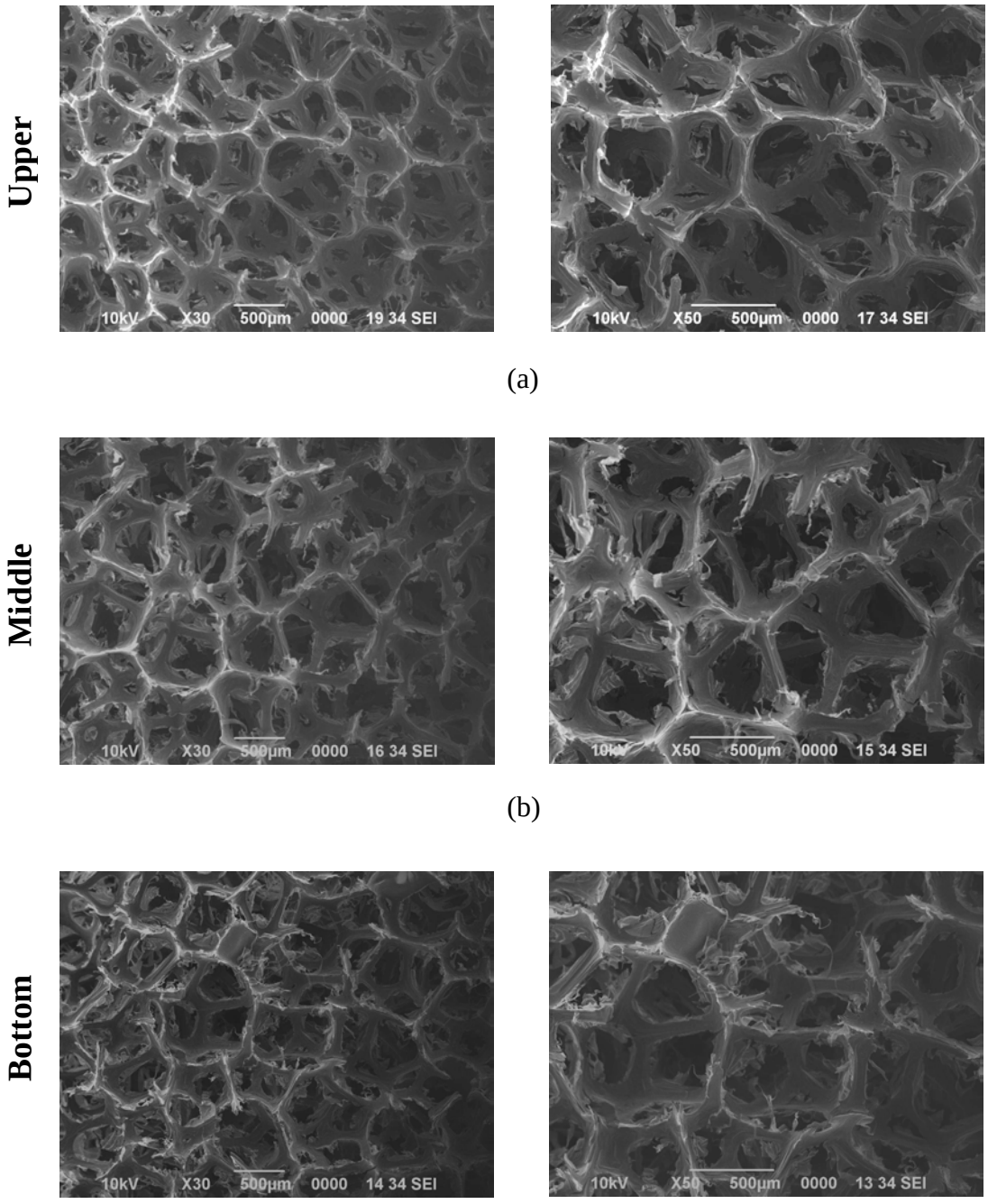

Figure 4.8 : SEM images of upper, middle, and bottom sections for the carbon foam with 1% (w/w) CNF additive produced at 5 atm in the z-direction.

The SEM images of the carbon foam with 1% CNF additive in the x-direction are shown in Figure 4.9. The spherical cell structure was mostly observed at the upper section compared to the other sections. The formation of cells and pores were mostly developed at the upper section. The cell geometries became spherical rather than

elongated spherical from bottom section to upper section. This phenomenon was good accordance with the literature explained by the bubble growth process in Section 3.3. As the temperature increases, the mesophase pitch first softens and then expand, the initial foam bubbles start to grow at upper section of the pitch and then the whole molten pitch are foamed. Therefore the bubble shape of foams shows a difference from top to bottom [17].

X-axis point of view

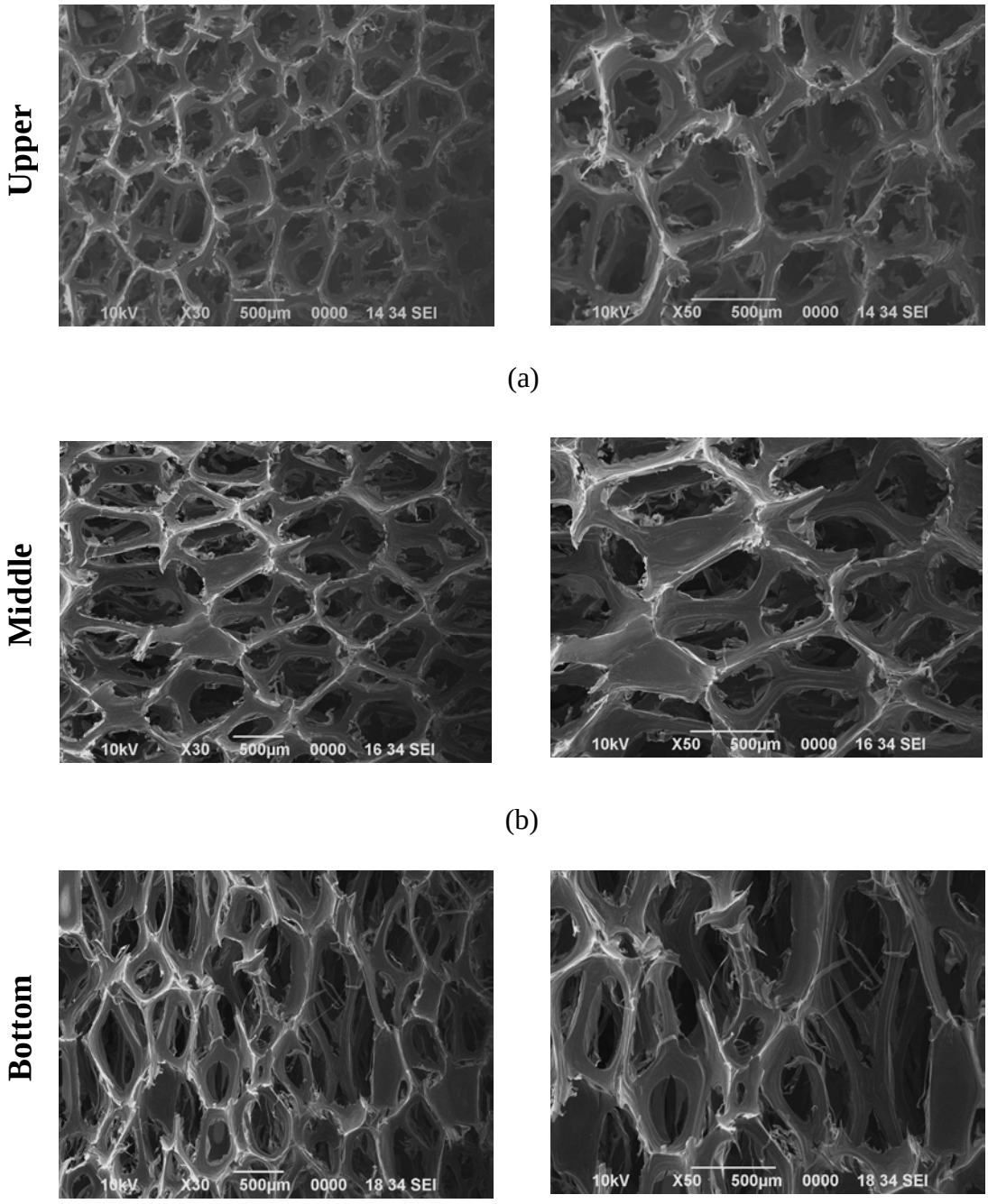

Figure 4.9 : SEM images of upper, middle, and bottom sections for the carbon foam with 1% (w/w) CNF additive produced at 5 atm in the x-direction.

X-ray diffraction spectra of the carbon foam sections are shown in Figure 4.10. The (002) peaks were obtained for all sections differing the intensity. As shown in Figure 4.4, the (002) peaks at middle and bottom sections did not appear distinctly in non-addition case. Comparison of XRD figures (Figure 4.10 and Figure 4.4) of additive

and non additive samples showed that addition of 1% CNF into pitch increased the (002) peak intensities for the middle and bottom sections, at 5 atm. This could be explained by more proper alignment of mesophase molecules in ligaments at the middle and bottom sections with the addition of 1% CNF.

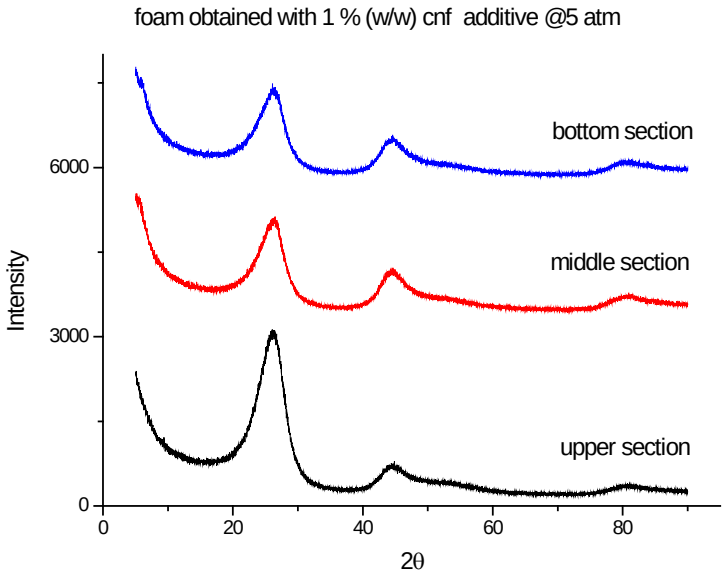

Figure 4.10 : XRD analysis of the carbon foam with 1% CNFadditive produced at 5 atm.

Table 4.4 presents the general properties of the carbon foam with 1% CNF additive produced at 5 atm (CF5-1). The skeletal and bulk densities of the upper section were lower than the other sections. The bottom and middle sections had slightly lower porosity than the upper section due to gravity induced porosity gradient that is inherent to the foaming process [169]. Also, the skeletal and bulk densities of the middle section were higher than that of the bottom section. More developed cell morphology at the middle section resulted in more dense structure compared to the bottom section. The density values of the carbon foam with the addition of 1% CNF were lower than that of the carbon foam without additive, 5 atm.

The compressive strength of the carbon foam produced was measured as 0.14 MPa. The compressive strength of the carbon foam with the addition of 1% CNF was lower than the carbon foam without additive, at 5 atm. Addition of 1% CNF into pitch caused a decrease in the strength value from 0.18 MPa to 0.14 MPa. This could be explained by the decrease in density values and weak ligament and cell formation with the addition of 1% CNF (parallel to SEM observations).

Ekşilioğlu reported that the addition of Bulgarian H_2O_2 treated isotropic pitch and graphite powder into pitch also reduced foam strength [90]. Gül also stated that the addition of polystyrene (PS) into pitch reduced the numbers of cells. Beside that the formation of ligaments and junctions could not complete in some areas with the addition of PS. In addition non porous structure was also observed. [88].

The interlayer spacings, d_{002}, and the crystal sizes in the c-direction, L_c, were 0.3374, 0.3401, and 0.3410 nm; and 1.5809, 1.5526, and 1.5498 nm as upper, middle, and bottom sections, respectively. The d_{002} values of CF5-1 increased and the L_c values of CF5-1 decreased from top to bottom depending on the cell formation and order of cells. According to the SEM observations, the foam structure became less ordered from top to bottom. The upper section was the most developed compared to the other sections and the middle section was well formed compared to the bottom section. More developed and uniform foam structure resulted in higher L_c value and lower d_{002} value.

The d_{002} values at the middle and bottom section of the carbon foam with 1% CNF additive were lower than the carbon foam without additive, at 5atm. The addition of 1% CNF into pitch caused a decrease in the d_{002} values at the middle and bottom sections. The d_{002} of the middle section decreased from 0.3427 nm to 0.3401 nm. The d_{002} of the bottom section decreased from 0.3434 nm to 0.3410 nm. These can be considered as indications for the enhancing alignment and arrangement of rod like mesophase molecules at the ligaments with the addition of CNF. Dispersion of CNF increased viscosity of the mesophase pitch. This led to complex morphological changes including changes in cell interlinking, porosity, and spherical geometry of cells [21]. The d_{002} value of the upper section was also changed with the addition of CNF. The d_{002} value of the upper section for the carbon foam with 1% CNF additive was higher than the carbon foam without additive, at 5 atm. Compared to the carbon foam without additive, the increase in d_{002} value of the upper section could be explained by loss of spherical geometry of cells which resulted in less ordered structure at the upper section.

The L_c values of the middle and bottom sections increased with the addition of 1% CNF compared to non-additive case, at 5 atm. However, the L_c value of the upper section for the carbon foam with the addition of 1% CNF was lower compared to the carbon foam without additive, at 5 atm. This was also in accord with the modification of carbon foam structure with the addition of CNF.

Table 4.4 : Properties of the carbon foam with 1% CNF additive produced at 5 atm.

Sample	**CF5-1**		
	U	**M**	**B**
CNF content (%)	1		
Skeletal density (g/cm^3)	1.6799	1.7395	1.7114
Bulk density (g/cm^3)	0.048	0.057	0.052
Porosity (%)	97.16	96.73	96.99
Compressive strength (MPa)	0.14		

The SEM images of the carbon foam with 3% CNF additive in the z-direction are given in Figure 4.11. From the SEM images in Figure 4.11; at the upper section, the cell formations were mostly developed; however, ligaments, junctions and walls were not formed distinctly. At the middle section, spherical cell formation reduced. The cell boundaries were unclear in some areas. At the bottom section, cells were distorted from spherical geometry. Ligaments, junctions and wall formation weakened. Pores increased in size.

Z-axis point of view

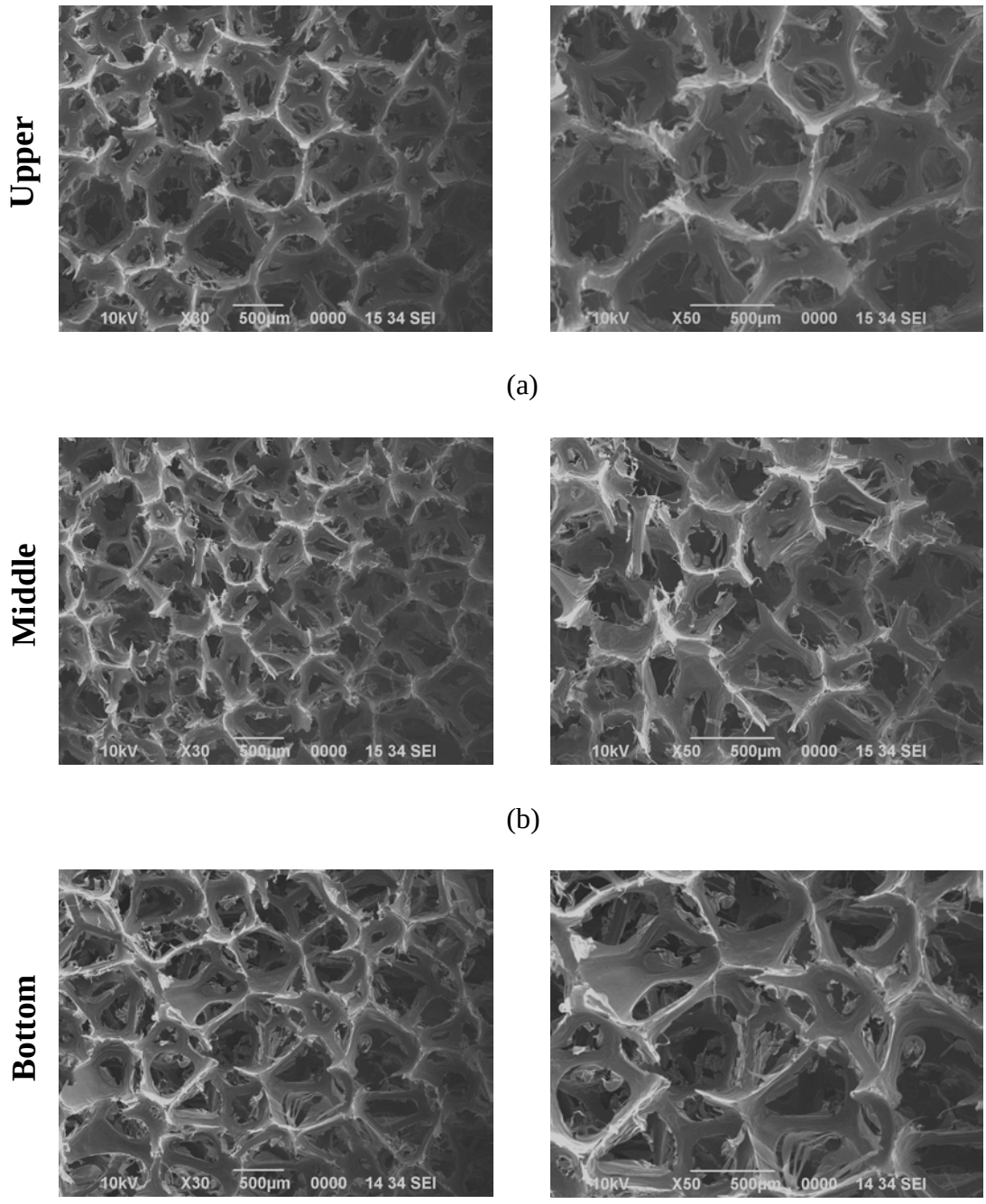

Figure 4.11 : SEM images of upper, middle, bottom sections for the carbon foam with 3% (w/w) CNF additive produced at 5 atm in the z-direction.

Figure 4.12 shows the SEM images of the carbon foam with 3% CNF additive in the x-direction. It is evident from Figure 4.12c that the formation of cells was not well developed and there were non-spherical cell formation at the bottom section. The non-uniform and less ordered foam structure was observed. At the bottom section,

stress is not enough to form the cells and the structure between the cells due to the low volatile amount [169]. In other words alignment of the rod-like mesophase molecules during the bubble growth was not effective. As it can be seen from Figure 4.12b and Figure 4.12a, the upper section showed similar geometry and structure to middle section. Graphene sheet (hexagonal) like geometry was observed.

X-axis point of view

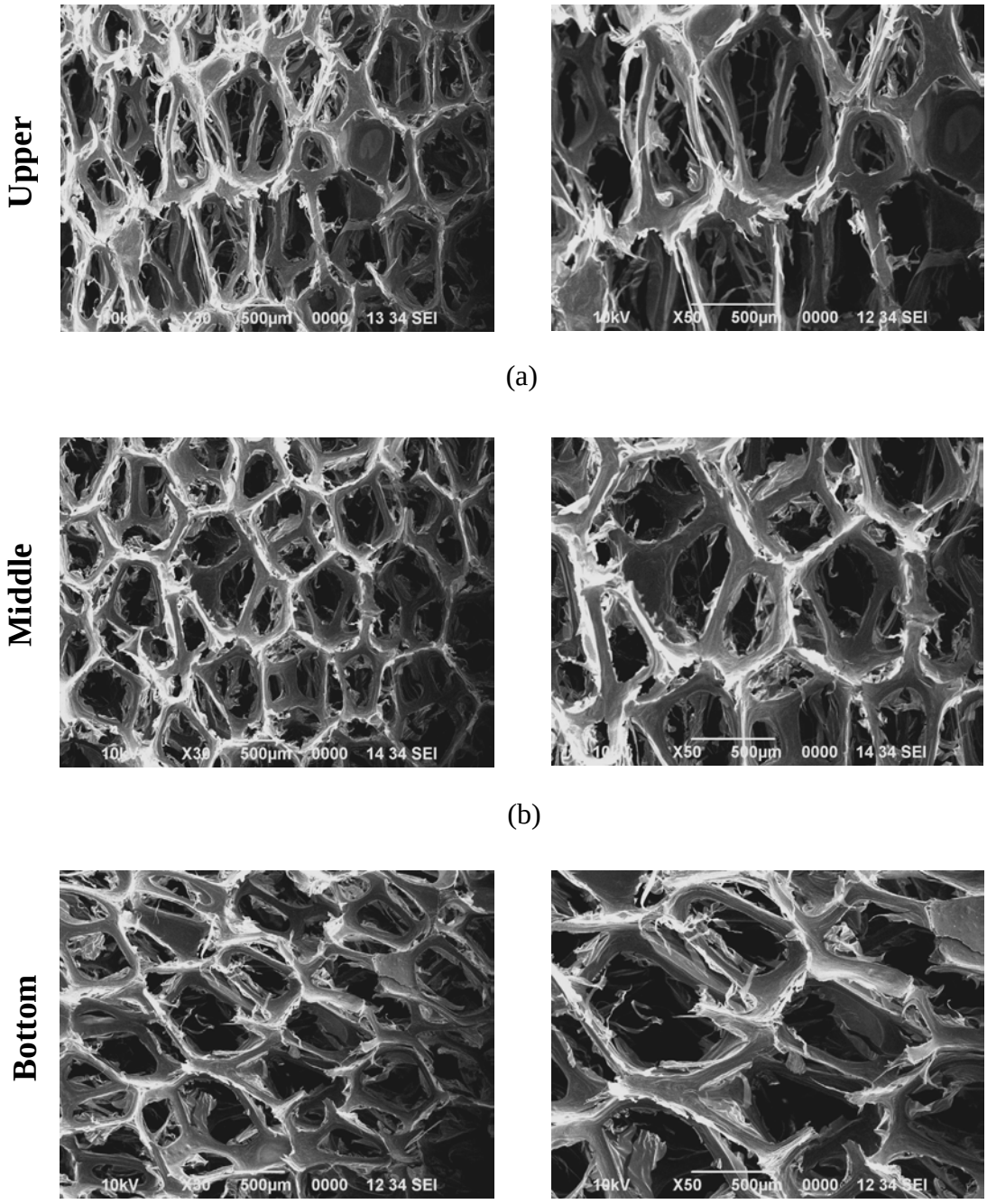

Figure 4.12: SEM images of upper, middle, and bottom sections for the carbon foam with 3% (w/w) CNF additive produced at 5 atm in the x-direction.

Figure 4.13 shows the XRD analysis results of the carbon foam with 3% CNF additive. The (002) peaks appeared for all sections. The intensities of the (002) peaks were different than each other. These observations indicated non-uniform alignment of mesophase molecules in ligaments with the addition of 3% CNF. The intensities

of (002) peaks decreased compared to the carbon foam with 1% CNF additive, at 5 atm. The decrease was originated from less ordered alignment of mesophase molecules due to deterioration in the foam formation.

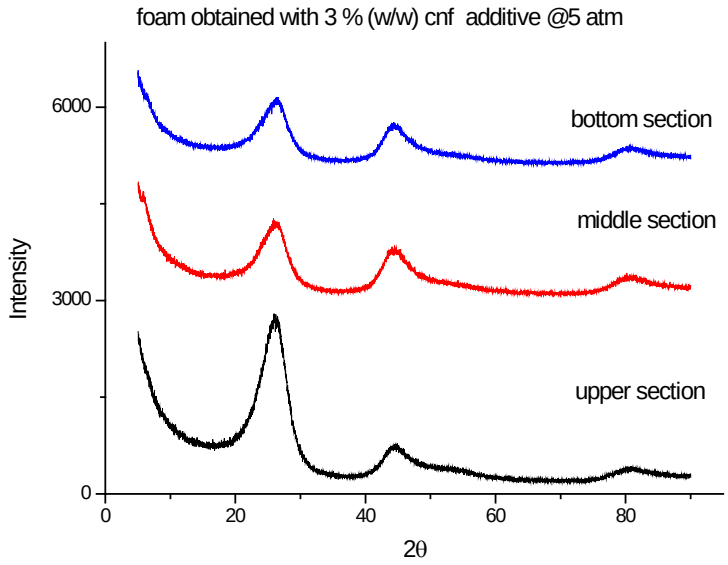

Figure 4.13 : XRD analysis of the carbon foam with 3% CNF additive produced at 5 atm.

The general properties of the carbon foam obtained with 3% CNF additive (CF5-3) are shown in Table 4.5. The skeletal densities were 1.6669, 1.7124, and 1.6803 g/cm^3 for upper, middle and bottom sections, respectively. The bulk densities of the carbon foam sections varied between 0.044-0.047 g/cm^3. The upper section of the carbon foam was the least dense compared to other sections. The middle section of foam was denser than the bottom section. This found in density behavior was also obtained for the carbon foam with the addition of 1% CNF previously. The density values of the carbon foam sections with the addition of 3% CNF were lower than that of the carbon foam with the addition of 1% CNF. The compressive strength of the carbon foam produced was measured as 0.09 MPa and it was lower compared to the carbon foam with the addiyion of 1% CNF. Addition of 3% CNF into pitch reduced the strength of the carbon foam from 0.14 MPa to 0.09 MPa. Weak cell, ligament and wall formation and increasing non-uniform structure caused a decrease in the carbon foam strength.

The interlayer spacings, d_{002}, and the crystal sizes in the c-direction, L_c, were 0.3378, 0.3417, and 0.3419 nm; and 1.5707, 1.5404, and 1.5359 nm as upper, middle, and

bottom sections, respectively. The d_{002} values of CF5-3 increased and the L_c values of CF5-3 decreased from top to bottom in accordance with the cell structure.

The d_{002} values for each section of the carbon foam with 3% CNF additive were higher than that of the carbon foam with 1% CNF additive, at 5atm. These can be considered as indications of the weak alignment and arrangement of rod like mesophase molecules at the ligaments with the addition of 3% CNF. The L_c values decreased with the addition of 3% CNF compared to the carbon foam with the addition of 1% CNF (parallel to foam structure).

Table 4.5 : Properties of the carbon foam with 3% CNF additive produced at 5 atm.

Sample	**CF5-3**		
	U	**M**	**B**
CNF content (%)	3		
Skeletal density (g/cm^3)	1.6669	1.7124	1.6803
Bulk density (g/cm^3)	0.044	0.047	0.045
Porosity (%)	97.36	97.26	97.32
Interlayer spacing of d_{002} (nm)	0.3378	0.3417	0.3419
L_c (nm)	1.5707	1.5404	1.5359
Compressive strength (MPa)	0.09		

Figure 4.14 and Figure 4.15 show the SEM images of the carbon foam with 5% CNF additive in the z- and x-directions, respectively. The shapes of cells with 5% CNF additive were far beyond spherical geometry compared to the carbon foam with 1% and 3% CNF additive, 5 atm. As it can be observed from Figure 4.14a; wall formations did not fully constitute in the upper section. The pore shapes were irregular and pore sizes were bigger compared to 1% and 3% additives samples. As it can be seen from Figure 4.14b; cells in the middle section were not developed well. At the bottom section, ligaments, junctions and cell wall formation could not be observed. The bottom section structure deteriorated in terms of ligament and cell formation compared to upper and middle sections.

Figure 4.15 showed that ligaments between the cells were significantly thinner compared to 1% and 3% CNF additives samples. Boundaries between the cells were unclear.

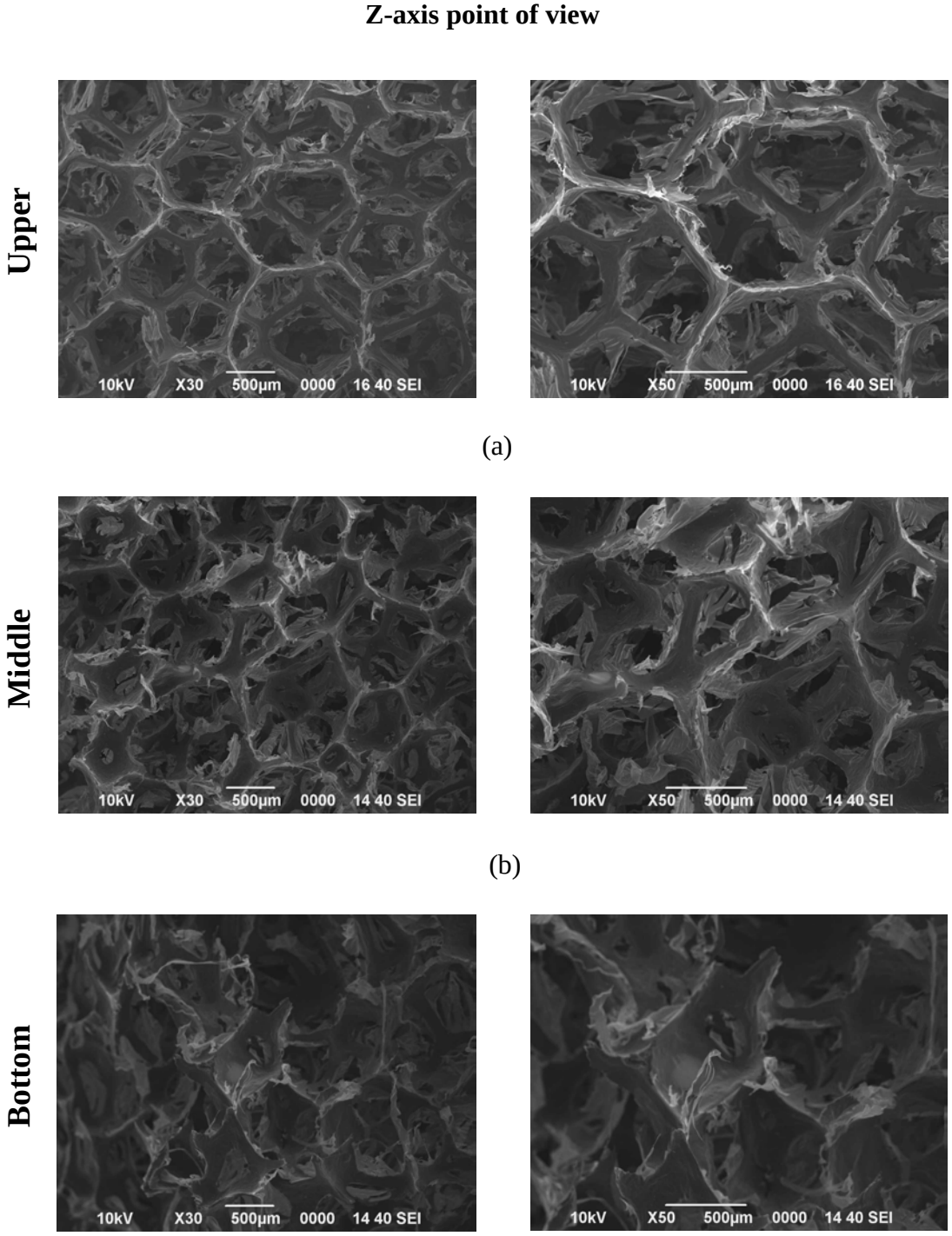

Figure 4.14 : SEM images of upper, middle, and bottom sections for the carbon foam with 5% (w/w) CNF additive produced at 5 atm in the z-direction.

X-axis point of view

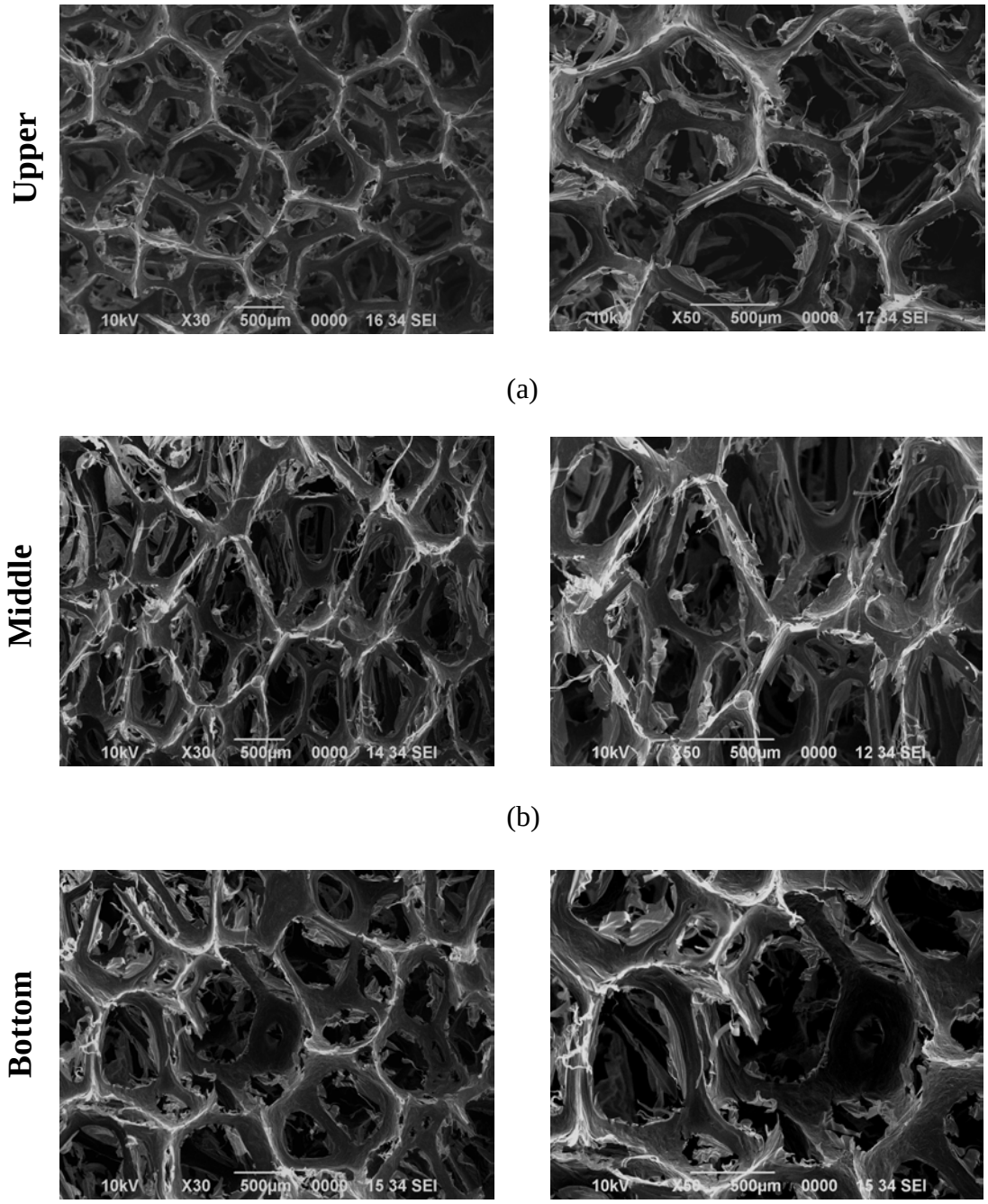

Figure 4.15 : SEM images of upper, middle, and bottom sections for the carbon foam with 5% (w/w) CNF additive produced at 5 atm in the x-direction.

Figure 4.16 shows the XRD analysis results of the carbon foam with 5% CNF additive. As it can be seen from Figure 4.16; XRD patterns and the (002) peak intensities for each section of the foam sample were similar to each other. The

intensities of (002) peaks of upper section for the carbon foam with 5% CNF additive were lower than carbon foam with 1% and 3 % CNF additive. The intensities of (002) peaks of the middle and bottom sections for the 5% CNF additive were higher than 1% and 3 % CNF additive.

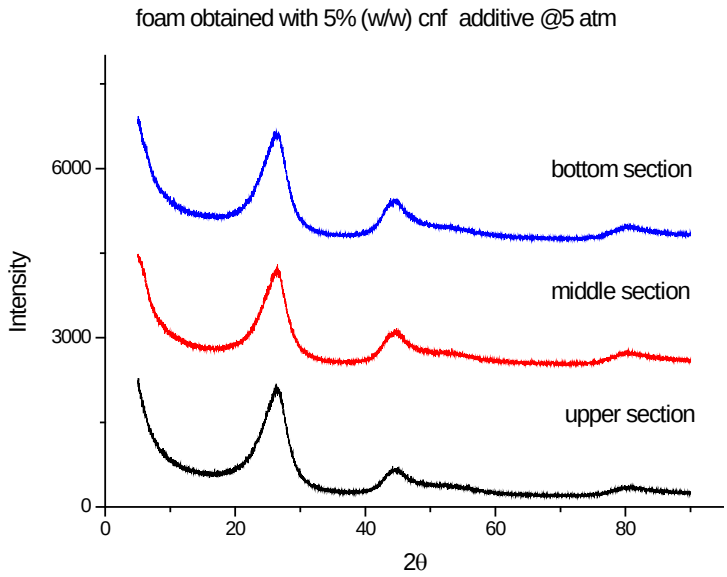

Figure 4.16 : XRD analysis of the carbon foam with 5% CNF additive produced at 5 atm.

Characteristic properties of the carbon foam with the addition of 5% CNF (CF5-5) can be seen in Table 4.6. The skeletal densities were 1.6446, 1.6938, 1.6795 g/cm^3 for the upper, middle, and bottom sections, respectively. At the upper section the bulk density of the foam was 0.043 g/cm^3, and porosity was 97.40%. At the middle section the bulk density of the foam was 0.046 g/cm^3, and porosity was 97.28%. At the bottom section the bulk density of the foam was 0.044 g/cm^3, and porosity was 97.38%. The density values of upper section were lower than the other sections. The middle section of the carbon foam was denser compared to upper and bottom sections. This trend in density was also obtained previously. The density values of the carbon foam with the addition of 5% CNF were lower than that of the carbon foam with the addition of 3% CNF.

The compressive strength of CF5-5 foam was 0.06 MPa. The strength of foam with 3% CNF additive was higher than foam with 5% CNF additive. Addition of 5% CNF decreased the strength of foam from 0.14 MPa to 0.06 MPa. The strength of foam reduced due to weaker cell formations and less dense structure with 5% CNF additive compared to the carbon foam with 3% CNF additive.

The d_{002} values of the foam sections varied between 0.3392-0.3398 nm. The L_c values of the foam sections varied between 1.5651-1.5604 nm. The d_{002} values of CF5-5 increased and the L_c values of CF5-5 decreased from top to bottom in accordance with the cell structure. The cell structures distorted at middle and bottom sections compared to the upper section, therefore, the alignment of mesophase molecules at the ligaments weakened. This caused a decrease in the L_c values and a increase in the d_{002} values from top to bottom.

The upper section of the carbon foam with the addition of 5% CNF had higher d_{002} value compared to upper section of CF5-3. This could be showed that weak alignment of mesophase molecules at the upper section with the addition of 5% CNF. The d_{002} values of the middle and bottom sections were lower compared to CF5-3 foam. Compared to the carbon foam with the addition of 3% CNF, the alignment of mesophase molecules at the middle and bottom sections were improved with the addition of 5% CNF.

Table 4.6 : Properties of carbon foam with 5 % CNF additive produced at 5 atm.

Sample	**CF5-5**		
	U	**M**	**B**
CNF content (%)	5		
Skeletal density (g/cm^3)	1.6446	1.6938	1.6795
Bulk density (g/cm^3)	0.043	0.046	0.044
Porosity (%)	97.40	97.28	97.38
Compressive strength (MPa)	0.06		

Figure 4.17 and Figure 4.18 are the SEM images of the samples with 7% CNF additive in the z- and x-directions, respectively. As it can be seen from Figure 4.17 and Figure 4.18; at the upper section, the structure of the foam more developed in terms of cell and ligament formation compared to the other sections. The foam structure was more deformed at the middle and bottom sections.

Z-axis point of view

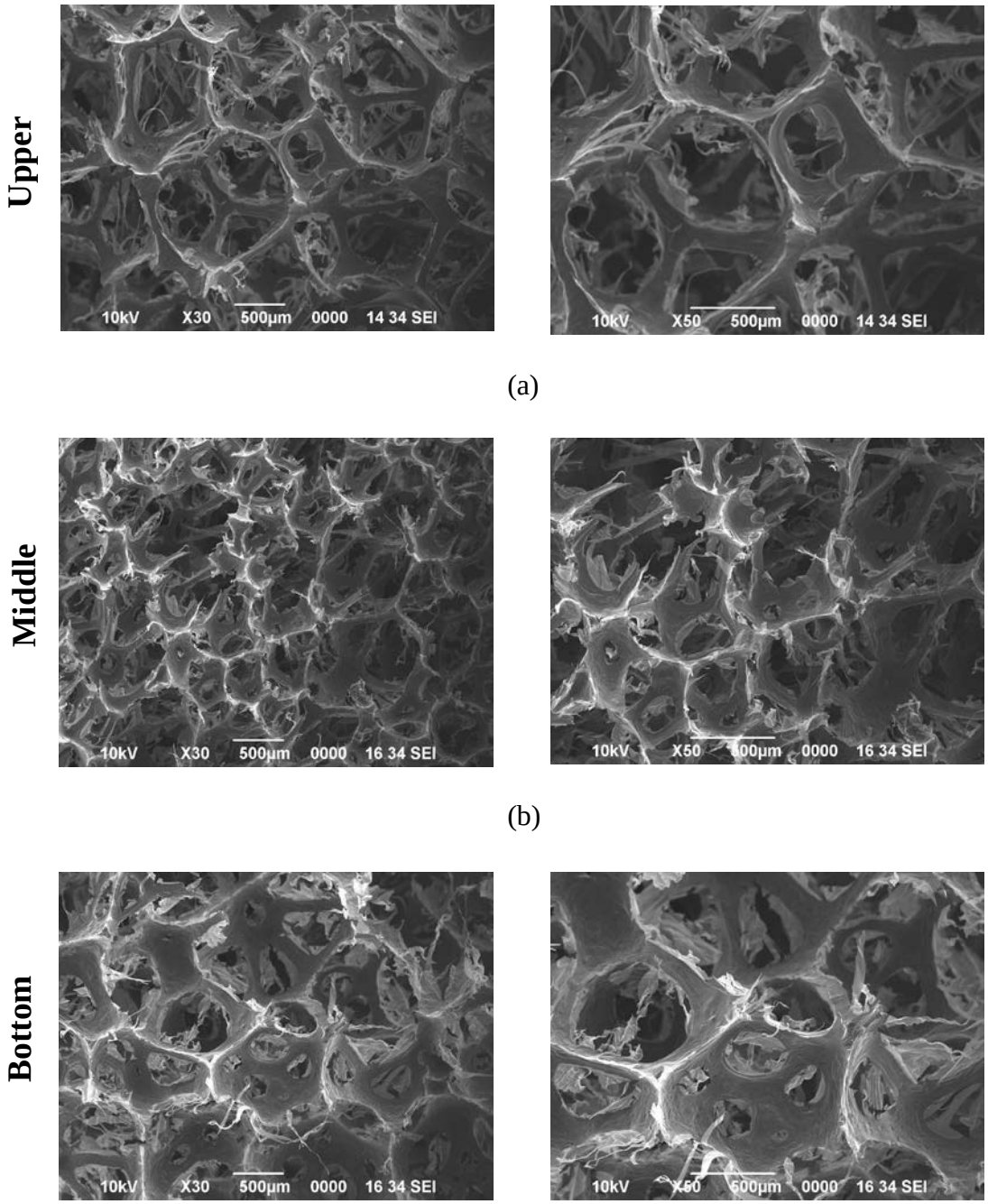

Figure 4.17 : SEM images of upper, middle, and bottom sections for the carbon foam with 7% (w/w) CNF additive produced at 5 atm in the z-direction.

X-axis point of view

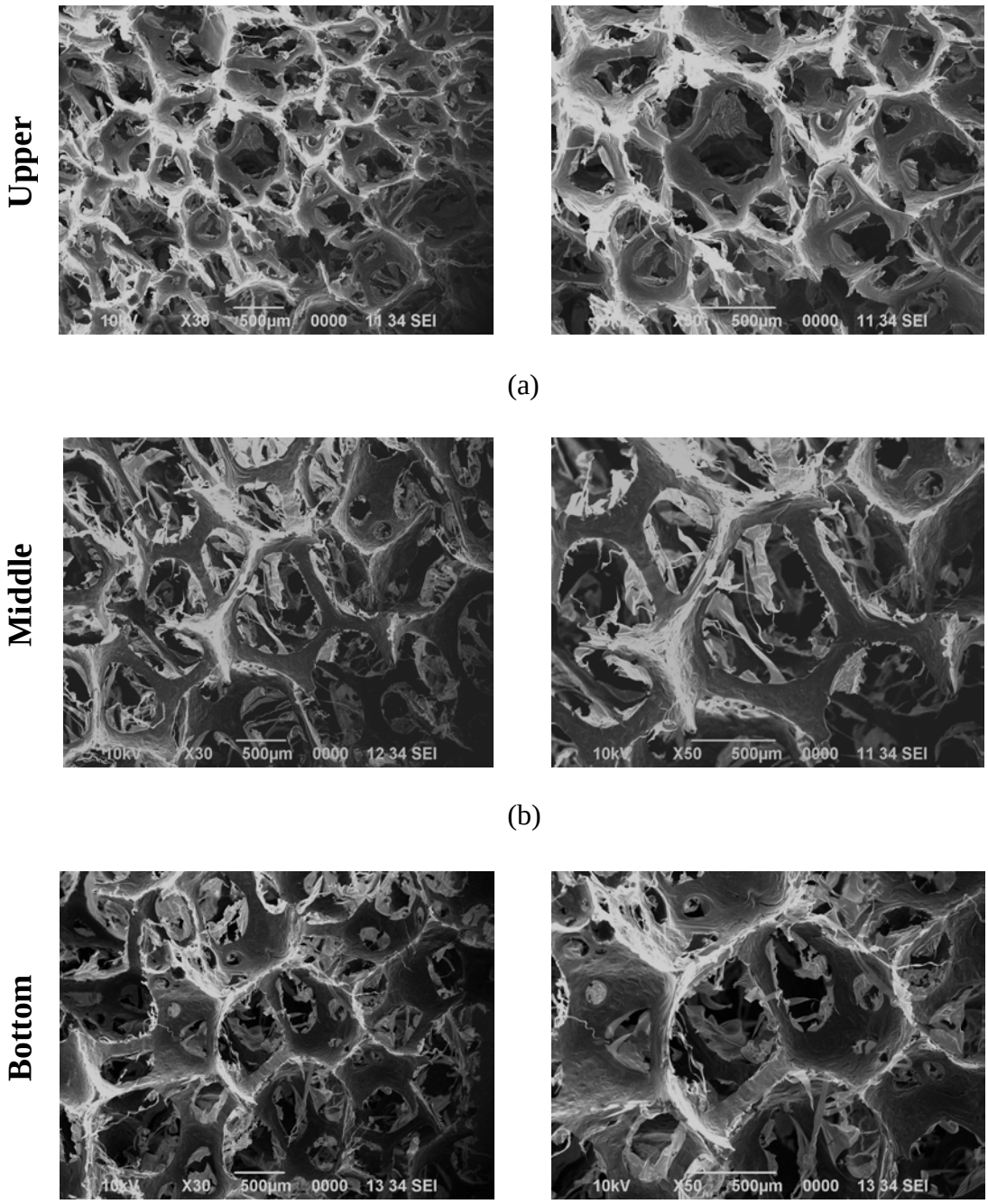

Figure 4.18 : SEM images of upper, middle, and bottom sections for the carbon foam with 7% (w/w) CNF additive produced at 5 atm in the x-direction.

X-ray diffraction patterns of the carbon foam sections are presented in Figure 4.19. The XRD patterns for each section were almost identical. The intensities of (002) peaks of the carbon foam sections were lower compared to the carbon foam with the addition of 5% CNF. This could be explained by weak cell structure of the foam as shown in Figure 4.17 and 4.18.

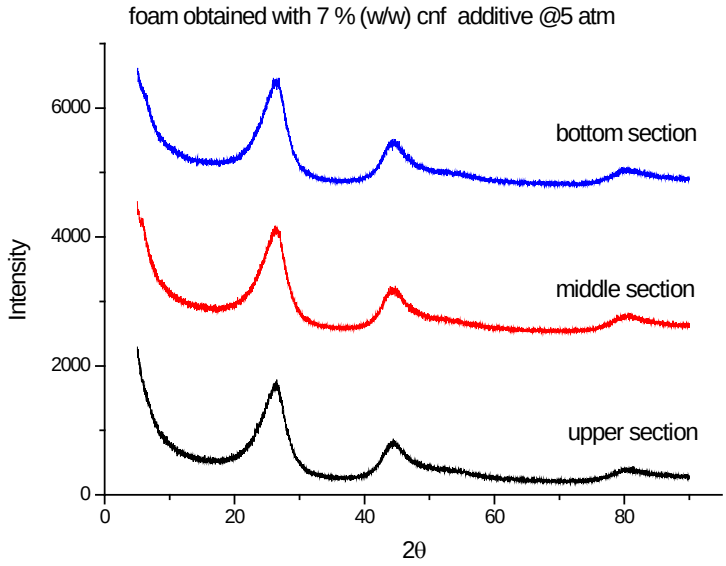

Figure 4.19 : XRD analysis of the carbon foam with 7% CNF additive produced at 5 atm.

The other characterization results of the carbon foam with 7% CNF additive (CF5-7) were also compiled in Table 4.7. At the upper, middle and bottom sections; skeletal and bulk density and porosity values were 1.6385 g/cm^3, 0.042 g/cm^3, and 97.44%; 1.6809 g/cm^3, 0.045 g/cm^3, and 97.32%; 1.6716 g/cm^3, 0.043 g/cm^3, and 97.43%, respectively. The middle section was denser than the other sections. The density values at the upper section were lower compared to the middle and bottom sections. This behavior was explained by foaming mechanism previously. The density values of the carbon foam with the addition of 7% CNF were lower than that of the carbon foam with the addition of 5% CNF.

The compressive strength of foam is 0.04 MPa. Addition of 7% CNF into pitch reduced the carbon foam strength compared to the carbon foam with the addition of 5% CNF. The cell formation for the carbon foam with the addition of 7% CNF was weaker than the carbon foam with the addition of 5% CNF (as explained in the SEM images before).

The d_{002} values of the foam were 0.3399, 0.3400, and 0.3401 nm; the L_c values of the foam were 1.5552, 1.5531, and 1.5511 nm for the upper, middle and bottom section, respectively. The d_{002} and L_c values were almost identical for each section.

The d_{002} values of CF5-7 were higher than that of CF5-5. The L_c values of CF5-7 were lower than that of CF5-5. Compared to the carbon foam with the addition of 5% CNF, weak cell formation in the carbon foam with the addition of 7% CNF resulted in lower alignment of mesophase molecules. This caused a decrease in the L_c values and increased in the d_{002} values.

Table 4.7 : Properties of the carbon foam with 7% CNF additive produced at 5 atm.

Sample	**CF5-7**		
	U	**M**	**B**
CNF content (%)	7		
Skeletal density (g/cm^3)	1.6385	1.6809	1.6716
Bulk density (g/cm^3)	0.042	0.045	0.043
Porosity (%)	97.44	97.32	97.43
Compressive strength (MPa)	0.04		

The SEM images of the carbon foam with 10% CNF additive in the z- and x-directions are given in Figure 4.20 and Figure 4.21, respectively.

In the z-direction; non-formed cell structures were observed in the upper section of the carbon foam. This non-formed cell structure continued in the middle and bottom sections.

In the x-direction; cell structures occurred at the upper and middle sections. However, foam structure was not observed at the bottom section. Cell and pore shapes in the upper section were different than the middle section.

The structures of the sample in the z-direction were completely different than the structure of the sample in the x-direction. Although cells could not occur in the z-direction, the sample had some cells at the upper and middle sections in the x-direction. Foam structure was non-homogenous. The difference in the structure was much more obvious compared to CF5-1, CF5-3, CF5-5, and CF5-7.

Z-axis point of view

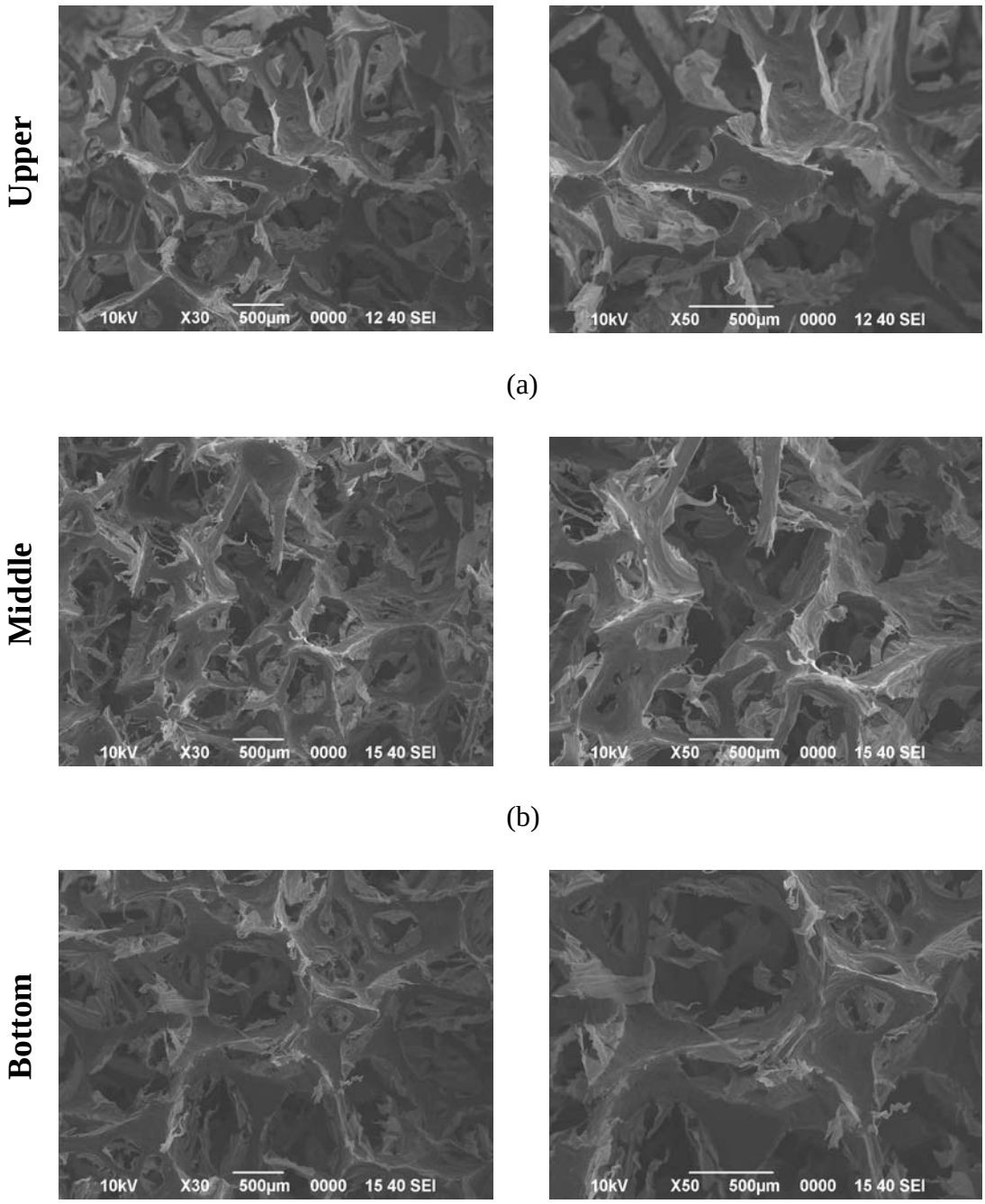

Figure 4.20 : SEM images of upper, middle, and bottom sections for the carbon foam with 10% (w/w) CNF additive produced at 5 atm in the z-direction.

X-axis point of view

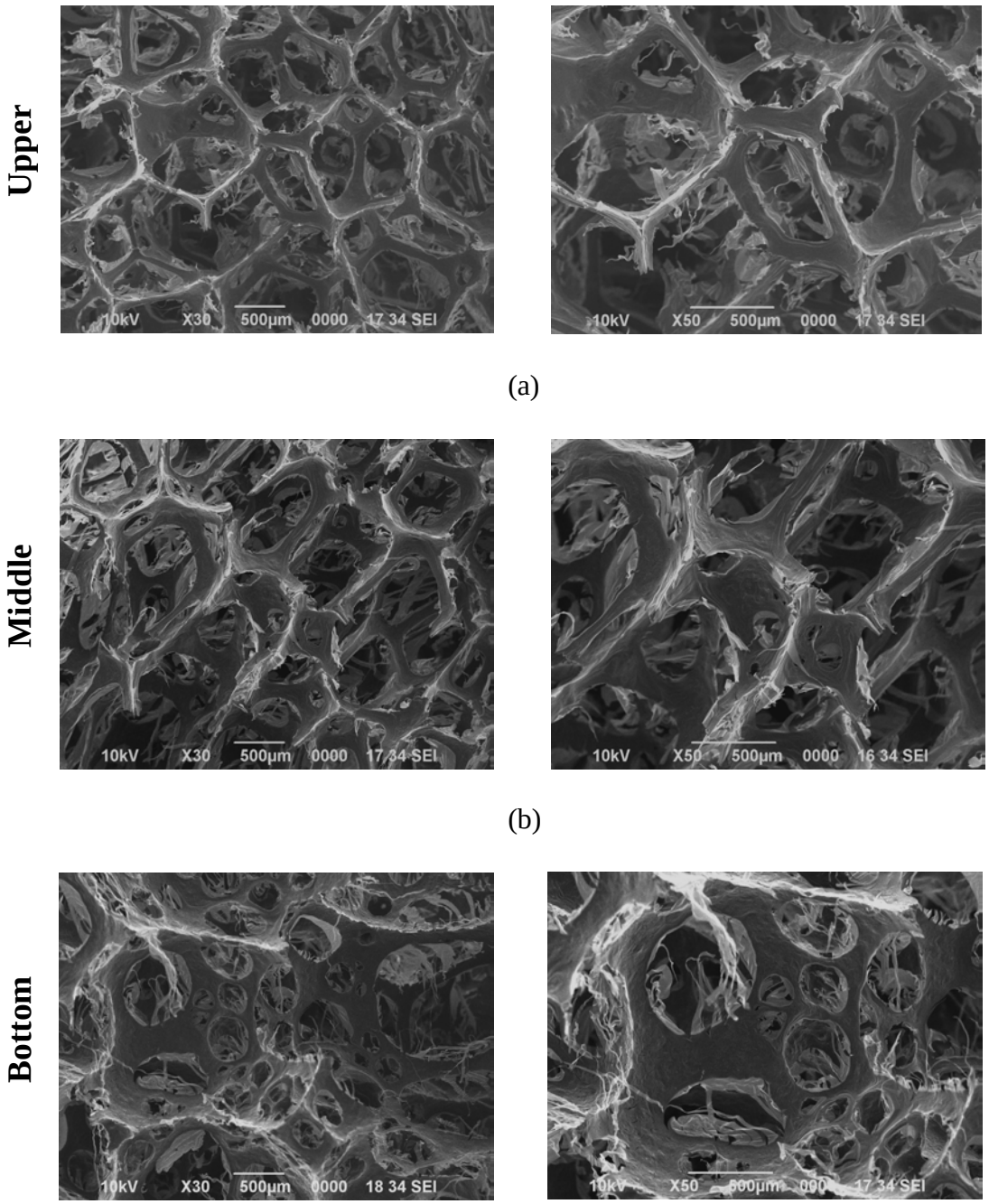

Figure 4.21 : SEM images of upper, middle, and bottom sections for the carbon foam with 10% (w/w) CNF additive produced at 5 atm in the x-direction.

The XRD patterns of each section of the carbon foam obtained with 10% CNF additive are given in Figure 4.22. The XRD patterns of each section were similar. The (002) peaks in each section had very low intensities and they were wide compared to the other additive samples. The 10% CNF additive made the foam weaker in terms of alignment of mesophase molecules.

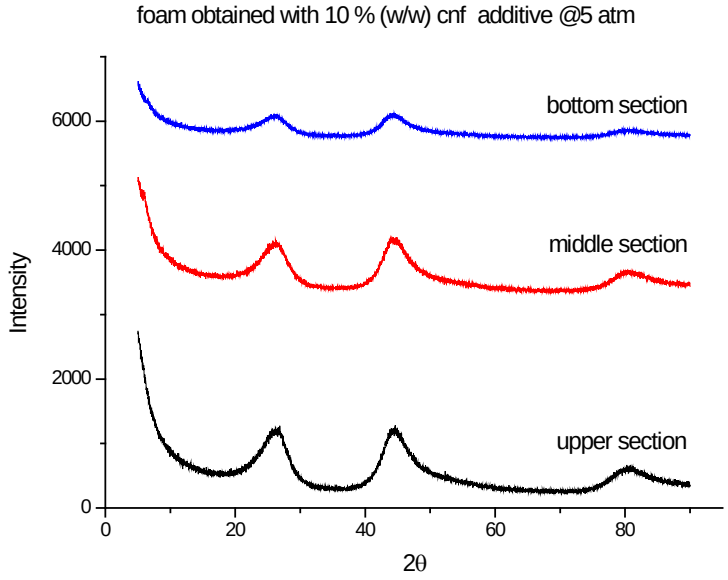

Figure 4.22 : XRD analysis of the carbon foam with 10% CNF additive produced at 5 atm.

The other characterization results of the carbon foam with 10% CNF additive (CF5-10) were also compiled in Table 4.8. The skeletal densities of sections of the carbon foam (upper, middle, and bottom) were 1.5989, 1.6373, 1.6235 g/cm^3, respectively. At the upper section the bulk density of the carbon foam was 0.038 g/cm^3, and porosity was 97.62%. At the middle section the bulk density of the carbon foam was 0.042 g/cm^3, and porosity was 97.43%. At the bottom section the bulk density of the foam was 0.040 g/cm^3, and porosity was 97.54%. The density values of the upper section were the lowest compared to the middle and bottom sections. The middle section was denser than other sections. The bottom section of the carbon foam was denser than upper section due to gravity force. The density values of the carbon foam with the addition of 10% CNF were lower than that of the carbon foam with the addition of 7% CNF. This behavior in density values could be explained by the loss of foam structure obtained with the addition of 10% CNF.

The compressive strength of the carbon foam produced was determined as 0.03 MPa. The strength of CF5-7 was higher compared to CF5-10. The addition of 10% CNF into pitch reduced the foam strength from 0.14 to 0.03 MPa. The CF5-10 was less dense than CF5-7. Also the structure of CF5-10 had weak in terms of cell formation compared to CF5-7 (as parallel to SEM images). This caused a decrease in the foam strength.

The d_{002} values of the carbon foam produced were 0.3418, 0.3424, and 0.3436 nm; the L_c values of the carbon foam produced were 1.5159, 1.4674, and 1.4258 nm for the upper, middle and bottom sections, respectively. The d_{002} values of CF5-10 increased and the L_c values of CF5-10 decreased from top to bottom. This trend could be explained by the weak cell structure from top to bottom in accordance with the SEM images obtained.

The d_{002} values for CF5-10 were higher compared to CF5-7. The L_c values were lower than CF5-7. The decrease in L_c values and increase in d_{002} values could be explained by less ordered structure in the CF5-10 compared to CF5-7.

Table 4.8 : Properties of the carbon foam with 10 % CNF additive produced at 5 atm.

Sample	**CF5-10**		
	U	**M**	**B**
CNF content (%)	10		
Skeletal density (g/cm^3)	1.5989	1.6373	1.6235
Bulk density (g/cm^3)	0.038	0.042	0.040
Porosity (%)	97.62	97.43	97.54
Interlayer spacing of d_{002} (nm)	0.3418	0.3424	0.3436
L_c (nm)	1.5159	1.4674	1.4258
Compressive strength (MPa)	0.03		

4.2.2 Properties of the carbon foams with the addition of CNF produced at 10 atm

In this section of the study; the experimental results of the carbon foams produced at pressure of 10 atm and temperature of 600 ^{o}C and rapid pressure release time of 5 sec were given. The properties of the carbon foams produced were investigated with respect to the CNF additive. CNF was added to mesophase pitch in five different weight ratios; 1%, 3%, 5%, 7%, and 10%. The carbon foams produced were carbonized and then split into three sections as upper, middle and bottom. Each section was analyzed separately.

The carbon foams produced were firstly characterized by taking the SEM images of the structure. The SEM images of the carbon foams produced were taken for two different magnifications. In these images; a, b, and c represents upper, middle, and bottom sections for the carbon foams produced, respectively.

Figure 4.23 and 4.24 showed the SEM images of the carbon foams with the addition of 1% CNF in the z- and x-directions, respectively. In the z-direction, the cells were more developed at the upper section. The ligaments, junctions and cell boundaries at the upper section were almost well formed compared to the other sections. The formation of cells having clear boundaries decreased from top to bottom. Similar observations were also obtained for the carbon foam with the addition of 1% CNF produced at 5 atm. The better foam structure at upper section could be explained by the foaming mechanism as previously discussed. In the x-direction, the foam structure at the upper section was more developed than the middle and bottom sections; moreover, the shapes of cells were more spherical and ligaments between the cells were more clear at the upper section compared to the other sections.

Z-axis point of view

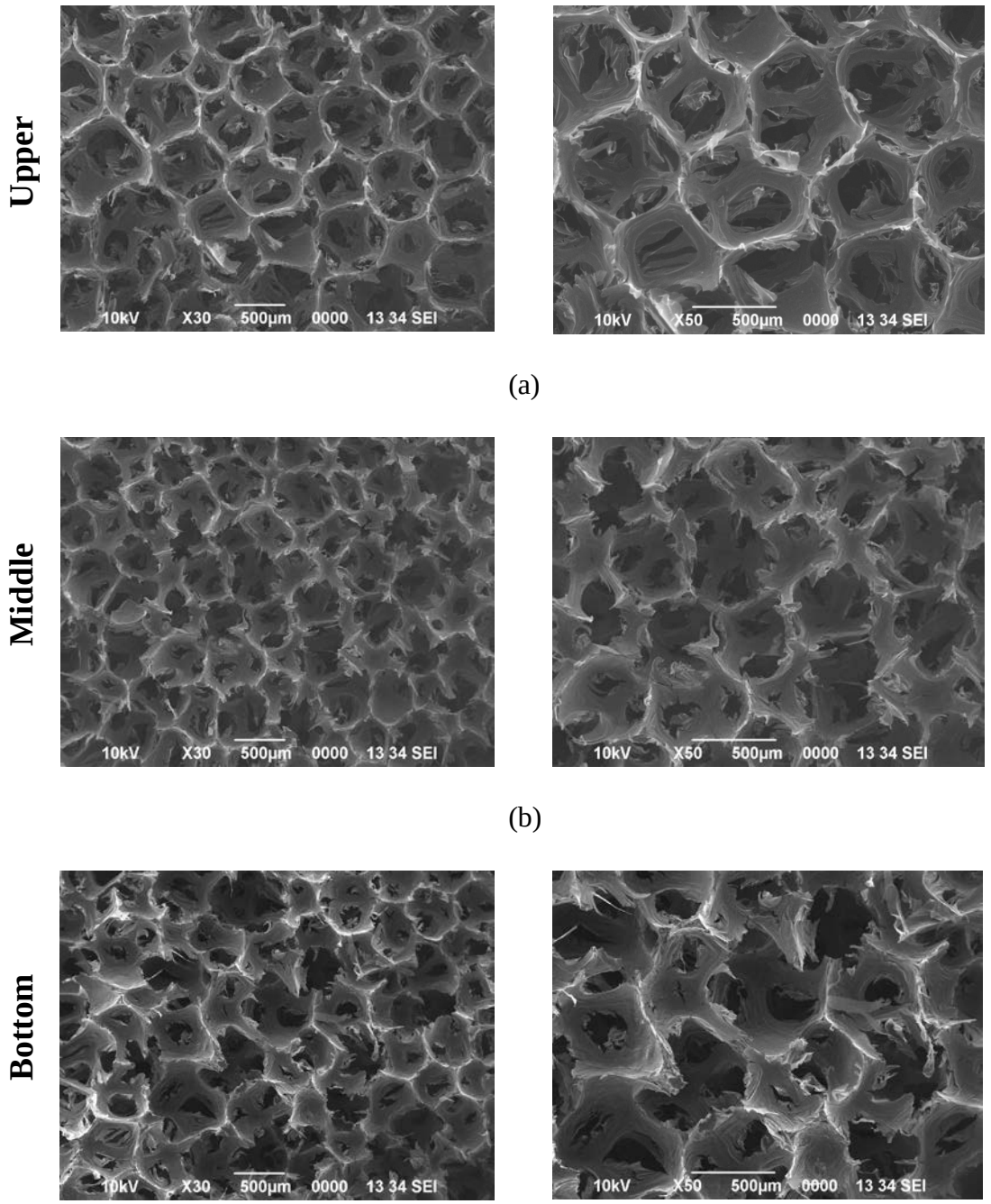

Figure 4.23 : SEM images of upper, middle, and bottom sections for the carbon foam with 1% (w/w) CNF additive produced at 10 atm in the z-direction.

. **X-axis point of view**

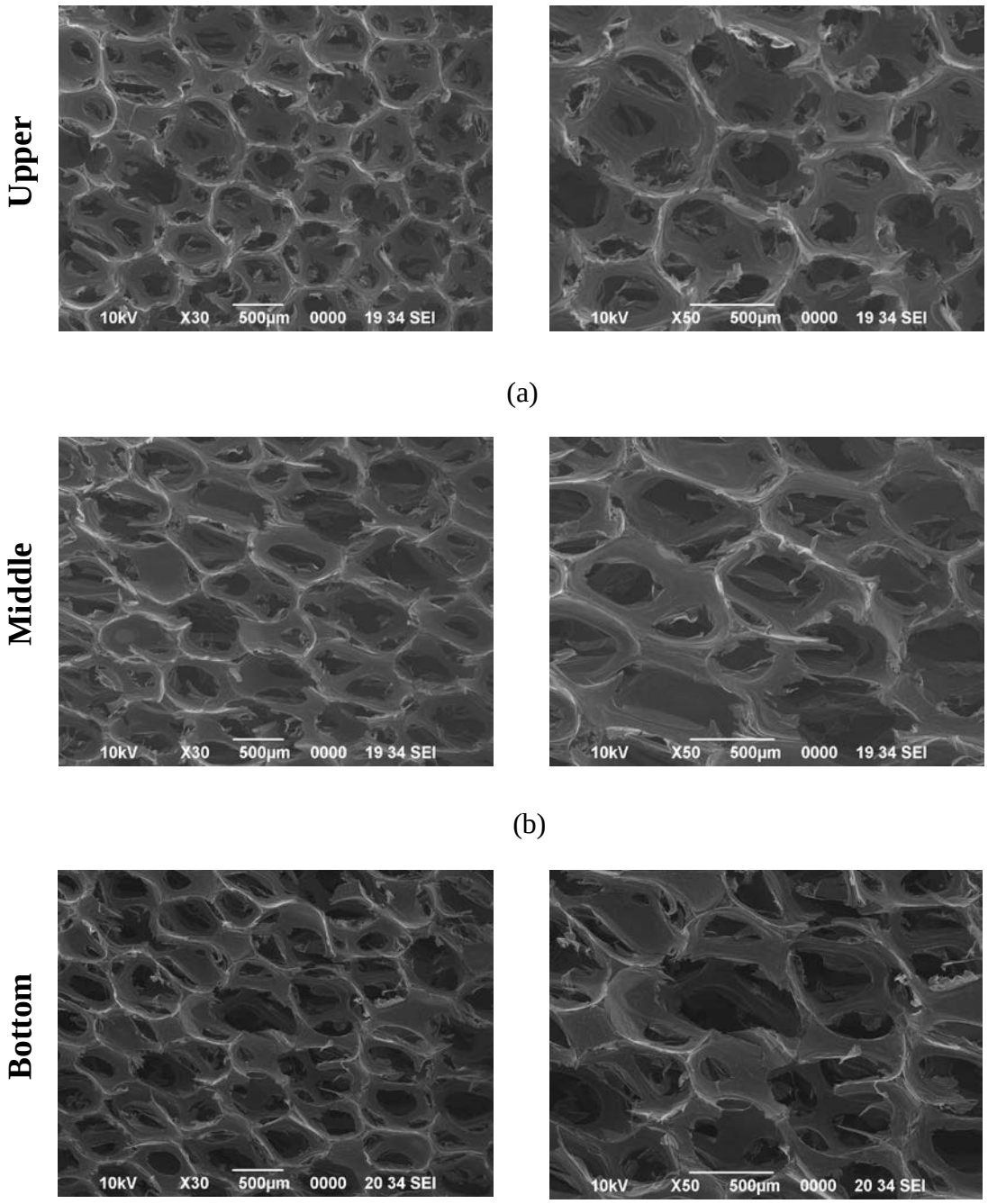

Figure 4.24 : SEM images of upper, middle, and bottom sections for the carbon foam with 1% (w/w) CNF additive produced at 10 atm in the x-direction.

The XRD patterns of the carbon foam sections are shown in Figure 4.25. Each section displayed diffraction peaks near $2\theta = 26^{o}$ which are characteristic of ordered carbonaceous structure as discussed in previous section. The intensities of the (002) peaks decreased slightly from top to bottom. The differences in intensities of the (002) peaks could be explained by the non-uniform stacking of mesophase molecules in the structure of carbon foam produced as discussed before.

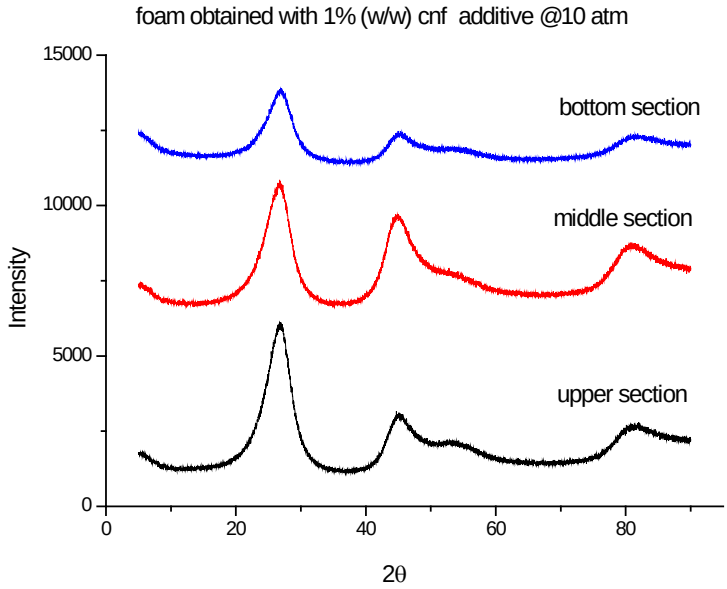

Figure 4.25 : XRD analysis of the carbon foam with 1 % CNF additive produced at 10 atm.

The properties of the carbon foam with 1% CNF additive produced at 10 atm (CF10-1) were given in Table 4.9. Bulk densities of upper, middle and bottom sections were 0.067, 0.082, and 0.072 g/cm^3, respectively. The skeletal densities were measured as 1.9577, 2.1335, and 2.0446 g/cm^3 for upper, middle and bottom sections, respectively. The porosities of upper, middle and bottom sections were 96.58%, 96.16%, and 96.48%, respectively. The compressive strength of the carbon foam produced was 0.38 MPa.

The upper section density was lower than the middle and bottom sections due to gravity force which make denser lower portion of foam as discussed before. The middle section density was higher compared to the bottom section. Same behavior was also obtained for other additive samples produced at 5 atm. The decrease in density from middle section to bottom section could be explained by the relatively more oriented structure in the middle section in terms of cell formation. The SEM

images taken from the middle section indicated that shapes of cells were more spherical and ligaments were more clear and thicker compared to the bottom section.

The density of the carbon foam with 1% CNF additive were lower than that of the carbon foam without additive, at 10 atm. CNF addition caused some deformation. The pore and cell formation was rather distorted compared to foam without additive, at 10 atm. Because density of the carbon foam with 1% CNF additive were lower than the carbon foam without additive, compressive strength of the carbon foam produced was comparatively lower than without additive, at 10 atm.

The d_{002} values of the carbon foam with the addition of 1% CNF increased from upper section to bottom section. The carbon foam with the addition of 1% CNF produced at 5 atm was showed same trend in the d_{002} values. For the carbon foam with the addition of 1% CNF produced at 5 and 10 atm, the better arrangement of mesophase molecules in ligaments was obtained at the upper section. The L_c values decreased towards bottom section in consistent with the formation of the (002) peaks.

The d_{002} value of the upper section for the carbon foam with 1% CNF additive was higher than the carbon foam without additive, at 10 atm. The loss of spherical geometry of cells resulted in less ordered structure at the upper section compared to the carbon foam without additive, at 10 atm. The d_{002} values of the middle and bottom section for the carbon foam with 1% CNF additive were lower than the carbon foam without additive, at 10atm. The d_{002} value of the middle section decreased from 0.3372 nm to 0.3368 nm. The d_{002} value of the bottom section decreased from 0.3378 nm to 0.3373 nm. This behaviour in crystal parameters were also observed between CF5-0 and CF5-1. The alignment and arrangement of mesophase molecules were modified with the addition of CNF.

The L_c values of the middle and bottom sections increased with the addition of 1% CNF compared to non-additive case, at 10 atm. However, the L_c value of the upper section for the carbon foam with the addition of 1% CNF was lower compared to the carbon foam without additive, at 10 atm. The L_c values were also in accord with the d_{002} values for each section. The variation in crystal parameters between CF5-0 and CF5-1 showed same trend.

Table 4.9 : Properties of the carbon foam with 1% CNF additive produced at 10 atm.

Sample	**CF10-1**		
	U	**M**	**B**
CNF content (%)	1		
Skeletal density (g/cm^3)	1.9577	2.1335	2.0446
Bulk density (g/cm^3)	0.067	0.082	0.072
Porosity (%)	96.58	96.16	96.48
Interlayer spacing of d_{002} (nm)	0.3360	0.3368	0.3373
L_c (nm)	1.7668	1.7561	1.5906
Compressive strength (MPa)	0.38		

Figure 4.26 and 4.27 present the cell morphology of the carbon foam with the 3% CNF additive in the z- and x-directions, respectively. From Figure 4.26, more homogeneous structure was obtained with 3% CNF additive compared to other foams with or without additive, at 10 atm. The distribution of pores and cells of the carbon foam were seen nearly similar in each section. Ligament, junction, and wall formation in each section did not differ distinctly to each other. Cell geometry in the upper section seemed to be similar to the other sections which were nearly spherical in shape. The 3% CNF additive modified the foam structure and formed more uniform structure. These observations were also obtained for the SEM images in the x-direction. These results were consistent with the density, strength, and XRD measurements.

Z-axis point of view

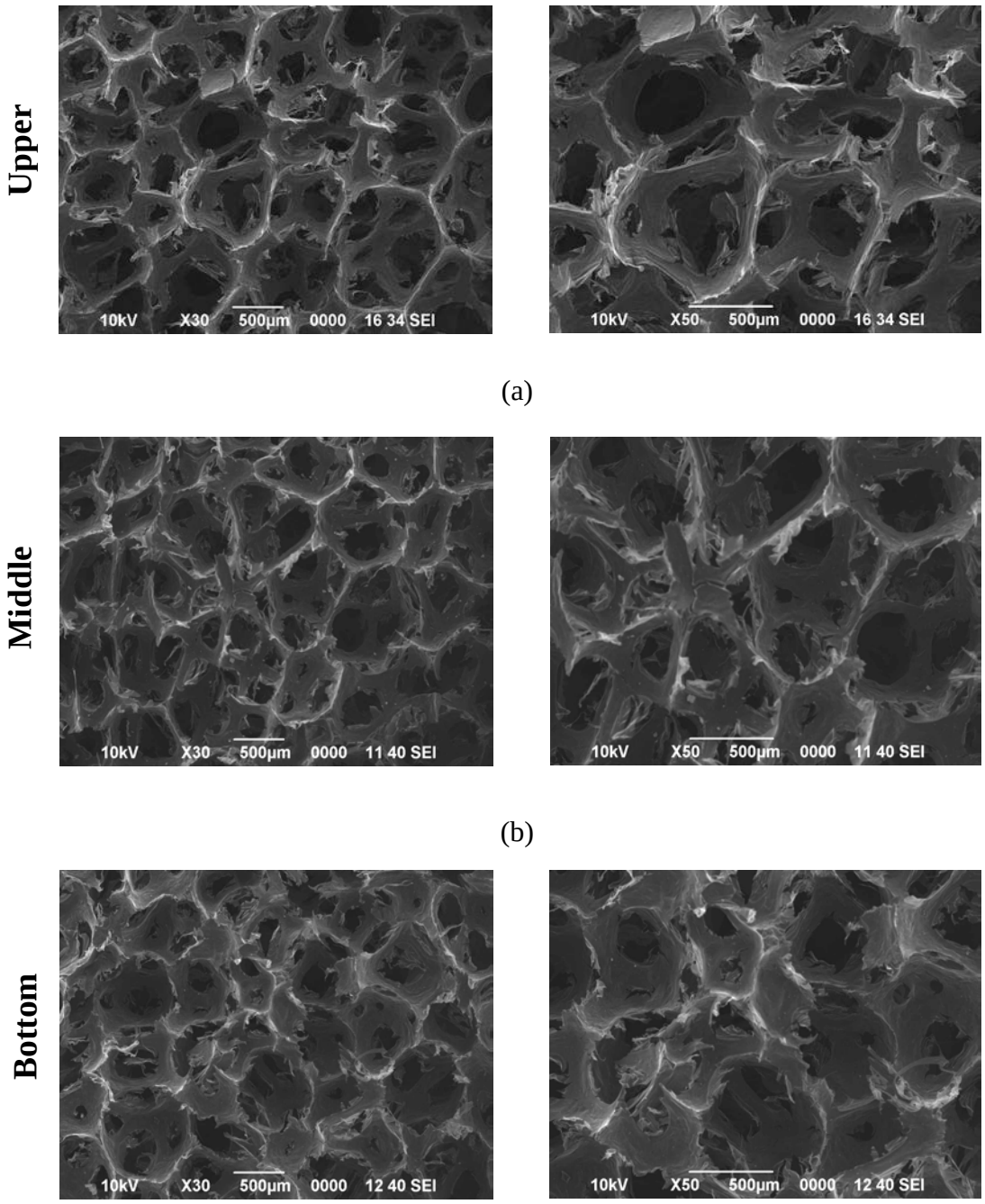

Figure 4.26 : SEM images of upper, middle, and bottom sections for the carbon foam with 3% (w/w) CNF additive produced at 10 atm in the z-direction.

X-axis point of view

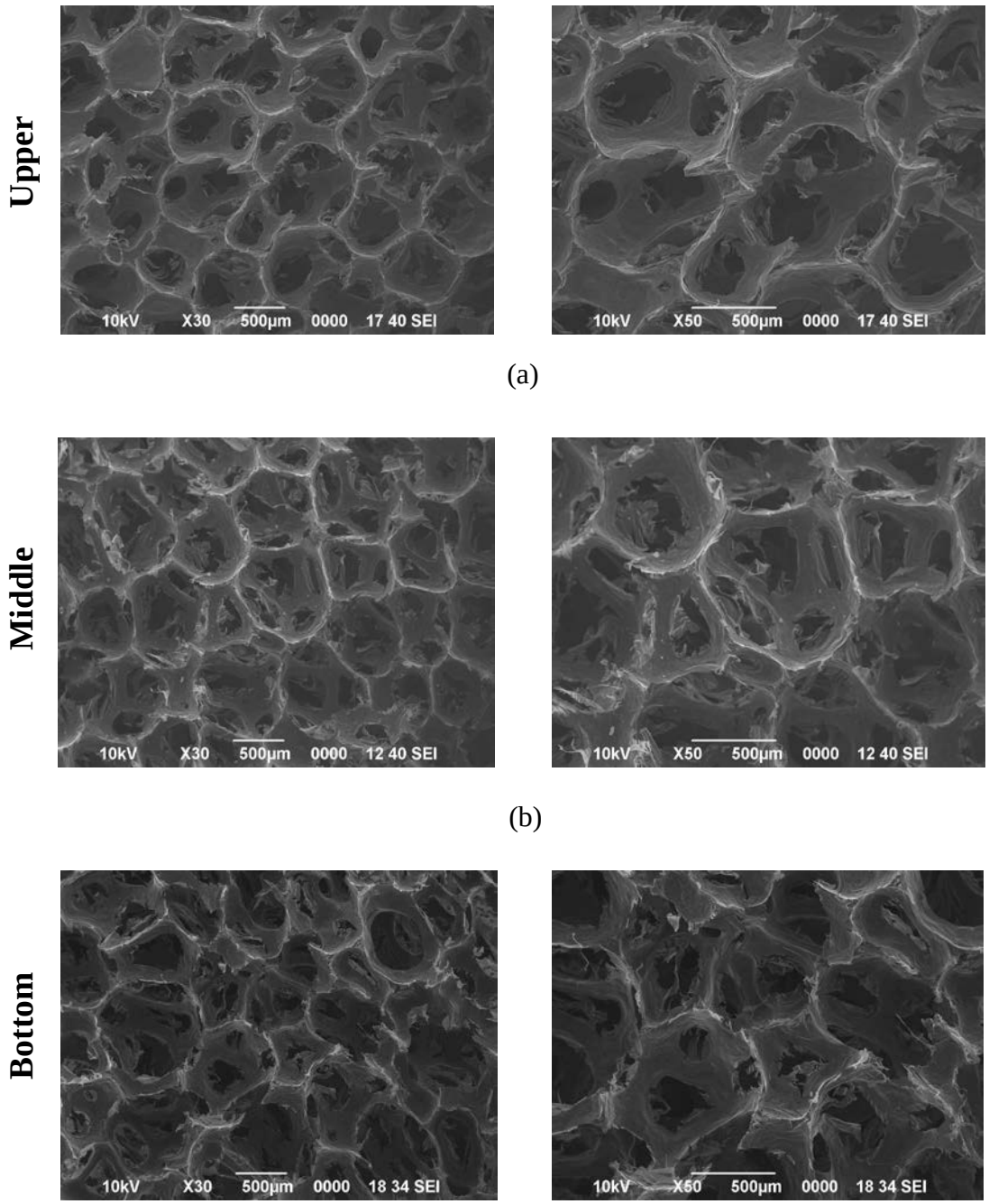

Figure 4.27 : SEM images of upper, middle, and bottom sections for the carbon foam with 3% (w/w) CNF additive produced at 10 atm in the x-direction.

Figure 4.28 represents the XRD patterns for the carbon foam with the 3% CNF additive. The XRD patterns for each section were nearly similar. The presence of a

similar XRD patterns indicated uniform alignment of mesophase molecules as well as uniform structure for each section of the 3% CNF additive foam.

The intensity of (002) peak of the upper section for the carbon foam with the 3% CNF additive were lower than the carbon foam with the addition of 1%CNF, at 10 atm. However, the intensity of (002) peak of the middle and bottom sections for the carbon foam with the addition of 3% CNF were higher than the carbon foam with the addition of 1%CNF.

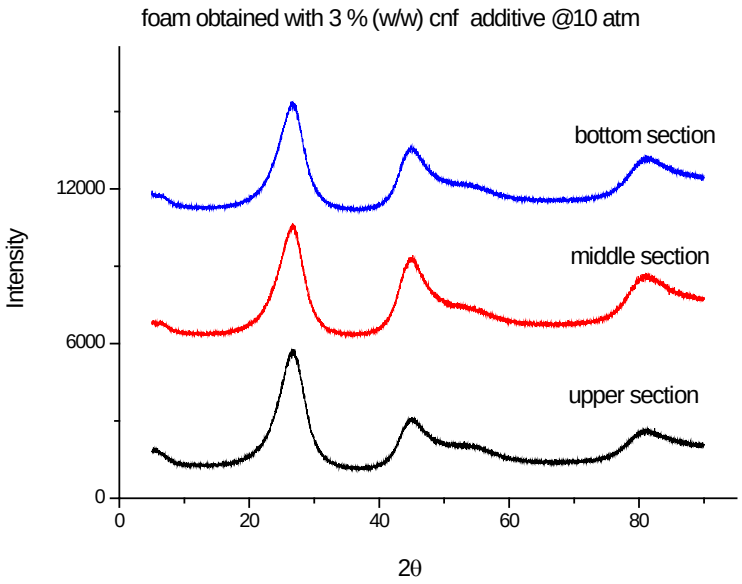

Figure 4.28 : XRD analysis of the carbon foam with 3% CNF additive produced at 10 atm.

The properties of the carbon foam with 3% CNF additive produced at 10 atm (CF10-3) are given in Table 4.10. The skeletal densities of the carbon foam section (upper, middle, and bottom) were 1.9355, 2.1132, and 1.9594 g/cm^3, respectively. At the upper section, the bulk density of the foam was 0.062 g/cm^3, and porosity was 96.80%. At the middle section, the bulk density of the foam was 0.070 g/cm^3 and porosity was 96.69 %. At the bottom section, the bulk density of the foam was 0.064 g/cm^3, and porosity was 96.73%. The d_{002} values of upper, middle and bottom sections were 0.3363, 0.3364, and 0.3366 nm, respectively. The L_c values of upper, middle and bottom sections were measured as 1.7568, 1.7566 and 1.7565 nm, respectively. The strength of the carbon foam produced was 0.33 MPa.

The density values of the carbon foam with the addition of 3% CNF were lower than that of the carbon foam with or without CNF additive, at 10 atm. However, the density differences from top to bottom of the carbon foam with 3% CNF additive

was relatively less than the other carbon foams produced, at 10 atm. The percentages of changes in properties of the carbon foams produced at 10 atm are given in Appendix B. The skeletal density difference from upper section to middle section was 9.2% and the skeletal density difference from upper section to bottom section was 1.2% for the carbon foam with the addition of 3% CNF.

The d_{002} and L_c values of the carbon foam with 3% additive were almost identical to each other for each section. The d_{002} values of the upper section were higher than the carbon foam with the addition of 1% CNF, at 10 atm. However, the d_{002} values of the middle and bottom sections were lower than the carbon foam with the addition of 1% CNF, at 10 atm. The L_c values were also in accord with the d_{002} values for each section.

The properties of produced carbon foam showed more uniform structure in terms of foaming characteristic of the samples such as cell structure, density, porosity, d_{002}, and L_c. 3% CNF additive could not disturb foaming mechanism. The analysis of higher magnification images of the sample obtained with 3% CNF additive showed that carbon nanofibers were mostly located in junction regions as shown in Appendix C.

Table 4.10 : Properties of the carbon foam with 3% CNF additive produced at 10 atm.

Sample	**CF10-3**		
	U	**M**	**B**
CNF content (%)	3		
Skeletal density (g/cm^3)	1.9355	2.1132	1.9594
Bulk density (g/cm^3)	0.062	0.070	0.064
Porosity (%)	96.80	96.69	96.73
Interlayer spacing of d_{002} (nm)	0.3363	0.3364	0.3366
L_c (nm)	1.7568	1.7566	1.7565
Compressive strength (MPa)	0.33		

The SEM images of the carbon foam with the addition of 5% CNF in the z-direction are shown in Figure 4.29. Cell geometries in the upper and middle section were seen

similar to each other. Cells at the bottom section contained bigger pores compared to the other sections.

The SEM images of the carbon foam with the 5% CNF additive in the x-direction are shown in Figure 4.30. The more spherical cells were observed at the upper section compared to the other sections. The deformation in cell structure increased slightly from the middle section to bottom section. The shapes of cells seemed more likely elliptic in the middle and bottom section

Z-axis point of view

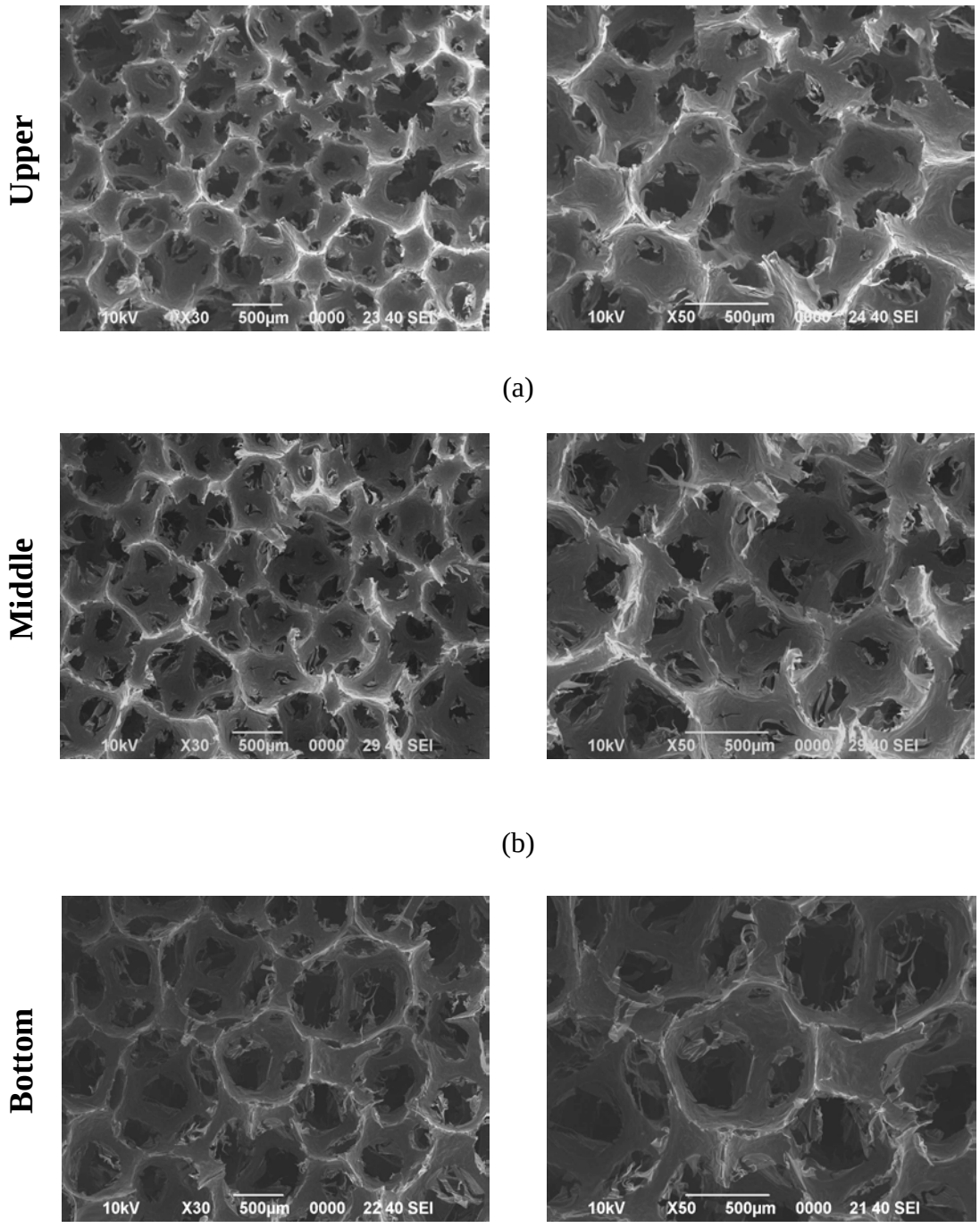

Figure 4.29 : SEM images of upper, middle, and bottom sections for the carbon foam with 5% (w/w) CNF additive produced at 10 atm in the z-direction.

Z-axis point of view

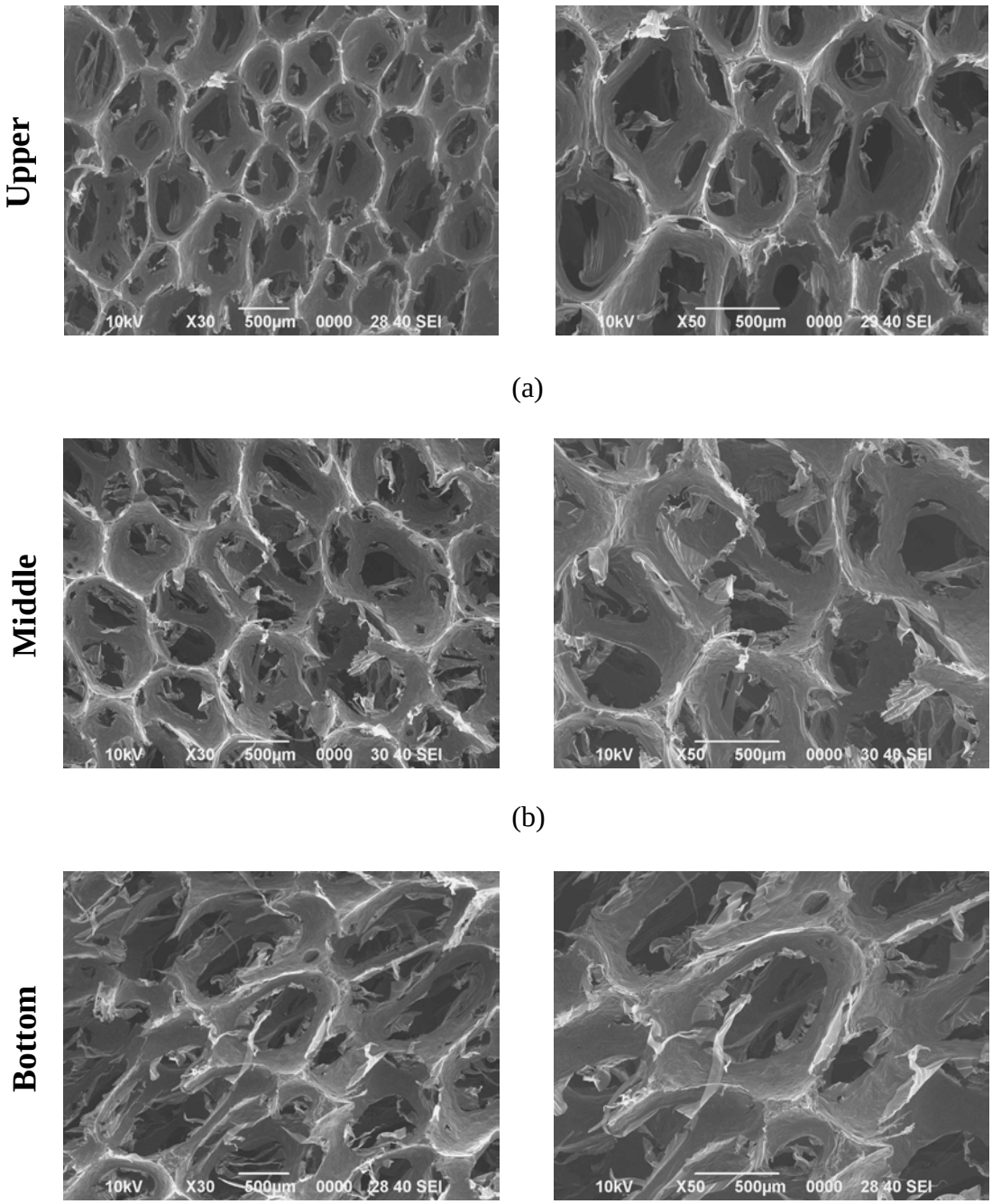

Figure 4.30 : SEM images of upper, middle, and bottom sections for the carbon foam with 5% (w/w) CNF additive produced at 10 atm in the x-direction.

Figure 4.31 shows XRD analysis results of the carbon foam with 5% CNF additive. The samples showed similar XRD patterns. Although the (002) peaks appeared for

each section, their patterns were wide compared to the carbon foam with 3% CNF additive, at 10 atm. The alignments of mesophase molecules on ligaments of the carbon foam with 5% CNF additive were weaker than that of foam with 3% CNF additive, at 10 atm. This was an indication that less ordered foam structure for the carbon foam with 5% CNF additive compared to the carbon foam with 3% CNF additive, at 10 atm.

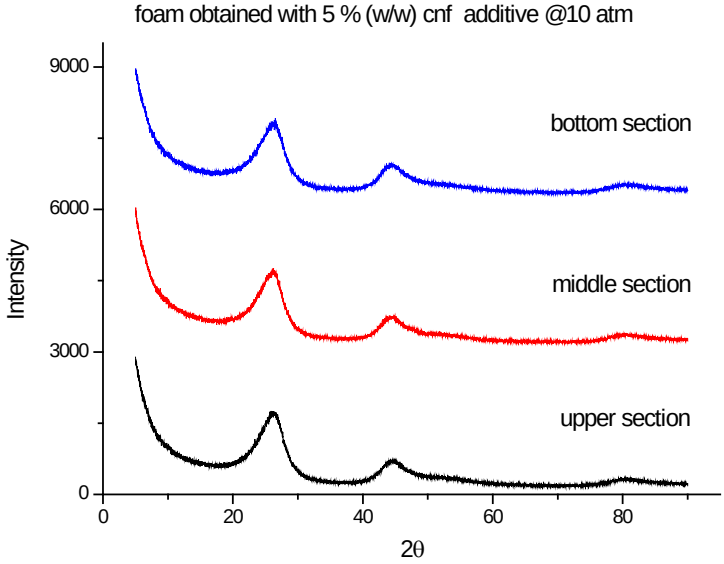

Figure 4.31 : XRD analysis of the carbon foam with 5 % CNF additive produced at 10 atm.

The general properties of the carbon foam produced with 5% CNF additive (CF10-5) are given in Table 4.11. The skeletal densities were 1.7610, 2.0866, and 1.8996 g/cm^3; bulk densities were 0.053, 0.067 and 0.058 g/cm^3; the porosities were 96.99%, 96.79%, and 96.95%, for upper, middle and bottom sections, respectively. The upper section had lower density values than the other sections. The middle section was denser compared to the other sections. This density trend was also obtained for CF10-3. The density values of the carbon foam with the addition of 5% CNF were lower than that of the carbon foam with the addition of 3% CNF.

The compressive strength of the carbon foam produced was 0.31 MPa. The strength of the carbon foam with the addition of 5% CNF was lower than that of the carbon foam with the addition of 3% CNF. The decrease in the compressive strength with 5% CNF additive was in good accordance with density measurements. The strength of foam reduced due to less dense structure with the addition of 5% CNF compared to the carbon foam with 3% CNF additive.

The d_{002} values of the foam were 0.3399, 0.3400, and 0.3405 nm, the L_c values of the foam were 1.5134, 1.5130, and 1.5092 nm for the upper, middle and bottom sections, respectively. The d_{002} and the L_c values of each section were almost similar to each other.

The d_{002} values of CF10-5 were higher than that of CF10-3. The L_c values of CF10-5 were lower than that of CF10-3. Compared to the carbon foam with the addition of 3% CNF, the weak cell structure with the addition of 5% CNF caused an increase in the d_{002} values and a decrease in the L_c values.

Table 4.11 : Properties of the carbon foam with 5% CNF additive produced at 10 atm.

Sample	**CF10-5**		
	U	**M**	**B**
CNF content (%)	5		
Skeletal density (g/cm^3)	1.7610	2.0866	1.8996
Bulk density (g/cm^3)	0.053	0.067	0.058
Porosity (%)	96.99	96.79	96.95
Interlayer spacing of d_{002} (nm)	0.3399	0.3400	0.3405
L_c (nm)	1.5134	1.5130	1.5092
Compressive strength (MPa)	0.31		

Figure 4.32 and 4.33 show the SEM images of the carbon foams with the 7% CNF additive in the z- and x-directions, respectively. The SEM images in the z- and x-directions showed that for the 7% CNF additive, the pore and cell formation were rather distorted compared to the carbon foam with 1%, 3%, and 5% CNF additive.

Z-axis point of view

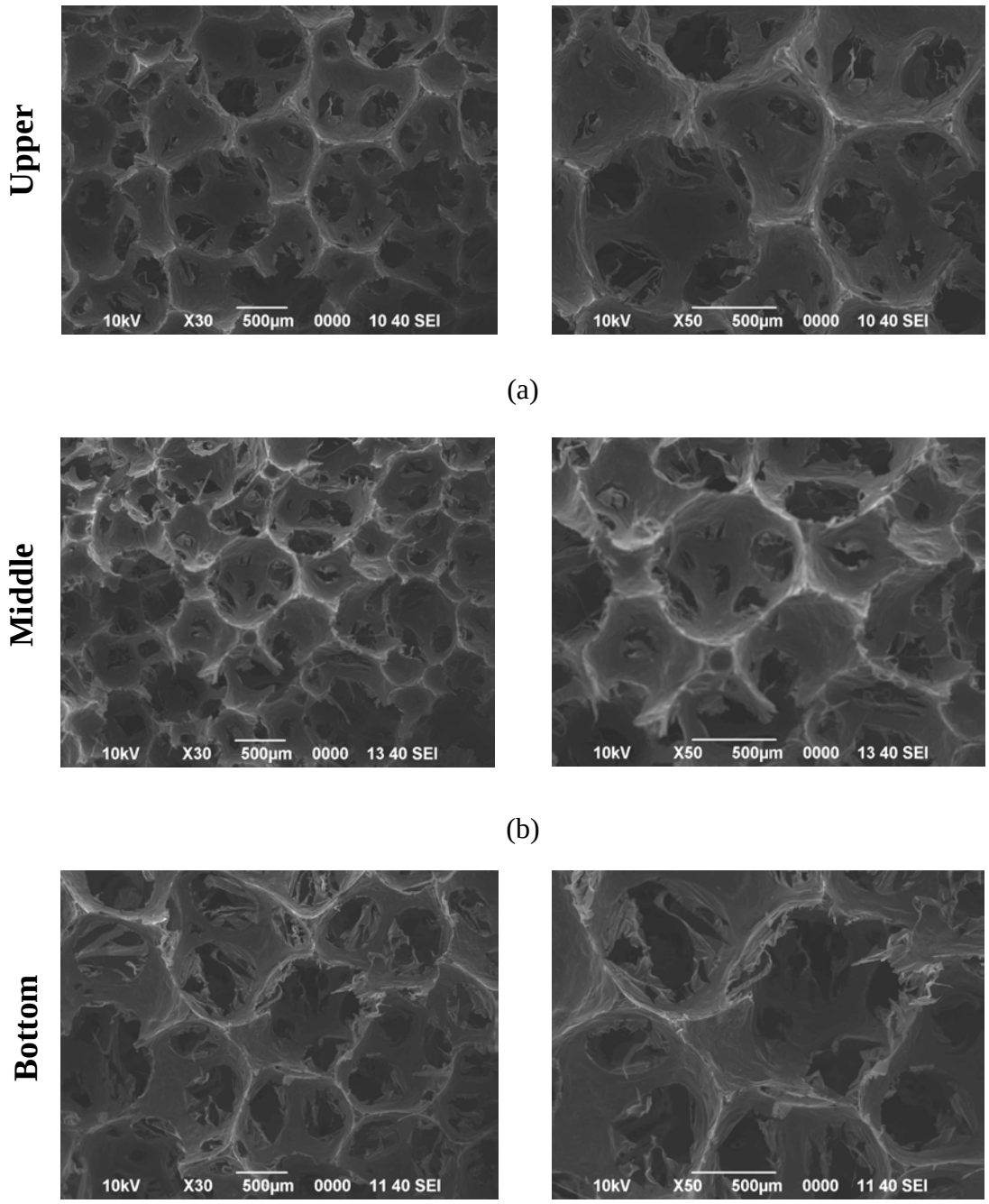

Figure 4.32: SEM images of upper, middle, and bottom sections for the carbon foam with 7% (w/w) CNF additive produced at 10 atm in the z-direction.

X-axis point of view

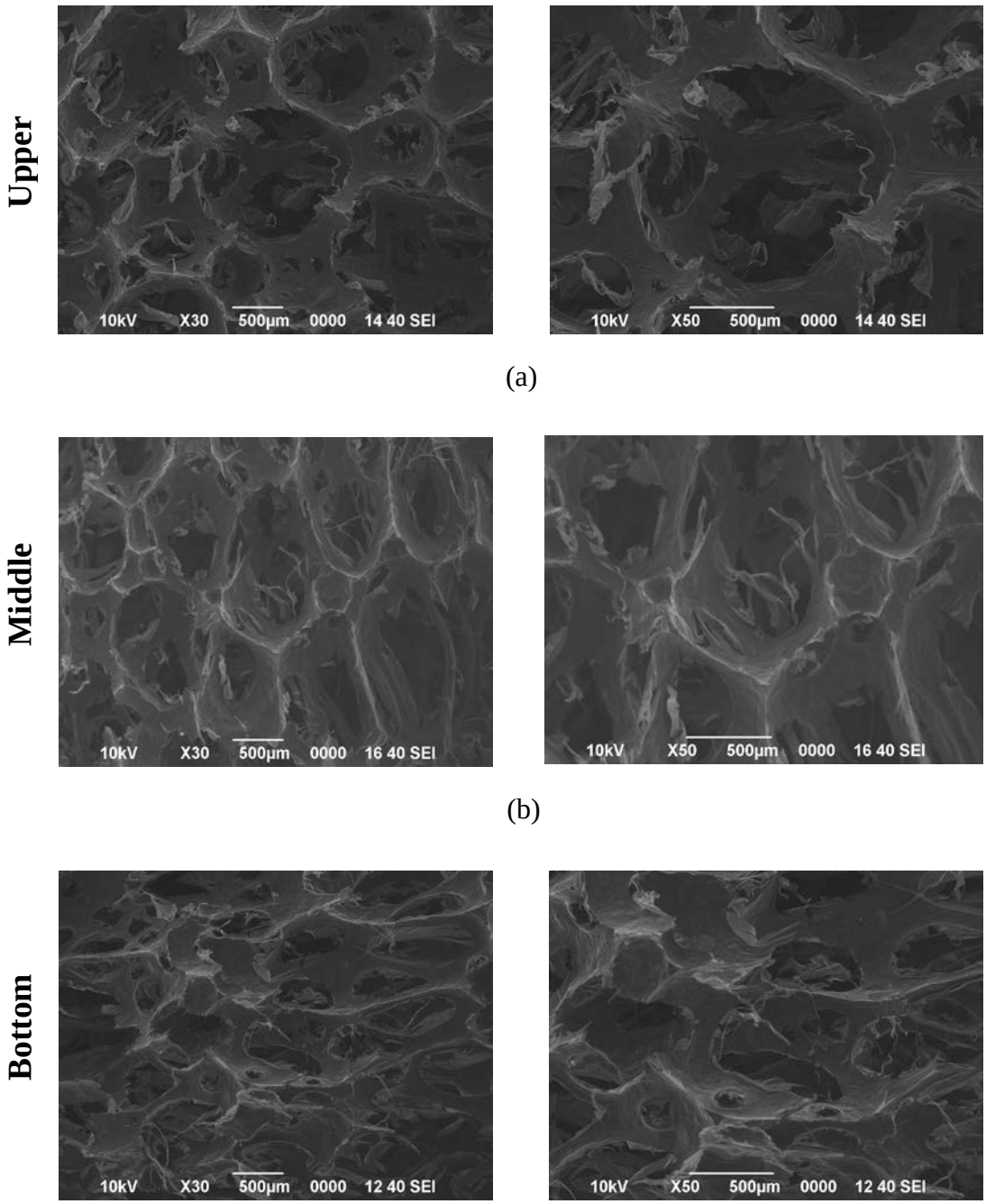

Figure 4.33 : SEM images of upper, middle, and bottom sections for the carbon foam with 7% (w/w) CNF additive produced at 10 atm in the x-direction.

The XRD analysis of the carbon foam produced is presented in Figure 4.34. The XRD patterns of each section were seen similar to each other. The (002) peaks for

each section almost disappeared. This was indication that weak alignment of the mesophase molecules for the carbon foam with the addition of 7% CNF.

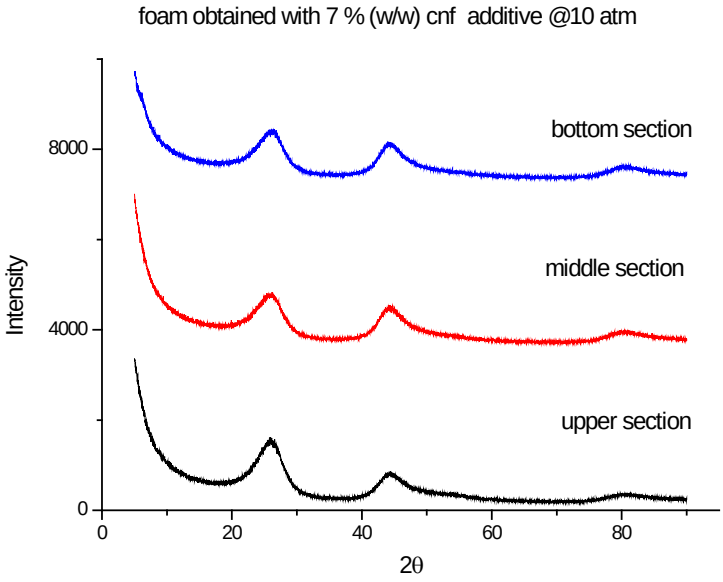

Figure 4.34 : XRD analysis of the carbon foam with 7% CNF additive produced at 10 atm.

Table 4.12 lists characteristic properties of the carbon foam with the addition of 7% CNF produced at 10 atm (CF10-7). The skeletal density values of the carbon foam produced were determined to be between 1.7441– 1.9466 g/cm^3. The densities of the carbon foam produced were measured between 0.051 g/cm^3 and 0.062 g/cm^3. The total porosities of the carbon foam produced were determined to be 97.08%, 96.81%, and 96.83% for upper, middle and bottom sections, respectively. The compressive strength of the carbon foam with 7% CNF additive was measured as 0.14 MPa. The interlayer spacings, d_{002}, and the crystal sizes in the c-direction, L_c, were 0.3408, 0.3424, and 0.3425 nm; and 1.5009, 1.4290, and 1.4121 nm as upper, middle, and bottom sections, respectively.

The density values of the upper section were lower compared to the middle and bottom sections. The middle section was denser than the other sections. This trend in density was also obtained for the other additive samples produced at 5 and 10 atm.

The density values of the carbon foam with 7% CNF additive were less than that of the carbon foam with 5% CNF additive, at 10 atm. As a result of lower dense structure, the strength of the carbon foam with 7% CNF additive was also low compared to the carbon foam with 5% CNF additive.

The d_{002} value of the upper section was lower than the other sections. The middle and bottom sections had nearly same d_{002} values. The L_c values decreased from top to bottom for the carbon foam with the addition of 7% CNF.

The d_{002} values of CF10-7 were higher than that of CF10-5. The L_c values of CF10-7 were lower than that of CF10-5. From SEM investigations, the structure was more developed for the carbon foam with the addition of 5% CNF compared to the carbon foam with the addition of 7% CNF, at 10 atm. The weak cell formation ended up a reduction in the alignment of mesophase molecules for the carbon foam with the addition of 7% CNF compared to the carbon foam with the addition of 5% CNF, at 10 atm. This caused a decrease in the L_c values and increased in the d_{002} values with 7% CNF additive compared to the 5% CNF additive, at 10 atm.

Table 4.12 : Properties of the carbon foam with 7% CNF additive produced at 10 atm.

Sample	**CF10-7**		
	U	**M**	**B**
CNF content (%)	7		
Skeletal density (g/cm^3)	1.7441	1.9466	1.7989
Bulk density (g/cm^3)	0.051	0.062	0.057
Porosity (%)	97.08	96.81	96.83
Interlayer spacing of d_{002} (nm)	0.3408	0.3424	0.3425
L_c (nm)	1.5009	1.4290	1.4121
Compressive strength (MPa)	0.14		

Figure 4.35 and 4.36 show the structure of foam with 10% CNF additive in the z- and x-directions, respectively. The 10% CNF addition into pitch disrupted the foam structure in terms of cell formation and ligament development. Cell size in the upper section was bigger compared to the foam with 7% CNF additive. Cells contained too many pores in number at the upper section. Spherical cell formation could not be observed in each section. Cells were irregular in shape at the middle and bottom sections.

Z-axis point of view

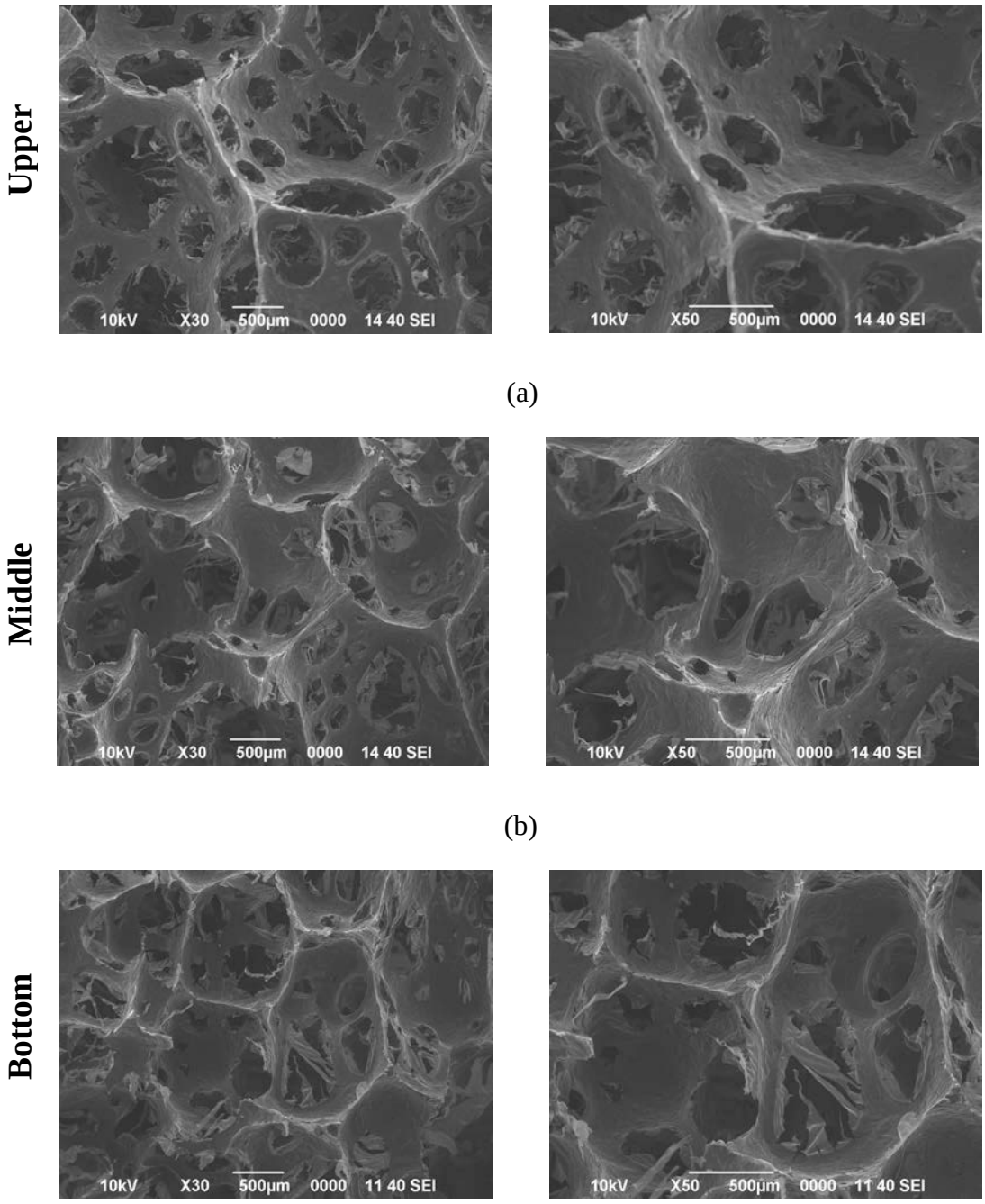

Figure 4.35 : SEM images of upper, middle, and bottom sections for the carbon foam with 10% (w/w) CNF additive produced at 10 atm in the z-direction.

X-axis point of view

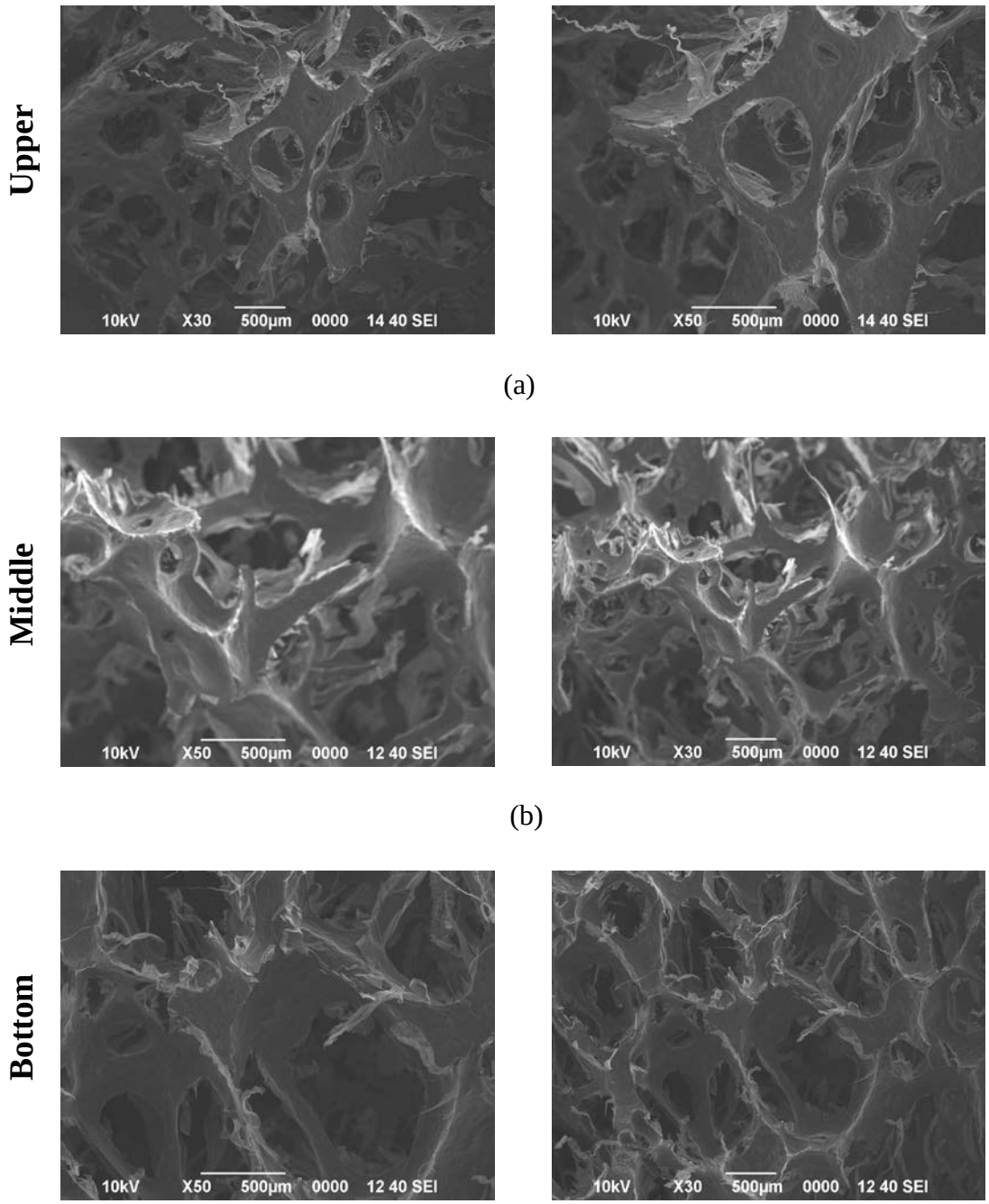

Figure 4.36 : SEM images of upper, middle, and bottom sections for the carbon foam with 10% (w/w) CNF additive produced at 10 atm in the x-direction.

The XRD patterns of the carbon foam with 10% CNF additive are shown in Figure 4.37. It is seen from the Figure 4.37 that each section showed similar patterns. The

(002) peaks were weak in each section. This revealed less developed cell formation for the carbon foam with 10% CNF additive.

The (002) peak intensities of the upper section were lower for the carbon foam with the addition of 10% CNF compared to the carbon foam with the addition of 7% CNF, at 10 atm. The (002) intensities of the middle and bottom sections increased slightly with the 10% CNF additive compared to the carbon foam with 7% CNF additive, at 10 atm.

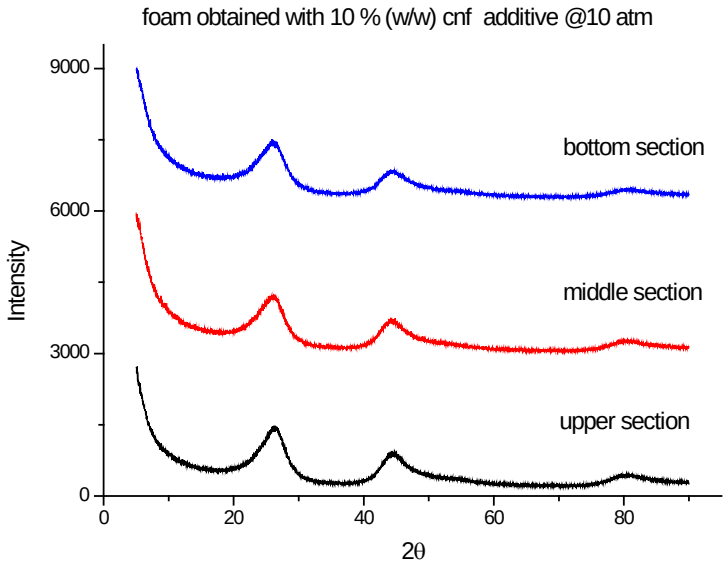

Figure 4.37 : XRD analysis of the carbon foam with 10% CNF additive produced at 10 atm.

The properties of the carbon foam with 10% CNF additive produced at 10 atm (CF10-10) is shown in Table 4.13. The middle section was denser than other sections. The density values of the upper section were the lowest compared to the other sections. The density values of the carbon foam with the addition of 10% CNF were lower than that of the carbon foam with the addition of 7% CNF.

The 10% CNF additive caused a much more deterioration in the foaming mechanism resulting with high number of pore formation. This behaviour was also in accordance with the other properties as shown in Table 4.13. The density values of each section were the lowest compared to other additives samples, at 10 atm. The carbon foam obtained with 10% CNF additive had the highest porosity and the lowest strength between all percentages samples studied, at 10 atm.

The d_{002} values of the carbon foam with the addition of 10% CNF increased from upper section to bottom section. Also the L_c values decreased towards bottom section in consistent with the formation of the (002) peaks.

The d_{002} values of upper section were higher than the carbon foam with 7% CNF additive, at 10 atm. The d_{002} values of middle and bottom sections were lower than the carbon foam with 7% CNF additive, at 10 atm.

The L_c values of upper section for the carbon foam with 10% CNF additive were lower than the carbon foam with 7% CNF additive, at 10atm. The L_c values of middle and bottom sections for the carbon foam with 10% CNF additive were higher than the carbon foam with 7% CNF additive, at 10atm.

Table 4.13 : Properties of the carbon foam with 10% CNF additive produced at 10 atm.

Sample	**CF10-10**		
	U	**M**	**B**
CNF content (%)	10		
Skeletal density (g/cm^3)	1.6898	1.9082	1.7780
Bulk density (g/cm^3)	0.045	0.054	0.049
Porosity (%)	97.34	97.17	97.24
Interlayer spacing of d_{002} (nm)	0.3412	0.3417	0.3420
L_c (nm)	1.4898	1.4591	1.4323
Compressive strength (MPa)	0.07		

The carbon foams with the addition of CNF produced at 5 and 10 atm were compared in Table 4.14. Comparison of the carbon foams with the addition of CNF produced at 5 and 10 atm showed these findings. The bulk and skeletal density values of the carbon foam samples increased with the increase in operating pressure. The increase in density of carbon foams with increasing pressure can be explained according to the volatile evolution: As the pitch is heated above the softening point, volatile matter release takes place. For the case of higher pressures the stress created

on the peripheral area of the bubbles is higher than lower pressures therefore mesophase molecules are more effectively aligned and oriented to form cell walls, ligaments and junctions [88, 89]. The porosity values decreased with increasing pressure. Since compressive strength is inversely proportional with porosity, carbon foams of higher density presented much higher compressive strength.

The stack heights (L_c) were usually lower and the interlayer spacings (d_{002}) were usually higher for samples obtained at 5 atm compared to samples obtained at 10 atm.

As a conclusion, comparison of the samples with CNF additive produced at 5 and 10 atm showed that the carbon foams produced at 10 atm had better foam properties such as higher strength, higher density, and more ordered cell structure.

Table 4.14 : Comparison of the samples with the addition of CNF produced at 5 and 10 atm.

		5 atm						10 atm					
		Skeletal density (g/cm^3)	**Bulk density (g/cm^3)**	**Porosity (%)**	**Interlayer spacing of d_{002} (nm)**	**L_c (nm)**	**Compressive strength (MPa)**	**Skeletal density (g/cm^3)**	**Bulk density (g/cm^3)**	**Porosity (%)**	**Interlayer spacing of d_{002} (nm)**	**L_c (nm)**	**Compressive strength (MPa)**
CF1	**Upper**	1.6799	0.048	97.16	0.3374	1.5809	0.14	1.9577	0.067	96.58	0.3360	1.7668	0.38
	Middle	1.7395	0.057	96.73	0.3401	1.5526		2.1335	0.082	96.16	0.3368	1.7561	
	Bottom	1.7114	0.052	96.99	0.3410	1.5498		2.0446	0.072	96.48	0.3373	1.5906	
CF3	**Upper**	1.6669	0.044	97.36	0.3378	1.5707	0.09	1.9355	0.062	96.80	0.3363	1.7568	0.33
	Middle	1.7124	0.047	97.26	0.3417	1.5404		2.1132	0.070	96.69	0.3364	1.7566	
	Bottom	1.6803	0.045	97.32	0.3419	1.5359		1.9594	0.064	96.73	0.3366	1.7565	
CF5	**Upper**	1.6446	0.043	97.40	0.3392	1.5651	0.06	1.7610	0.053	96.99	0.3399	1.5134	0.31
	Middle	1.6938	0.046	97.28	0.3393	1.5607		2.0866	0.067	96.79	0.3400	1.5130	
	Bottom	1.6795	0.044	97.38	0.3398	1.5604		1.8996	0.058	96.95	0.3405	1.5092	
CF7	**Upper**	1.6385	0.042	97.44	0.3399	1.5552	0.04	1.7441	0.051	97.08	0.3408	1.5009	0.14
	Middle	1.6809	0.045	97.32	0.3400	1.5531		1.9466	0.062	96.81	0.3424	1.4290	
	Bottom	1.6716	0.043	97.43	0.3401	1.5511		1.7989	0.057	96.83	0.3425	1.4121	
CF10	**Upper**	1.5989	0.038	97.62	0.3418	1.5159	0.03	1.6898	0.045	97.34	0.3412	1.4898	0.07
	Middle	1.6373	0.042	97.43	0.3424	1.4674		1.9082	0.054	97.17	0.3417	1.4591	
	Bottom	1.6235	0.040	97.54	0.3436	1.4258		1.7780	0.049	97.24	0.3420	1.4323	

Comparison of the samples with CNF additives produced at 10 atm is shown in Table 4.15. The bulk and skeletal density of carbon foams exhibited a decreasing trend with increasing amount of additive. The porosity of the carbon foams increased with the decrease in density. The compressive strength of the carbon foams reduced with increasing porosity. This decrease in density and strength with additives were discussed previously.

The addition of CNF into pitch changed cell interlinking, porosity, and spherical geometry of cells as well as orientation of mesophase molecules. The d_{002} values usually increased and the L_c values usually decreased with the increase in amount of CNF.

The densities of bottom sections were always higher than upper sections. Hardcastle et al. also stated that the higher molecules compounds migrate due to gravity force thereby the bottom section of the foam was denser than top section of the foam [169].

The middle sections of the foams were found to be denser compared to the bottom sections in this study. The decrease in density from middle section to bottom section could be explained by formation of undeveloped cell and ligament structure in bottom sections.

The variation in density between upper and middle section of the foam with 3% CNF additive were less than that of all other produced carbon foams (except CF10-1), at 10 atm. Moreover, the percent change in density between upper and bottom section of the carbon foam with 3% CNF additive were the lowest compared to all other produced carbon foams, at 10 atm (see Appendix B).

Figure 4.38 shows the XRD patterns for all produced carbon foams with the addition of CNF, at 10 atm. The XRD patterns of each section differed to each other for the foam with 1% CNF additive. The (002) peak (which are characteristic of interlayer spacing) of the upper section was narrower and more intense than other sections for the foam with 1% CNF additive. The XRD patterns of each section were almost identical for the foam with 3% CNF additive. The (002) peak intensities and breadth of the each section were nearly similar to each other for the carbon foam with 3% CNF additive. Although XRD patterns were similar to each other for the foams with 5%, 7%, and 10% CNF additive, the (002) peak intensities were low compared to the foam with 3% CNF additive.

The similar XRD patterns for the carbon foam with 3% CNF additive indicated the more uniform alignment of mesophase molecules at ligaments compared to all other produced carbon foams, at 10 atm. This behaviour is also in accordance with the cell structure shown in

Figure 4.26 and 4.27. The foam with the 3% CNF additive showed more uniform structure in terms of cell morphology and ligament, junction, and wall formation compared to all other produced carbon foams as discussed previously, at 10 atm.

As a conclusion; the carbon foam with the addition of 3% CNF showed an ideal foam morphology with a more uniform structure (densities in each section were close to each other and having similar cell morphology from top to bottom), better foam properties (nearly identical XRD patterns and having clear (002) peak in each section), and moderate strength in this study.

Table 4.15 : Comparison of the carbon foams with CNF additives produced at 10 atm.

Sample	**CF10-1**			**CF10-3**			**CF10-5**			**CF10-7**			**CF10-10**		
	U	**M**	**B**	**U**	**M**	**B**	**U**	**M**	**B**	**U**	**M**	**B**	**U**	**M**	**B**
CNF Content	1			3			5			7			10		
Skeleton density (g/cm^3)	1.9577	2.1335	2.0446	1.9355	2.1132	1.9594	1.7610	2.0866	1.8996	1.7441	1.9466	1.7989	1.6898	1.9082	1.7780
Bulk density (g/cm^3)	0.067	0.082	0.072	0.062	0.070	0.064	0.053	0.067	0.058	0.051	0.062	0.057	0.045	0.054	0.049
Porosity (%)	96.58	96.16	96.48	96.80	96.69	96.73	96.99	96.79	96.95	97.08	96.81	96.83	97.34	97.17	97.24
Interlayer spacing of d_{002} (nm)	0.3360	0.3368	0.3373	0.3363	0.3364	0.3366	0.3399	0.3400	0.3405	0.3408	0.3424	0.3425	0.3412	0.3417	0.3420
L_c (nm)	1.7668	1.7561	1.5906	1.7568	1.7566	1.7565	1.5134	1.5130	1.5092	1.5009	1.4290	1.4121	1.4898	1.4591	1.4323
Compressive strength (MPa)	0.38			0.33			0.31			0.14			0.07		

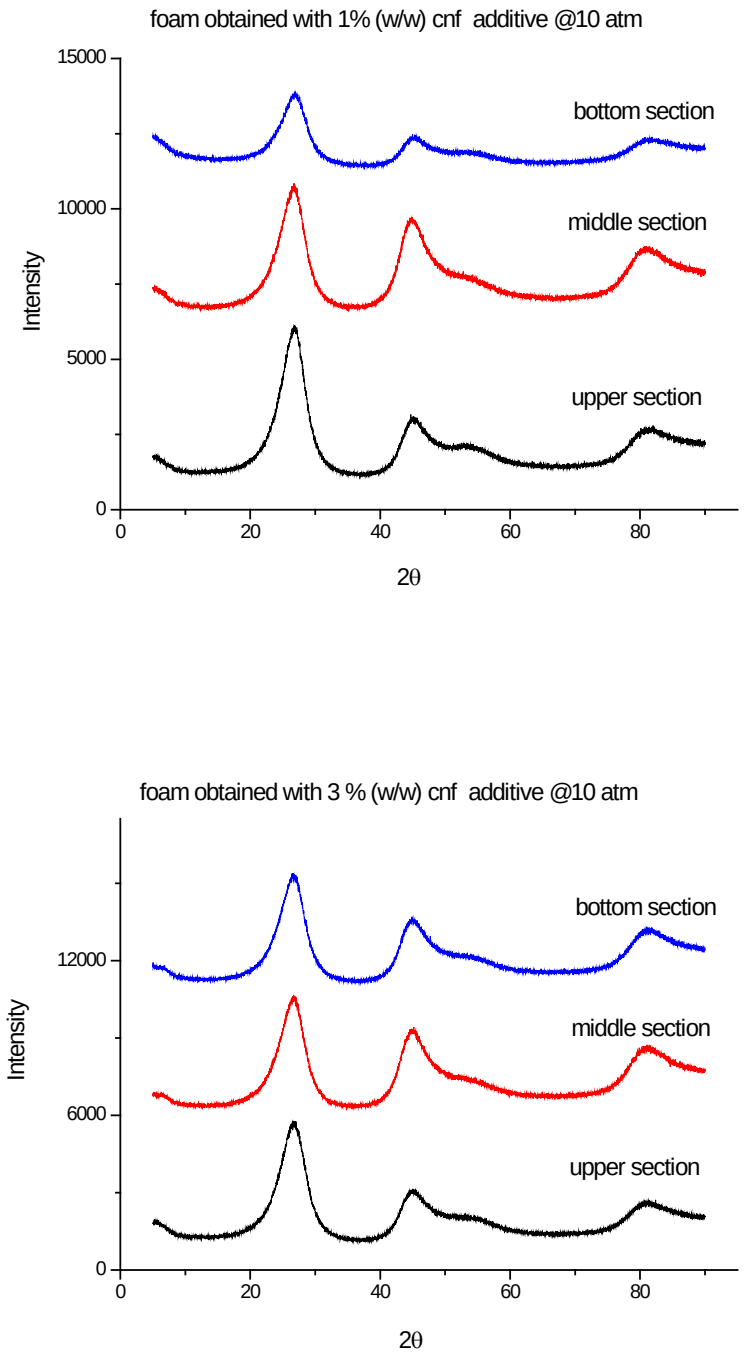

Figure 4.38: XRD patterns of the carbon foams with the addition of CNF produced at 10 atm.

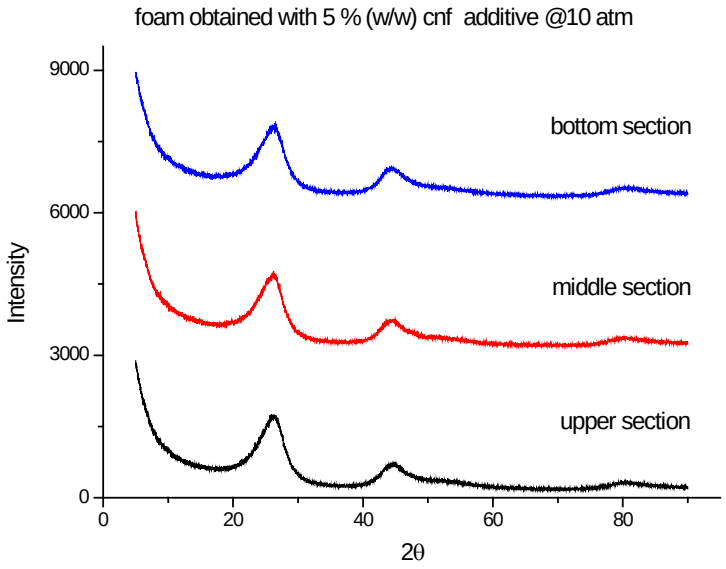

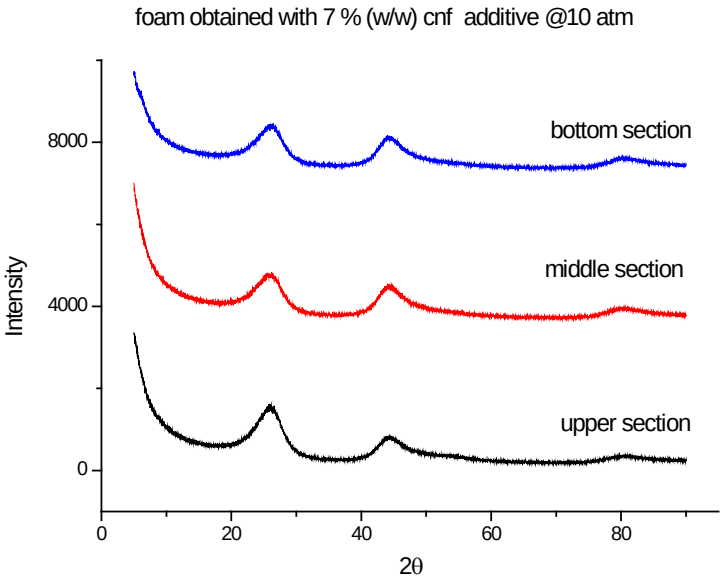

Figure 4.38 (continued) : XRD patterns of the carbon foams with the addition of CNF produced at 10 atm.

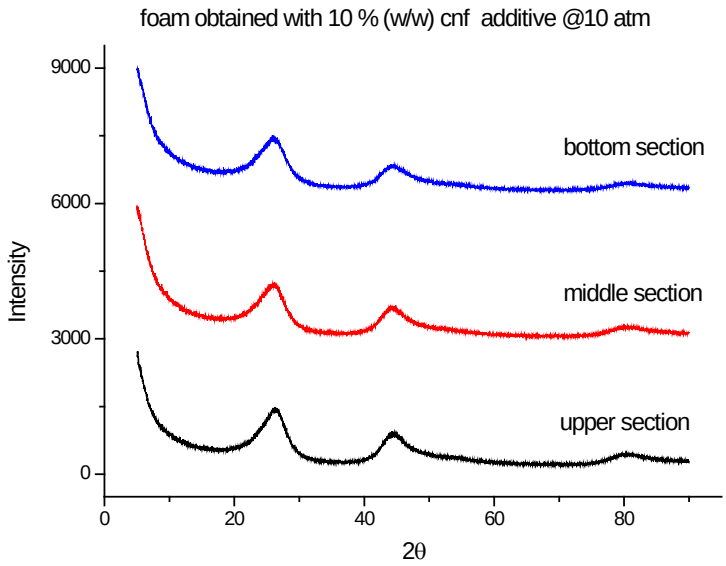

Figure 4.38 (continued) : XRD patterns of the carbon foams with the addition of CNF produced at 10 atm.

The carbon foams without additive and with 3% CNF additive produced at 10 atm were compared in order to get final comparative conclusion in this study. The SEM images of the carbon foams without additive and with 3% CNF additive indicated that the carbon foam without additive showed more difference in the cell structure from top to bottom. The comparison of properties of the carbon foams is shown in Table 4.16. The bulk and skeletal density values of the carbon foam without additive were higher and the porosity values of the carbon foam without additive were lower compared to the carbon foam with the addition of 3% CNF. The compressive strength was higher for the carbon foam without additive compared to the carbon foam with the addition of 3% CNF. Addition of 3% CNF into pitch reduced density and strength of the carbon foam produced. However, the variation in density between each section was lower for the carbon foam with the addition of 3% CNF compared to the carbon foam without additive (see Table B.1).

Figure 4.39 shows the XRD patterns of the carbon foams without additive and with 3% CNF additive produced at 10 atm. The XRD patterns of upper, middle and bottom sections for the carbon foam without additive differed than each other. The (002) peaks intensities and breadth for each section showed difference for the carbon foam without additive. The carbon foam with the addition of 3% CNF had almost identical XRD patterns for each section. The (002) peaks of each section showed similar intensities and breadth for the carbon foam with the addition of 3% CNF.

As a conclusion; the carbon foam with 3% CNF additive showed more uniform cell structure and close of density and XRD values in each section compared to all other produced carbon foams, at 5 and 10 atm.

Table 4.16 : Comparison between CF10-0 and CF10-3.

Sample	**CF10-0**			**CF10-3**		
	U	**U**	**B**	**U**	**M**	**B**
CNF content (%)	0			0		
Skeletal density (g/cm^3)	1.9848	2.3660	2.2498	1.9355	2.1132	1.9594
Bulk density (g/cm^3)	0.071	0.112	0.095	0.062	0.070	0.064
Porosity (%)	96.42	95.27	95.78	96.80	96.69	96.73
Interlayer spacing of d_{002} (nm)	0.3358	0.3372	0.3378	0.3363	0.3364	0.3366
L_c (nm)	1.7709	1.6760	1.5893	1.7568	1.7566	1.7565
Compressive strength (MPa)	0.69			0.33		

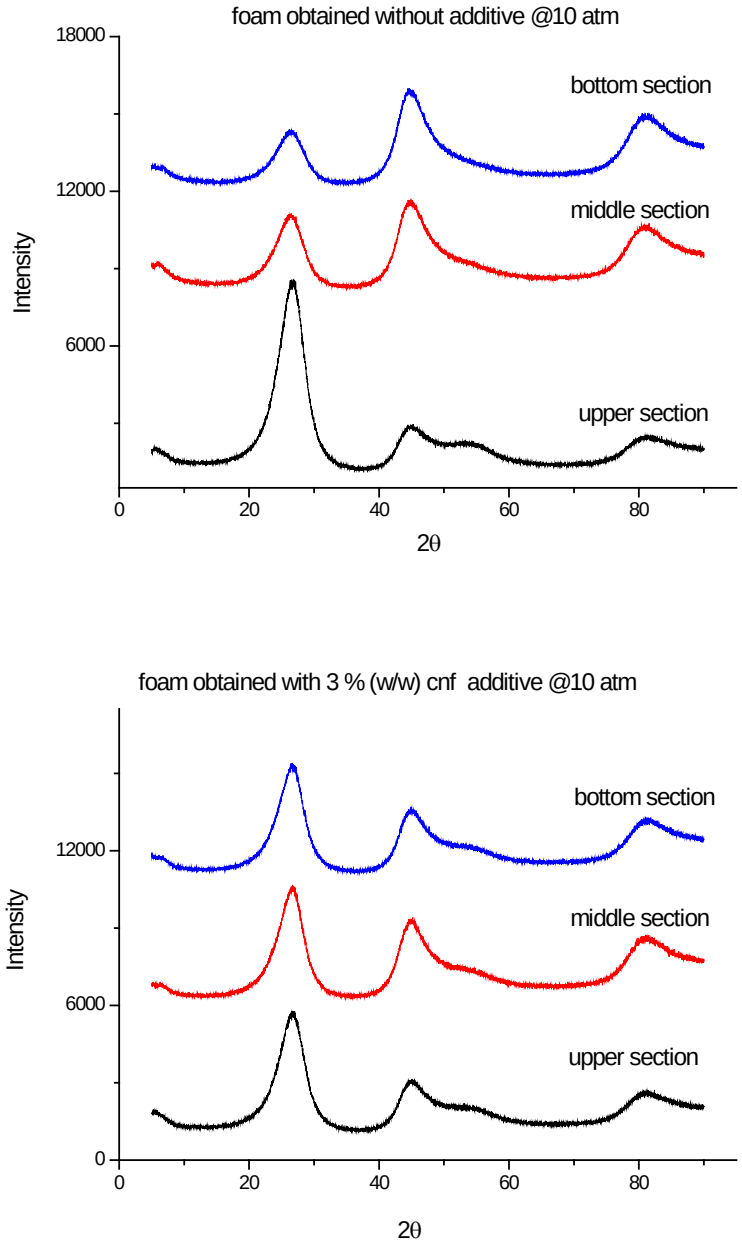

Figure 4.39 : XRD patterns of the carbon foams without additive and with the addition of 3% CNF produced at 10 atm.

5. CONCLUSIONS AND RECOMMENDATIONS

5.1 Conclusions

In this study, the effect of pressure and carbon nanofiber additive on the properties of carbon foam was investigated. The general results were summarized as follows:

1. General comparison results for the carbon foams without additive produced at 5 and 10 atm;
    a. The values of density and strength of the carbon foams increased with the increasing operating pressure.
    b. The porosity values of the carbon foams exhibited a decreasing trend with increasing operating pressure.
    c. The middle sections of the carbon foams produced at 5 and 10 atm were denser than upper and bottom sections
    d. The bottom sections of the carbon foams produced at 5 and 10 atm were denser than upper sections.
    e. Due to less dense structure in 5 atm samples, the stack heights (L_c) were lower and the interlayer spacings (d_{002}) were higher than 10 atm samples.
2. General results of CNF additives for the carbon foams produced at 5 atm;
    a. The bulk and skeletal density values of the carbon foams decreased with the increase in amount of CNF additive.
    b. The densities in bottom sections were always higher than upper sections and the middle sections were always denser than bottom sections.
    c. The porosity of foams increased with the increase in amount of CNF additive.

d. The compressive strengths of foams were inversely proportional with the amount of CNF additive.
e. The addition of CNF into pitch usually caused an increase in the d_{002} values and a decrease in the L_c values.
f. The SEM images for carbon foams with CNF additive showed that the formations of the cells were not well developed at bottom sections. Non-spherical cell formations decreased at middle sections. Well formed cells with interconnected pores were mostly observed at upper sections.

3. General results of CNF additives for the carbon foams produced at 10 atm;
    a. The bulk and skeletal density of the carbon foams exhibited a decreasing trend with increasing amount of additive. The porosity of the carbon foams increased with the decrease in density. The compressive strength of the carbon foams reduced with increasing porosity.
    b. The densities in bottom sections were always higher than upper sections and the middle sections were always denser than bottom sections.
    c. The addition of CNF into pitch usually caused an increase in the d_{002} values and a decrease in the L_c values.
    d. The SEM images stated that the cell formation at the bottom sections was relatively low compared to upper and middle sections. At middle sections, these textures seemed to be modified towards a comparatively more regular structure. At upper sections, the cell formation was more developed. Cells had more clear boundaries and ligaments compared to middle and bottom sections.
4. General comparison results of CNF additives for the carbon foams produced at 5 and 10 atm;
    a. The bulk and skeletal density values of the carbon foam samples increased with increase in operating pressure.
    b. The porosity decreased with increasing pressure. Since compressive strength was inversely proportional with porosity, carbon foams

having higher density presented much higher compressive strength. Therefore, the carbon foams produced at 10 atm showed higher strength compared to the carbon foams produced at 5 atm.

c. The stack heights (L_c) were usually lower and the interlayer spacings (d_{002}) were usually higher for the samples obtained at 5 atm compared to the samples obtained at 10 atm.

5. The percent change in density from top to bottom were the lowest for the carbon foam with 3% CNF additive compared to all other produced carbon foams, at 10 atm.
6. The least variation in properties (cell formation, density, and XRD values) between each section was obtained for the carbon foam with 3% CNF additive produced at 10 atm compared to all other carbon foams produced at 5 and 10 atm. The carbon foam with 3% CNF additive produced at 10 atm represented an ideal structure in terms of density distribution, cell structure, crystallography, and strength.

5. 2 Recommendations and Future Work

Investigation and characterization of the carbon foam under different process conditions were studied. As a result of the findings of this study, following research topics may be considered for further investigation:

- To modify process conditions in order to find specific application areas for the carbon foam produced at low pressure and with CNF additive.
- To investigate the effect of various kinds of additive on the foam structure and properties.
- Further heat treatment to improve the thermal and electrical properties and characterization of the further thermal treated sample.

REFERENCES

[1] **Bonzom A., Crepaux A.P., Moutard AM.,** (1981). Process for preparing pitch foams and products so produced, *United States Patent*, No: 4276246 dated 30.06.1981.

[2] **Kearns K.M., (**1999). Process for preparing pitch foams, *United States Patent*, No: 5868974 dated 09.02.1999.

[3] **Kearns K.M., (**1999). Pitch foams products, *United States Patent*, No: 5961814 dated 05.10.1999.

[4] **Wang M.X., Wang CY, Li Y.L, Zhang C.,** (2007). The use of optical microscopy to detect the bubble shape of carbon foams, *Carbon*, **45**, 687–689.

[5] **Gallego N.C., Klett J.W.,** (2003). Carbon foams for thermal management, *Carbon*, **41**, 1461–1466.

[6] **Li T.Q., Wang C.Y., An B.X., Wang H., (**2005). Preparation of graphitic carbon foam using size-restriction method under atmospheric pressure, *Carbon*, **43**, 2030–2032.

[7] **Klett J.W.,** (2001). Pitch-based carbon foams and composites, *United States Patent,* No: 6261485 dated 17.07.2001.

[8] **Klett J.W.,** (2000). Process for making carbon foams, *United States Patent,* No: 6033506 dated 07.03.2000.

[9] **Klett J.W., McMillan A.D., Gallego N.C., Burchell T.D., Walls C.A**., (2004). The role of structure on the thermal properties of graphitic foams, *Journal of Materials Science*, **39**, 3659-3676.

[10] **Gaies D., Faber K.T.,** (2002). Thermal properties of pitch derived graphite foam, *Carbon*, **10**, 1131-1150.

[11] **Chen A., Kennel E.B., Stiller A.H., Elliot B. K., Alfred H. S., Peter G. S., John W. Z**., (2006). Carbon foam derived from various precursors, *Carbon* , **44**, 1535-1543.

[12] **Klett J.W., Hardy R., Romine E., Walls C., Burchell T., (**2000). High thermal conductivity, mesophase pitch derived carbon foams: effect of precursor on structure and properties, *Carbon*, **40**, 953–973.

[13] **Druma A.M., Alam M.K., Duruma C.,** (2004). Analysis of thermal conduction in carbon foams, *International Journal of Thermal Sciences*, **43**, 7, 689-695.

[14] **Shin S., Roy A.K.,** (2004). Modelling and prediction of bulk properties of open-cell carbon foam, *Journal of the Mechanics and Physics of Solids*, **52**, 1, 167-191.

[15] **Beechem T, Lafdi K, Elgafy A**., (2005). Bubble growth mechanism in carbon foams, *Carbon*, **43**, 1055–1064.

[16] **Rosebrock G, Elgafy A, Beechem T, Lafdi K.**, (2005). Study of the growth and motion of graphitic bubbles, *Carbon*, **43**, 3075–3087.

[17] **Wang M, Wang C, Chen M, Li T, Hui Z.**, (2009). Bubble growth in the preparation of mesophase-pitch-based carbon foams, *New Carbon Materials*, **24**, 61–66.

[18] **Klett J.W., McMillan A.D., Gallego N.C., Burchell T.D., Walls C.A.,** (2004). Effects of heat treatment conditions on the thermal properties of mesophase pitch-derived graphitic foams, Carbon, **42**, 1849-1852.

[19] **Hardcastle, L.A., Sheppard, R.G., Dingus, D.F.,** (2002). Process for making carbon foam induced by process depressurization, *United States Patent*, No: 190414 dated 19.12.2002.

[20] **Luo R., Ni Y., Li J., Yang C., Wang S.,** (2011). The mechanical and thermal insulating properties of resin-derived carbon foams reinforced by $K_2Ti_6O_{13}$ whiskers, *Materials Science and Engineering: A*, **528**, 4-5, 2023-2027.

[21] **Fawcett W., Shetty D.K.,** (2010). Effects of carbon nanofibers on cell morphology, thermal conductivity and crush strength of carbon foam, *Carbon*, **48**, 68-80.

[22] **Li W.Q., Zhang H.B., Xiong X., Xiao F.,** (2010). Influence of fiber content on the structure and properties of short carbon fiber reinforced carbon foam, *Materials Science and Engineering: A*, **527**, 27-28, 7274-7278.

[23] **Wang S., Luo R., Ni Y.,** (2010). Preparation and characterization of resin-derived carbon foams reinforced by hollow ceramic microspheres, *Materials Science and Engineering: A*, **527**, 15, 3392-3395.

[24] **Li W.Q., Zhang H.B., Xiong X., Xiao F.,** (2010). Effect of zirconium addition on the microstructure and performance of carbon foam, *Materials Science and Engineering: A*, **527**, 12, 2993-2997.

[25] **Wang X., Luo R., Ni Y., R. Z., Wang S.,** (2009). Properties of chopped carbon fiber reinforced carbon foam composites, *Materials Letters*, **63**, 1, 25-27.

[26] **Wu X., Luo R., Ni Y., Xiang Q.,** (2009). Microstructure and mechanical properties of carbon foams and fibers reinforced carbon composites densified by CLVI and pitch impregnation, *Composites Part A: Applied Science and Manufacturing*, 40, 2, 225-231.

[27] **Wang,Y.,Xu,Z ,An,Q.Q , Wang,Y.M .,** (2007). High strength and high thermal conductivity carbon foam reinforced with graphite nanoparticles, *Cellular Polymers*, **26**, 5, 305-312.

[28] **Marsh, H.,** (1997). Carbon materials: an overview of carbon artifact, *Introduction to Carbon Technologies*, pp 1-34, Eds. Marsh, H., Heintz, E.A., and Rodriguez-Reinoso, F., Universaded de Alicante, Secretariade de Publicaciones.

[29] **Savage.G.,** (1993). *Carbon-Carbon Composites*, pp1-10, Chapman & Hall, London, UK.

[30] **Url-1**<*http://www.edinformatics.com/math_science/c_atom.htm*>, dated retrieved 03.11.2011.

[31] **Burchell,T**., (1999). Structure and Bonding in Carbon Materials, *Carbon Materials for Advanced Technologies*, p1-29, Amsterdam, New York, Pergamon.

[32] **Url-2**<*http://en.wikipedia.org/wiki/Diamond*>, dated retrieved 03.11.2011.

[33] **Url-3**<*http://www.chemguide.co.uk/atoms/structures/giantcov.html*>, dated retrieved 03.11.2011.

[34] **Url-4**<http://www.azonano.com/article.aspx?ArticleID=1858>, dated retrieved 03.11.2011.

[35] **Url-5**<*http://smarteconomy.typepad.com/smart_economy/2008/01/ what-came-befor.html* >, dated retrieved 03.11.2011.

[36] **Marsh,H.,** (2000). Structure in Carbons and Carbon Artifacts, *Science of carbon materials*, pp1-90, Eds: Marsh, H., Rodriguez-Reinoso, F., Universaded de Alicante, Secretariade de Publicaciones.

[37] **Marsh,H.,** (1989). Carbon Forms, *Introduction to Carbon Science*, pp10-15, Butterworth & Co. Ltd, England.

[38] **Ford W**., (1964). Method of making cellular refractory thermal insulating material, *United States Patent*, No: 3121050 dated 11.02.1964.

[39] **Googin, J., Napier, Scrivner, J.M.**, (1967). Method for manufacturing foam carbon products, *United States Patent*, No: 3345440 dated 3.10.1967

[40] **Vinton, C.S., Franklin, C. H., (**1977). Method for the preparation of vitreous carbon foams, *United States Patent*, No: 4022875 dated10.05.1977.

[41] **Raley et. al.,** (1976). Process for preparing macroporous open-cell carbon foam from normally crystalline vinylidene chloride polymer, *United States Patent*, No: 3960770 dated 01.06.1976.

[42] **Luhleich, H., et. al.**, (1975). Method of making carbonaceous bodies, *United States Patent*, No: 3927187 dated 16.12.1975.

[43] **Vinton, C., Franklin, C.,** (1975). Method for the preparation of carbon structures, *United States Patent*, No: 3927186 dated 16.12.1975.

[44] **Hopper et. al.,** (1988). Low density microcellular carbon or catalytically impregnated carbon foams and process for their preparation, *United States Patent*, No: 4756898 dated 12.07.1988.

[45] **Klett et. al., (**2000). Method for extruding pitch based foam, *United States Patent*, No: 6344159 dated 05.02.2002.

[46] **Klett, J., Burchell, T.,** (2002). Pitch Based Carbon Foam Heat Sink with Phase Change Material, *United States Patent*, No: 6399149 dated 04.06 2002.

[47] **Simandl,R. F., Brown, J. D.,** (1994). Microcellular carbon foam and method, *United States Patent*, No: 5300272 dated 05.04. 1994.

[48] **Kanno, K., Tsuruya, H., Fujiura, R., Koshikawa, T., Watanabe, F.**, (2004). *Carbon foam*, graphite foam and production processes of these, *United States Patent*, No: 6689336 dated 10.2.2004.

[49] **Tan,S.C**., (2002). Microcellular carbon foams and microcellular C/C composites fabricated therefrom, *United States Patent*, No: 6339031 dated 15.2.2002.

[50] **Murdie M., Parker C. A., Pigford J. F., Narasimhan D.; Dillon F.**, (2002). Process of stabilizing a carbonaceous pitch-based foam, *United States Patent*, No: 6342171 dated 29.6.2002.

[51] **Rogers D.K.**, (2004). Cellular coal products and processes, *United States Patent* No: 6814765 dated 9.11.2004.

[52] **Rogers D.K.**, **Plucinski J.W.**, (2003). Blended pitch/coal based carbon foams, *United States Patent*, No: 6656239 dated 2.12.2003.

[53] **Rogers, D. K.**, (2004). Petroleum pitch-based carbon foam, *United States Patent*, No: 6833012 dated 21.12.2004.

[54] **Mochida, I., Korai, Y., Ku, C., Watanabe F., Sakai, Y., 2000**. Chemistry of synthesis, structure, preparation and application of aromatic-derived mesophase pitch, *Carbon*, **38**, 305-328.

[55] **Murdie et al.,** 1993. Carbon-Carbon Matrix Materials, *Carbon-Carbon Materials and Composites*, Noyes Publications, Park Ridge, N.J., 105-167.

[56] **Murdie N., Parker C.A., Pigford J.F., Narasimhan D., Dillon F.**, (2001).Carbon-carbon composite material made from densified *carbon foam, United States Patent*, No: 6323160 dated 27.11.2001.

[57] **Klett J. W**., (2003). Pitch-based carbon foam and composites, *United States Patent*, No: 6656443 dated 02.12.2003.

[58] **Prasad K.R., Munichandraiah N.**, (2002). Electrocatalytic efficiency of polyaniline by cyclic voltammetry and electrochemical impedance spectroscopy studies, *Synthetic Metals*, **126**, 61-68.

[59] **Stiller A. H., Stansberry P. G.**, **Zondlo J. W., (**2002). Method of making a carbon foam material and resultant product, *United States Patent*, No: 6346226 dated 12.02. 2002.

[60] **Chen W., Wen T., Teng H.**, (2003). Polyaniline-deposited porous carbon electrode for supercapacitor, *Electrochimica Acta ,* **48**, 641-649.

[61] **Murdie N., Parker, C. A., Pigford, J. F., Narasimhan, D., Dillon, F.**, (2000). Process of making carbon-carbon composite material made from densified carbon foam, *United States Patent*, No: 6077464 dated 20.06. 2000.

[62] **Zhang Q., Zhoua X., Yang H.,** (2004). Capacitance properties of composite electrodes prepared by electrochemical polymerization of pyrrole on carbon foam in aqueous solution, *Journal of Power Sources*, **125**, 141–147.

[63] **Knippenberg W.F., Lersmacher B.,** (1976). Carbon Foam, *Philips Technical Review*, **36** (4), 93-103.

[64] **Arnold J.R., Aubert J.H., Clough R.L., Rand P.B., Sylwester A.P., (**1989). Low-density microcellular carbon foams and method of preparation, *United States Patent*, No: 4832881 dated 23.05.1989.

[65] **Landrock A. H.,** (1995). Thermosetting foams, *Handbook of Plastic foams Types, properties, Manufacture and applications*, pp 11-139, Ashida, K., Iwasaki K., Noyes Publications, Park Ridge, New Jersey, U.S.A.

[66] **Url-6**<http://www.ergaerospace.com/RVC-properties.htm>, dated retrieved 03.11.2011.

[67] **Pekala R.W., Hopper R.W.,** (1987). Low-density microcellular carbon foams, *Journal of Materials Science*, **22**, 5, 1840–1844.

[68] **Benton S.T., Schmitt C.R.,** (1972). Preparation of syntactic carbon foam, *Carbon*, **10,** 2, 185–190.

[69] **Nicholson J., Thomas C.R.,** (1973). Syntactic carbon foams, *Carbon*, **11**, 1, 65–66.

[70] **Mercuri R.A., Wessendorf T.R., Criscione J.M.**, (1968). Carbon foam: its preparation and properties, PreprPap-AmChem Soc, Div Fuel Chem, 1**2**, 4, 103–108.

[71] **Fay T.F, Ferla R.L., Sherman A.J., Stankiewicz E.P.,** (2000). Foam catalyst support for exhaust purification. *United States Patent*, No: 6040266 dated 21.03.2000

[72] **Duffy A.J., Kaplan R.B., Racik S.A., Stankiewicz E.P., Tuffias R.H., Williams B.E.**, (1994). Filter and method of forming. *United States Patent*, No: 5372380 dated 13.12.1994

[73] **Stankiewicz E.P.,** (2000). Method for producing controlled aspect ratio reticulation carbon foam and the resultant foam, *United States Patent*, No: 6103149 dated 15.08.2000.

[74] **Shiwen L., Quangui G., Jingli S.,Lang L.,** (2010). Preparation of phenolic- based carbon foam with controllable pore structure and high compressive strength, *Carbon*, **48**, 2644 –2673.

[75] **Tsyntsarski B., Petrova B., Budinova T., Petrov N., Krzesinska M., Pusz S.,Majewska J., Tzvetkov P.,** (2010). Carbon foam derived from pitches modified with mineral acids by a low pressure foaming process, *Carbon*, **48**, 12, 3523-3530.

[76] **Krevelen, D.W**., **(**1993). Coal--typology, physics, chemistry, constitution *Elsevier* Amsterdam, New York.

[77] **Url-7** <http://www.cfoam.com >, dated retrieved 03.11.2011.

[78] **Url-8** <http://www.cfoam.com/pdf/Composite_Tooling_CFOAM.pdf >, dated retrieved 03.11.2011.

[79] **Stiller A.H., Stansberry P.G., Zondlo J. W.,** (2001). Method of making a carbon foam material and resultant product, *United States Patent*, No: 6241957 dated 05.06.2001.

[80] **Stiller, A.H., Yocum, A., Plucinski, J.,** 1999. Method of Making a Reinforced Carbon Foam Material and Related Product, *United States Patent*, No: 6183854 dated 06.02.2001.

[81] **Gibson, L.J., Ashby, M. F., (**1997). *Cellular solids: structure and properties***,** 2^{nd} ed. Cambridge University Press, Cambridge, UK.: 183-234.

[82] **Hager J.W., (**1992). *Materials Research Society Symposium Proceedings*, **270**, 41-46.

[83] **Mochida et al.,** (1995). Carbon fibers from aromatic hydrocarbons, *Chemtech*, **25**, 2, 29-37.

[84] **Marsh, H.**, 2000. Tar and pitch: composition and application, *Science of Carbon Materials*, pp173-203 Eds. Menendez, R., Bermejo, J., Fiqueiras, A., Universaded de Alicante, Secretariade de Publicaciones.

[85] **Mochida I., Yoon S.H., Korai Y., Kanno K., Sakai Y., Komatsu E., (**2000). Mesophase pitch from aromatic hydrocarbons, *Science of Carbon Materials*, pp.1-97, Eds. Marsh., Rodriguez-Reinoso, F., Universaded de Alicante, Secretariade de Publicaciones.

[86] **Url-9** <*http://en.wikipedia.org/wiki/Foam*>, dated retrieved 03.11.2011.

[87] **Ruiying L., Yongfeng N., Jinsong L., Caili Y. Shaobo W.,** (2011). The mechanical and thermal insulating properties of resin-derived carbon foams reinforced by $K_2Ti_6O_{13}$ whiskers, *Materials Science and Engineering A*, **528**, 2023–2027.

[88] **Gül, A,** (2005). Mesophase pitch derived graphitic carbon foam, Graduate School of Science Engineering and Technology, Master's Thesis, Istanbul Technical University, Istanbul, Turkey.

[89] **Gencay, N.,** (2004). A mesophase pitch derived carbon foam: effect of pressure and release time, Graduate School of Science Engineering and Technology, Master's Thesis, Istanbul Technical University, Istanbul, Turkey.

[90] **Eksilioglu, A.,** (2004). Effect of temperature, solvent type and additives on the properties of mesophase pitch based carbon foam, Graduate School of Science Engineering and Technology, Master's Thesis, Istanbul Technical University, Istanbul, Turkey.

[91] **Sipahi M.,** (2006). Influence of thin conductive polymer coating on the morphological and electrical properties of carbon foam, Graduate School of Science Engineering and Technology, Master's Thesis, Istanbul Technical University, Istanbul, Turkey.

[92] **Stiller A.H., Pluncski J., Yocum A.,** Method of making a carbon foam material and resultant product, *United States Patent*, No: 6506354 dated 14.06.2003

[93] **Url-10**<*http://www.ornl.gov/sci/de_materials/documents/8GraphiteFoamsv2.pdf* >, dated retrieved 03.11.2011.

[94] **Brooks J.D.,Taylor G.H.,** (1965). The formation of graphitizing carbons from the liquid phase, *Carbon*, **3**, 185-193.

[95] **Stiller A. H., Stansberry P. G., Zondlo J. W., (**1999). Method of making a carbon foam material and resultant product, *United States Patent*, No: 5888469 dated 30.03.1999.

[96] **Reznek et. al.,** (2002). Carbon foams and methods of making the same, *United States Patent*, No: 6500401 dated 31.12.2002.

[97] **Klett J.W.,** (2002). Pitch-based carbon foam and composites, *United States Patent*, No: 6387343 dated 14.05.2002.

[98] **Klett J.W., Gallego N.C.,** (2003). Carbon foams for thermal management, *Carbon*, **41,** 1461–1466.

[99] **Klett, J.W.,** (1999). High thermal conductivity mesophase pitch-derived carbon foams, *Composites in Manufacturing*, **14,** 4, 1-19.

[100] **Wiechmann, L.,** (2000). Graphite foam with high thermal conductivity and diffusivity conducts heat in all directions, *Material Research Society Bulletin*, 10-11.

[101] **Url-11**<http://www.thirdwave.de/3w/tech/mnt/cfoamoverview.pdf> dated retrieved 03.11.2011.

[102] **Oshida K., Bonnamy S., (**2002). Primary carbonization of an anisotropic mesophase pitch compared to conventional isotropic pitch, *Carbon*, **40**, 2699-2711.

[103] **Miura K., Nakagawa H., Hashimoto K., (**1995). Examination of the oxidative stabilization reaction of the pitch-based carbon fiber through continuous measurement of oxygen chemisorption and gas formation rate, *Carbon*, **33**, 3, 275-282.

[104] **Hugh O., (**1993). Handbook of carbon, graphite, diamond and fullerenes: properties, processing and applications. Noyes Publications, NJ, USA.

[105] **Liedtke V., Hüttinger K. J., (**1996). Mesophase pitches as matrix precursor of carbon fiber reinforced carbon part II: stabilization of mesophase pitch matrix by oxygen treatment, *Carbon*, **34**, 9, 1067-1079.

[106] **RogersD. K., Plucinski J.W.,** (2003). Coal-based carbon foam, *United States Patent*, 6656238 dated December 2, 2003.

[107] **Pierson H.O.,** (1993). Carbon as an element, Handbook of carbon, graphite, diamond, and fullerenes, Noyes Publications, pp1-44, USA

[108] **Mochida I., Yoon S.H., Qiao W.,** (2006). Catalysts in Synthesis of Carbon and Carbon Precursors, *Journal of the Brazilian Chemical Society*, **17**, 6, 1059-1073.

[109] **Teo K.B., Singh C., Chhowalla M., Milne W.I.,** (2003). *Encyclopedia of Nanoscience and Nanotechnology*. Edited by H.S. Nalwa, Catalytic synthesis of carbon Nanotubes and Nanofibers, p 1-22.

[110] **Yoon S.H. , Lim S., Hong S., Qiao W., Whitehurst D. D., Mochida I. , An B., Yokogawa K.,** (2005). A conceptual model for the structure of catalytically grown carbon nano-fibers, *Carbon*, **43**, *9*, 1828-1838.

[111] **Dumanlı, A.G,** (2008). Effect of metal catalyst and tailoring the conditions for CNF/CNT growth through CVD, PhD Thesis, Sabancı University, Istanbul,Turkey.

[112] **Yoon C.M., Long D., Jang S.M. , Qiao W. , Ling L. , Miyawaki J., Rhee C.K. , Mochida I., Yoon S.H.,** (2011). Electrochemical surface oxidation of carbon nanofibers *Carbon*, **49**, 1, 96-105.

[113] **Barbaro P., Bianchini C.,** (2009). Catalysis for sustainable energy production, *Selective synthesis of carbon nanofibers as better catalyst supports for low temperature fuel cells*, Hang, S-H., Jun, M-S, Mochida, I., Yoon S-H ,71-87.

[114] **Tanaka A., Yoon S.H. , Mochida I. ,** (2004). Formation of fine Fe–Ni particles for the non-supported catalytic synthesis of uniform carbon nanofibers *Carbon*, **42**, 7, 1291-1298.

[115] **Yoon S.H., Lim S.,. Song Y, Ota Y., Qiao W., Tanaka A.,** (2004). Mochida I KOH activation of carbon nanofibers, *Carbon*, ***42***, *8-9, 1723-1729*.

[116] **Yoon S.H., S.Lim, Hong S., Mochida I.**, **An B., Yokogawa K.,** (2004). Carbon nano-rod as a structural unit of carbon nanofibers, *Carbon*, **42**, 15, 3087-3095.

[117] **Jang S.M., Miyawaki J., Tsuji M., Mochida I. , Yoon S. H. , Kang F.,**(2010). Preparation of a carbon nanofiber/natural graphite composite and an evaluation of its electrochemical properties as an anode material for a Li–ion battery, *New Carbon Materials*, **25,** 2, 89-96.

[118] **Yoon S.H. , Park C.W., Yang H., Korai Y., Mochida I. , Baker R.T.K, Rodriguez N.M.,** (2004). Novel carbon nanofibers of high graphitization as anodic materials for lithium ion secondary batteries, *Carbon*, **42**,1,21-32.

[119] **Qiao W.M., Lim S.Y., Yoon S.H. , Mochida I. , Ling L.C., Yang J.H**., (2007*)*. Synthesis of crystalline SiC nanofiber through the pyrolysis of polycarbomethylsilane coated platelet carbon nanofiber, *Applied Surface Science*, **253**, 10, 4467-4471

[120] **Baker, R. T. K., Barber, M. A., Harris, P. S., Feates, F. S., Waite, R. J.,** (1972). Nucleation and growth of carbon deposits from the nickel catalyzed decomposition of acetylene, *Journal of Catalyst*, **26**, 1, 51-62.

[121] **De Jong, K. P., Geus, J. W.,** (2000). Carbon nanofibers: Catalytic synthesis and applications, *Cat. Rev. - Sci. Eng*, **42**, 4, 481–510.

[122] **Url-12** < http://www.industrialheating.com/Articles/Feature_Article/ 0b5e3d79d0cb7010V gnVCM100000f932a8c0>, dated retrieved 03.11.2011

[123] **Url-13**<http://www.cfoam.com/fireproofcore.htm>, dated retrieved 03.11.2011

[124] **Url-14**<http://www.cfoam.com/mirrors.htm>, dated retrieved 03.11.2011

[125] **Url-15**<http://www.cfoam.com/finishing.htm>, dated retrieved 03.11.2011

[126] **Klett J, Conway, B.** (1998). Thermomechanical behavior of a graphite foam. Proceedings of the 43rd International SAMPE Symposium and Exhibition, SAMPE, Covina, CA pp. 745-755.

[127] **Klett, J.W.,** (1998) .High thermal conductivity, pitch-based carbon foam, *Proceedings of the 43rd International SAMPE Symposium*, May 31-June 4, Anaheim, California, SAMPE.

[128] **Coursey J.S, Roh, H, Kim J, and Boudreaux P.J.,** (2002). Graphite foam thermosyphon evaporator performance: Parametric investigation of the effects of working fluid, liquid level, and chamber pressure, *Proceedings of the ASME IMECE*, New Orleans, LA, paper No.2002-33733.

[129] **Kyungbin L., Hongkoo R.,** (2005). Thermal characteristics of graphite foam thermosyphon for electronics cooling, *Journal of Mechanical Science and Technology*, **19,** 10, 1932-1938.

[130] **Coursey J.S., Kim J., Kim J.,** (2005). Performance Of Graphite Foam Evaporator For Use, *Journal of Electronic Packaging*, **127**, 127-134.

[131] **Gandikotaa V., Fleischera A.S., (**2009). Experimental investigation of the thermal performance of graphite foam for evaporator enhancement in both pool boiling and an FC-72 thermosyphon, *Heat Transfer Engineering*, **30**, 8, 643–648.

[132] **Klett J.W, McMillan A, Gallego N,** (2002).Carbon foam for electronics cooling. National Laboratory Fuel Cell Annual Report, FY.

[133] **Klett, J.W.,** (2000). Thermal management solutions utilizing high thermal conductivity graphite foams, Oak Ridge National Laboratory, Metals and Ceramic Division, internal report, Tennessee, USA.

[134] **Morgan D.R, Biggers S.B, Grujicic M.** (2004). Engineering, construction, and operations in challenging environments. ASCE, 960-967, Houston TX, USA

[135] **Lafdi K., Mesalhy O., Elgafy A.,** (2008). Graphite foams infiltrated with phase change materials as alternative materials for space and terrestrial thermal energy storage applications, *Carbon*, **46**, 159 –168.

[136] **Klett J.W., Burchell T.D.,** (2007). Pitch-based carbon foam heat sink with phase change material, *United States Patent*, No: 7166237 dated 23.01.2007.

[137] **Zhong Y., Guo Q., Li S., Shi J., Liu L.,** (2010). Heat transfer enhancement of parafin wax using graphite foam for thermal energy storage, *Solar Energy Materials & Solar Cells*, **94**, 1011–1014.

[138] **Spradling DM, Guth RA,** (2003).Carbon foams, Advanced Materials & Processes, Nov., pp. 29-31.

[139] **Url-16**<http://www.ornl.gov/sci/oetd/documents/graphite_foam_2.pdf dated retrieved 03.11.2011.

[140] **Blacker J.M., Merriman D.J.,** (2008). Carbon Foam EMI Shield, *United States Patent*, No: US2008078576 dated 03.04.2008.

[141] **Url-17**<http://www.cfoam.com/emishielding.htm> dated retrieved 03.11.2011

[142] **Chen Y., Chen B., Shi X.C., Xu H., Shang W., Yuan Y., Xiao L.**, (2008). Preparation and electrochemical properties of pitch-based carbon foam as current collectors for lead acid batteries, *Electrochimica Acta*, **53**, 2245–2249.

[143] **Ma L.W., Chen B.Z., Chen Y., Yuan Y.,** (2009). Pitch-based carbon foam electrodeposited with lead as positive current collectors for lead acid batteries, *Journal of Applied Electrochemisty*, **39**, 609–1615.

[144] **Firefly Energy website**. www.Fireflyenergy.com (2009) Technical White Paper.

[145] **Url-18**<http://www.fireflyenergy.com/index.php?option=com_content&task=view&id=204&Itemid=89 dated retrieved 03.11.2011.

[146] **Lucas R., Danford H.,** *(*2009). Case Studies: Low Cost, High-Strength, Large Carbon Foam Tooling, *Sampe Journal*, **45**, 1.

[147] **Klett J.,** (2001). Pitch Based Foam with Particulate, *United States Patent*, No: 6287375 dated 11.09.2001.

[148] **Url-19**<http://www.industrialheating.com/Articles/Feature_Article/ 0b5e3d79d0cb7010VgnVCM100000f932a8c0> dated retrieved 03.11.2011.

[149] **Klett JW, Tee C, Stinton DP, Yu NA.,** (2000). Heat exchangers based on high thermal conductivity graphite foam, *Proceedings Of The 1st World Conference on Carbon*, July 9-15, Berlin, Germany, p.244.

[150] **Hajiesmaili S., Josset S., Bégin D., Huu C. P., Keller N., Keller V.,** (2010). 3D solid carbon foam-based photocatalytic materials for vapor phase flow-through structured photoreactors, *Applied Catalysis A: General,* **382,** 122–130.

[151] **Gallego N.C., Burchell T. D., Klett J. W.,** (2006). Irradiation effects on graphite foam, *Carbon*, **44**, 618–628.

[152] **Davis B. K. and Weber S.*G.*,** (1990). Electrochemical Characterization of a Microcellular Carbon Foam/Epoxy Composite Electrode, *Anal. Chem.*, ***62,*** 1000-1003.

[153] **Url-20**<http://www.mgc.co.jp/eng/products/abc/pdf/ar.pdf> dated retrieved 03.11.2011.

[154] **Endo, M., Hyashi T., Kim Y.A., Muramatsu H.,** (2006). Development and application of carbon nanotubes, *Japanese Journal of Applied Physic*s **45**, 6A,4883–4892.

[155] **Yanagisawa, T., Hayashi T, A. Y. Kim, Fukai Y., Endo M.** (2002). Structure and basic properties of cup-stacked type carbon nanofiber, *Molecular Crystals and Liquid Crystals*, **387**, 167–171.

[156] **Zhao, T.J., Chen D., Dai Y., Yuan W., Holmen A.,** (2007). The effect of graphitic platelet orientation on the properties of carbon nanofiber supported Pd catalysts synthesized by ion exchange. *Topics in Catalyst*, **45**, (1–4), 87–91.

[157] **Van Der Lee, M.K.,** Van Dillen AJ**,** Bitter JH**,** De Jong KP**,** (2005). Deposition precipitation for the synthesis of carbon nanofiber supported nickel catalysts, *Journal of the American Chemical Society,* **127**, 13573–13582.

[158] **Bennett B., Stiller A.,** (2004). Method of making carbon foam at low pressure, *United States Patent*, No: 6797251 dated 28.09.2004.

[159] **Wang, M., Wang, C., Li, T., Hu, Z.,** 2008. Preparation of mesophase-pitch based carbon foams at low pressures, *Carbon*, **46**, 84-91.

[160] **Işıksal E.,** (2009). Stabilizasyon aşaması olmadan karbon köpük üretimi ve proses parametrelerinin incelenmesi, Graduate School of Science Engineering and Technology, Master's Thesis, Istanbul Technical University, Istanbul, Turkey.

[161] **Klett J.W., Burchell T.D., Choudhury A., (**2006). Pitch based carbon foam and composites and use thereof , *United States Patent*, No: 7070755, 04.06.2006.

[162] **Hardcastle L., Sheppard R.G., Dingus D.F.,** (2002). Process for making carbon foam induced by process deppessurization, *United States Patent*, No: 6576168 dated 19.12.2002.

[163] **Eksilioglu, A., Gencay, N., Yardim, M.F., Ekinci, E.,** (2006). Mesophase AR Pitch derived carbon Foam: Effect of Temperature, Pressure and Pressure Release Time, *Journal of Material Science*, **41**, **10**, 2743-2748.

[164] **Klett, J., (**2001). Pitch based foam with particulate, *United States Patent*, No: 6287385, dated 29.03.2001

[165] **Dumont M., Chollon G, Dourges M.A, Pailler R, Bourrat X, Naslain R, Bruneel J.L, Couzi M,** (2002). Chemical, microstructural and thermal analyses of a naphthalene-derived mesophase pitch, *Carbon*, **40**, 9, 1475-1486.

[166] **Li S., Tian Y., Zhong Y., Yan X., Song Y., Guo Q., Shi J., Liu L.,** (2011). Formation mechanism of carbon foams derived from mesophase pitch, *Carbon*, **49**, 2, 618-624.

[167] **Wang M., Wang C., Chen M., Li T.,Hu Z.,** (2009). Bubble growth in the preparation of mesophase-pitch-based carbon foams, *New Carbon Materials*, **24**, 1, 61-66.

[168] **Beauharnois M. E., Edie D. D., Thies M. C.,** (2001). Carbon fibers from mixtures of AR and supercritically extracted mesophases, *Carbon*, **39**, 2101–2111.

[169] **Straatman A.G., Gallego N.C., Thompson B.E., Hangan H.,** (2006). Thermal characterization of porous carbon foam—convection in parallel flow, *International Journal of Heat and Mass Transfer*, **49**, 1991–1998.

[170] **Wang M., Wang C-Y, Li T-Q, Hu Z-J,** (2008). Preparation of mesophase-pitch-based carbon foams at low pressures, *Carbon*, **46**, 1, 84-91.

[171] **Yadav A., Kumar R., Bhatia G., Verma G.L.,** (2011*).* Development of mesophase pitch derived high thermal conductivity graphite foam using a template method *Carbon*, **49**, 11, 3622-3630.

[172] **Li T-Q, Wang C-Y, An B-X, Wang H.,** (2005). Preparation of graphitic carbon foam using size-restriction method under atmospheric pressure, *Carbon*, **43**, 9, *2030-2032.*

[173] **Fathollahi B., Zimmer J.,** (*2007).* Microstructure of mesophase-based carbon foam,*Carbon*, **45**, 15, 3057-3059.

[174] **Lifshin, E.,** (1999). *X-ray Characterization of Materials*, Wiley-VCH, Germany.

[175] **Suryanarayana, C, Norton, G.M., (**1998). *X-ray Diffraction: a practical approach*, Plenum Press, USA.

[176] **Savage,G.,** (1993). *Carbon Carbon Composites*, pp13-26, Chapman&Hall, London, UK.

[177] **El-Baradie EM, Shoeib MA, Maamoun MA.** (2005). Pore-size effect on the properties of open-cell Al–Ni foam. *Materials Research Innovations*, **9**, 19–20.

[178] **Tondi G., Fierro V., A. Pizzi, Celzard A.** (2009). Tannin-based carbon foams, *Carbon*, **47**, 1480 –1492.

[179] **Celzard A., Zhao W., Pizzi A., Fierro V.,** (2010). Mechanical properties of tannin-based rigid foams undergoing compression, *Materials Science and Engineering: A*, **527**, 16–17, 4438-4446.

[180] **Tondi G, Zhao W, Pizzi A, Du G, Fierro V, Celzard A.** (2009). Tannin-based rigid foams: a survey of chemical and physical properties, *Bioresource Technology*, **100**, 21, 5162-9.

[181] **Celzard A., Fierro V., Amaral-Labat G., Pizzi A., Torero J.,** (2011). Flammability assessment of tannin-based cellular materials, *Polymer Degradation and Stability*, **96**, 4, 477-482

[182] **Tondi G, Blacher S., Léonard A., Pizzi A., Fierro V., Leban J.M., Celzard A.,** (2009). X-ray microtomography studies of tannin-derived organic and carbon foams, *Microscopy and Microanalysis*, **15**, 5, 384-394.

[183] **Lu Y., Li Z., Wang P., Yang C.,** (2011). Preparation of mesophase pitch-based carbon foams with supercritical toluene, *Journal of Applied Polymer Science*, **121**, 1, 336–341.

[184] **Li J., Wang C., Cheng G., Wang Y.L., Zhan L., Qiao W.M., Ling L.C.,** (2010). Preparation of carbon foams with supercritical, toluene *Journal of Porous Materials*, **17**, 6, 685-691.

[185] **Gallego N.C., Klett J.W., McMillan A.D.,** (2003). Effects of processing conditions on properties of carbon foam. http://www.ornl.gov/~webworks/cppr/y2001/pres/114424.pdf.

[186] **Wang Y.G., Min Z.H., Cao, M., Xu D.P.,** (2009). Effect of heating conditions on pore structure and performance of carbon foams, *New carbon materials*, **24**, 4, 321-326.

[187] **Zhang Z., Wang F., Yu X., Wang Y., Yan Y., Li K., Luan Z.,** (2009). Porous silicon carbide ceramics produced by a carbon foam derived from mixtures of mesophase pitch and Si particles, *Journal of the American Ceramic Society*, **92**, 1, 260–263.

[188] **Wang M.X., Wang C.Y., Li T.Q., Hu Z.J.,** (2008). Preparation and characterization of mesophase-pitch-based foam/natural graphite composites, *Composites Science and Technology*, **68**, 10–11, 2220-2223.

[189] **Hu H.L., Hwang J.D., Ko T.H**., (2009). The structure of the carbon foam derived from mesophase coal-tar pitch, *Mater. & Chem. Res. Lab.*, 678 – 680.

[190] **Li, S., Guo,Q., Song,Y., Shi,J., Liu L.,** (2010). Effects of pitch fluoride on the thermal conductivity of carbon foam derived mesophase pitch, *Carbon*, **48**, 1312-1320.

[191] **Wang, X., Zhong,J., Wang,Y., Yu,M.,** (2006). A study of the properties of carbon foam reinforced by clay, *Carbon*, **44**, 1560-1564.

[192] **Sihn S., Roy A.K.,** (2004). Modelling and prediction of bulk properties of open-cell carbon foam, *Journal of the Mechanics and Physics of Solids*, **52**,167 – 191.

APPENDICES

APPENDIX A : Electron microscopy images of HCNF

APPENDIX B : Table of the percentage of changes in some properties of produced carbon foams, 10 atm

APPENDIX C :SEM images of Carbon nanofibers located in the carbon foam produced

APPENDIX D : The general properties of various carbon foam

APPENDIX A

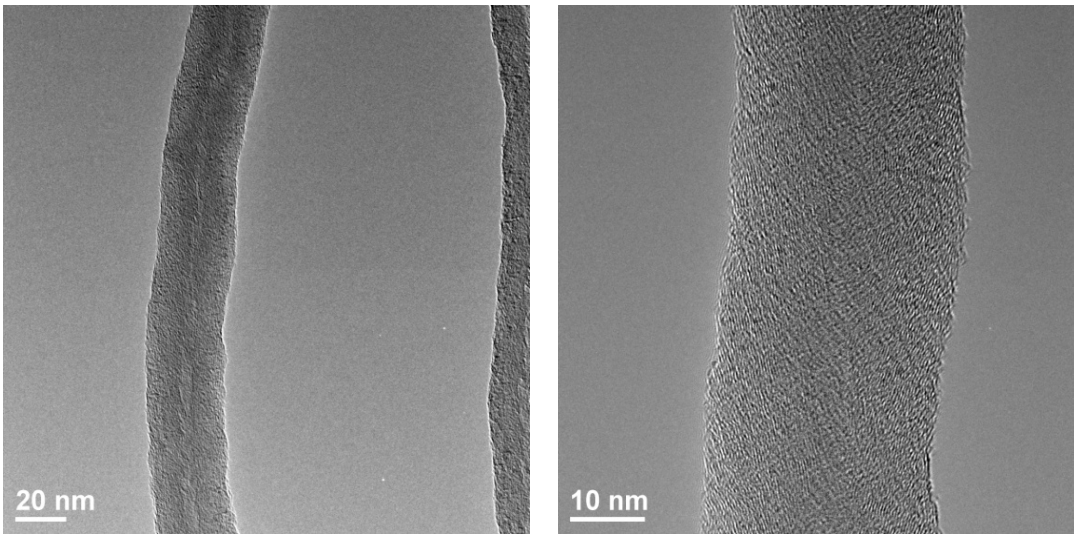

Figure A.1: TEM images of HCNF.

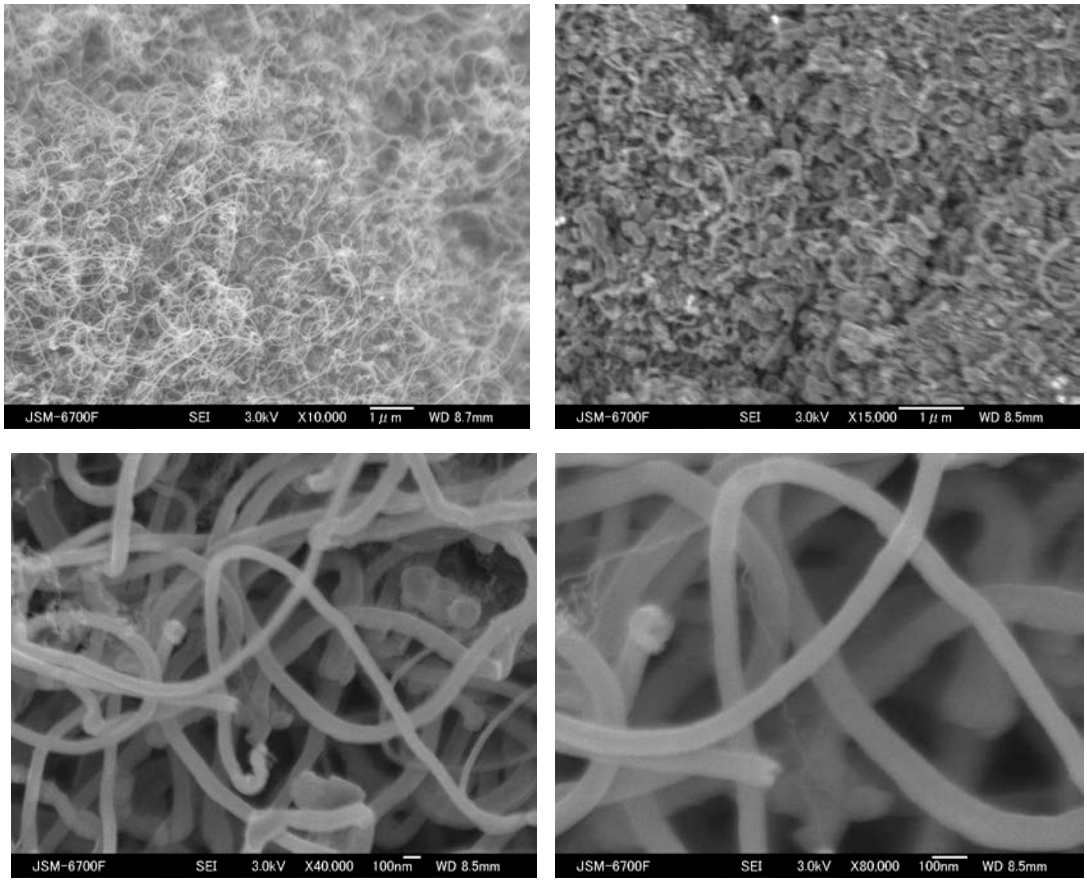

Figure A.2: SEM images of HCNF.

APPENDIX B

Table B.1 : The percentage of changes in some properties of produced carbon foams, at 10 atm.

Sample	**CF10-0**		**CF10-1**		**CF10-3**		**CF10-5**		**CF10-7**		**CF10-10**	
	U-M	**U-B**	**U-M**	**U-B**	**U-M**	**U-B**	**U-M**	**U-B**	**U-M**	**U-B**	**U-M**	**U-B**
Skeleton density difference (%)	19.2	13.4	9.0	4.4	9.2	1.1	18.5	7.9	11.6	3.1	12.9	5.2
Bulk density difference (%)	57.7	33.8	22.4	7.5	12.9	3.2	26.4	9.4	21.6	11.8	20.0	8.9

U-M: percentage of differences between upper section and middle section
U-B: percentage of differences between upper section and bottom section

APPENDIX C

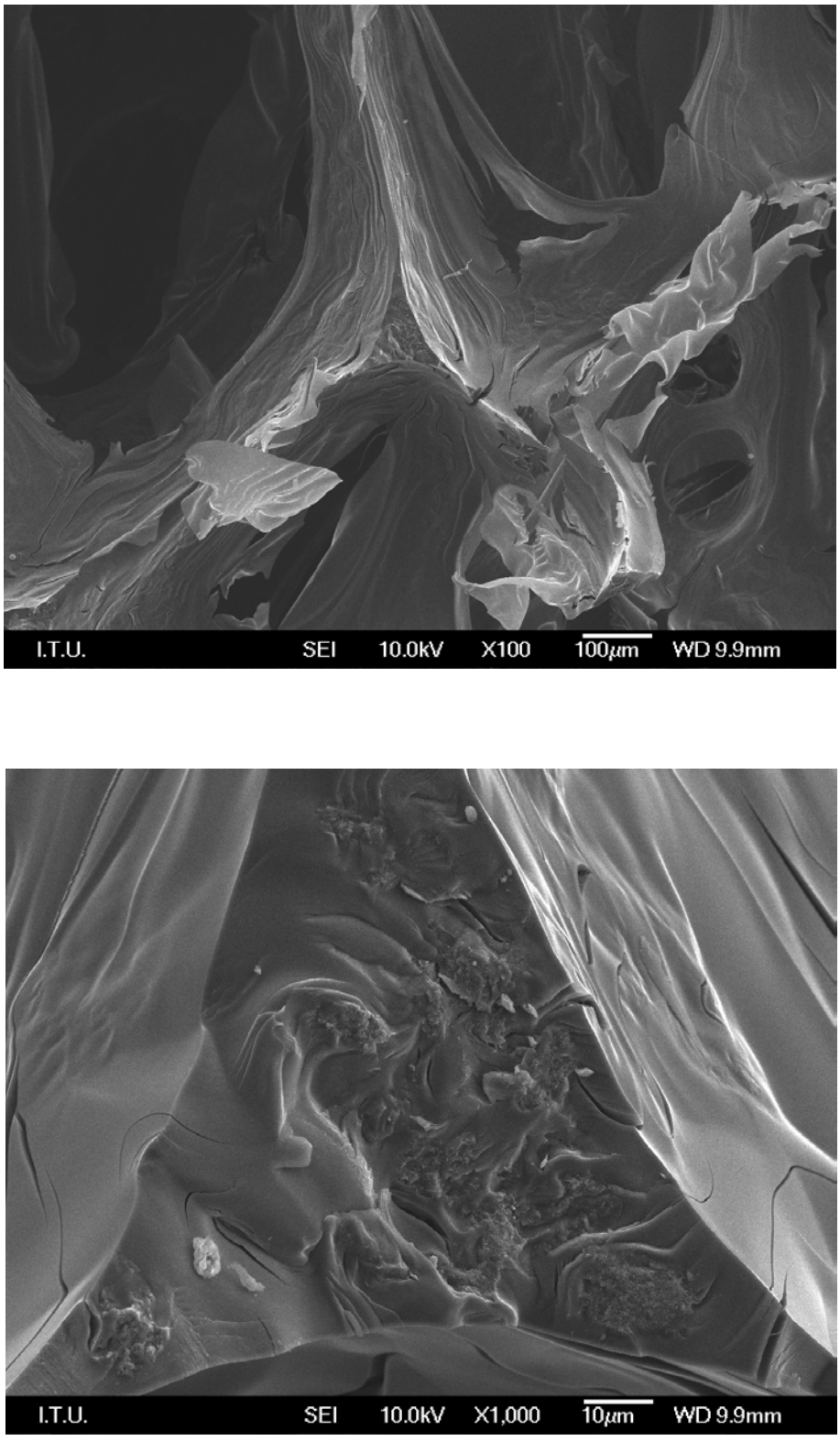

Figure C.1: Carbon nanofibers located in foam junction area (CF10-3).

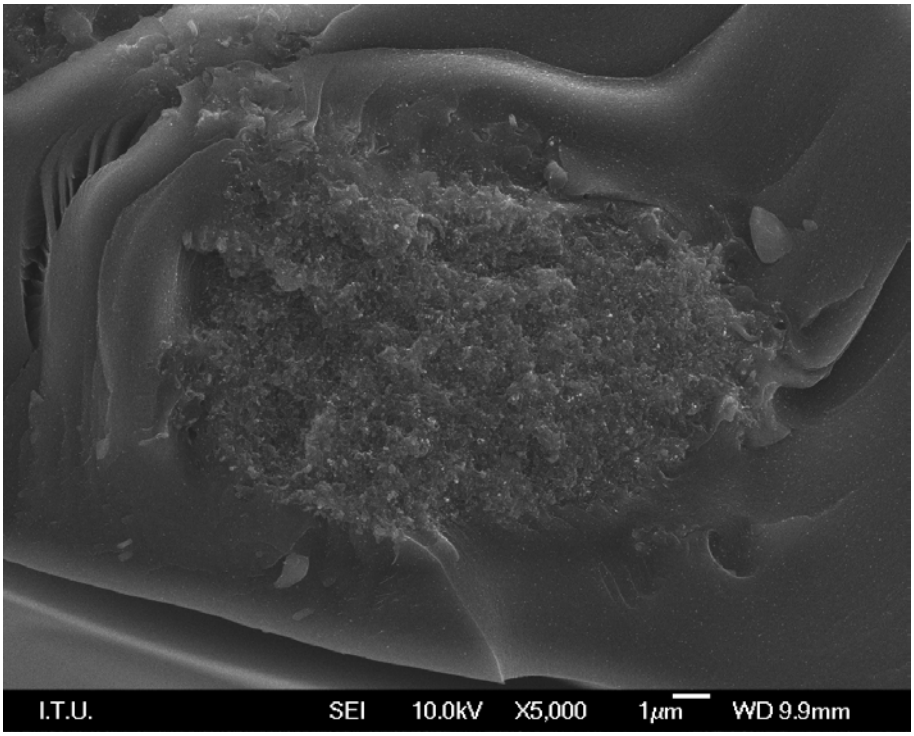

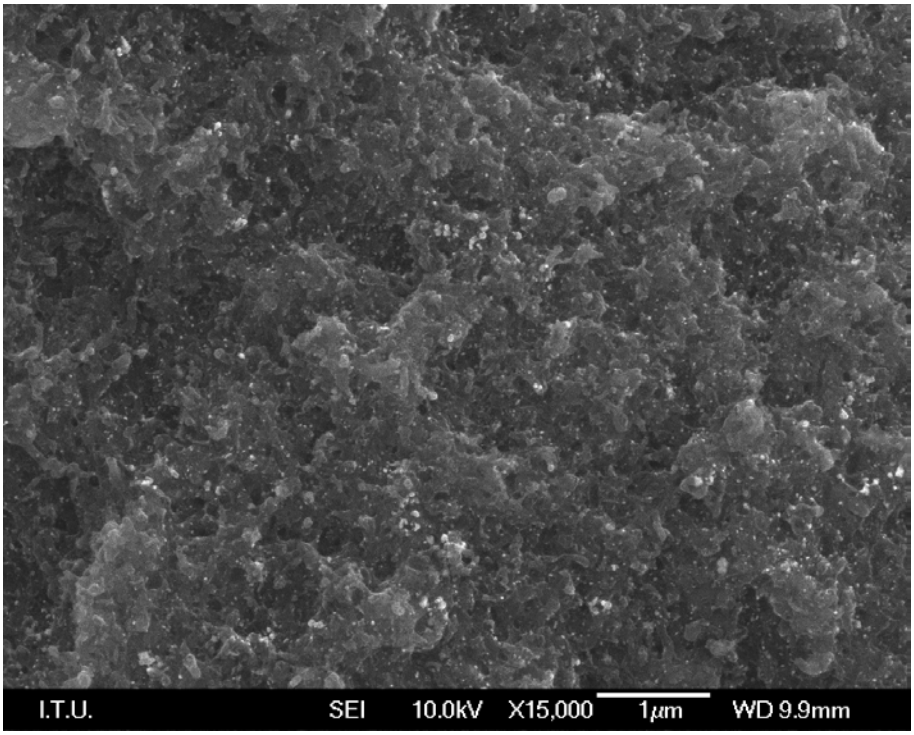

Figure C.1 (Continued): Carbon nanofibers located in foam junction area (CF10-3).

APPENDIX D

Table D.1 : The general properties of various carbon foams.

Pitch	Max. Heat Temperature (^oC)	Foaming pressure (psi)	d spacing (nm)	L_a (nm)	Bulk density (g/cm^3)	Porosity (%)
AR [161]	1000	400			0.22	
AR [161]	1000	600			0.37	
AR [161]	1000	800			0.44	
AR [161]	1000	1000	0.3362	20.30	0.54	
AR [161]	2800	400	0.3364	11.80	0.25	
AR [161]	2800	600	0.3362	17.80	0.39	
AR [161]	2800	800	0.3360	21.50	0.48	
AR [161]	2800	1000	0.3356	21.40	0.57	
Coal derived pitch [75]	2000	145	0.3469-0.3424	2.26-30.3	0.52-0.59	68.1-73.4
Phenolic [25]					0.31- 0.32	77.2-82.3
Phenolic [74]	800	580			0.24-0.73	
Mesophase pitch [167]	1000	145			0.14-0.22	78-86.2
Mesophase pitch [189]	1000	1000	0.3640	1.20		
Mesophase pitch [189]	2500		0.3560	3.60		
Coal tar pitch [21]	3000	200			0.39	77.4
Coal tar pitch carbon nanofiber (0.01) [21]	3000	200			0.42	76.0
Coal tar pitch carbon nanofiber (0.04) [21]	3000	200			0.47	74.8
Mitsubishi mesophase pitch [166]	2600	435	0.3362	252	0.55	
Mitsubishi mesophase pitch/fluorine(1%) [166]	2600	435	0.3357	377	0.53	
Mitsubishi mesophase pitch/fluorine (3%) [166]	2600	435	0.3356	324	0.51	
Mesophase pitch[167]	1000	145			0.14-0.22	78-86.2

Table D.1 (continued) : The general properties of various carbon foams.

Pitch	Max Heat Temperature (^oC)	Foaming pressure (psi)	d spacing (nm)	L_a (nm)	Bulk density (g/cm^3)	Porosity (%)
Coal tar pitch [137]	1200	1160			0.73	75
Coal tar pitch-clay (2%) [137]	1200	1160			0.73	63
Coal tar pitch-clay (5%) [137]	1200	1160			0.61	57
Coal tar pitch-clay (10(%) [137]	1200	1160			0.71	45
Mesophase pitch	2300	1522	0.3373		0.75	63.8
Mesophase pitch-carbon fiber (2%) [22]	2300	1522	0.3379		0.76	62.7
Mesophase pitch-carbon fiber (4%) [22]	2300	1522	0.3388		0.78	61.5
Mesophase pitch-carbon fiber (6%) [22]	2300	1522	0.3390		0.80	57.2
Mesophase pitch-carbon fiber (8%) [22]	2300	1522	0.3401		0.81	55.4
Mesophase pitch [188]	2800		0.3373		0.17	
Mesophase pitch natural graphite (5%) [188]	2800		0.3365		0.21	
Mesophase pitch natural graphite (10%) [188]	2800		0.3366		0.20	
Mesophase pitch natural graphite (15%) [188]	2800		0.3370		0.20	
Mesophase pitch natural graphite (20%) [188]	2800		0.3373		0.18	
Mesophase pitch natural graphite (25%) [188]	2800		0.3373		0.15	
Mesophase pitch natural graphite (30%) [188]	2800		0.3378		0.12	

CURRICULUM VITAE

Candidate's full name: Ayşenur Gül

Place and date of birth: Istanbul 27.11.1978

E-Mail: gulaysenur@hotmail.com

Universities and Colleges attended:

- 2005-2012 Ph.D., Material Science and Engineering Program, Advanced Technologies in Engineering Department, Istanbul Technical University
- 2002-2005 M.Sc., Material Science and Engineering Program, Advanced Technologies in Engineering Department, Istanbul Technical University
- 1998-2002 Chemical Engineering, Istanbul Technical University
- 1997-1998 English Preparatory School, Istanbul Technical University
- 1993-1996 Private Üsküdar Science School, Istanbul
- 1990-1993 Beşiktaş High School, Istanbul
- 1985-1990 Barbaros Primary School, Istanbul

WORK EXPERIENCE:

January 2003-…	Research Assistant, Material Science and Engineering, ITU
January-July 2009	Visiting Researcher, Kyushu University, Japan
11 -17 April 2005	Visiting Researcher, Bulgaria Science Academy, Sofia, Bulgaria
November 2003-January 2004	Visiting Researcher, Gunma University, Japan

VOLUNTEER WORKING: I assisted in international conferences as a part of organisation team. My duties was included registration and organisation. Conferences that I worked are listed below:

29 May-June 1, 2012	Assistant, The sixth International Conference on Thermal Engineering Theory and Applications, Istanbul Technical University, Turkey.
18-19 March 2010	Conference Secretariat, Carbon Materials for Today and Future, Istanbul Technical University, Turkey.

24-25 April 2008	Assistant, Development and Technology of Carbons German-Turkish Joint Symposium, Istanbul Technical University, Turkey.
1-3 July 2000	Training Assistant, Aimos Networking Conference, Istanbul Technical University, Turkey.
2-5 December 1999	Training Assistant, International Conference On The Kocaeli Earthquake, Istanbul Technical University, Turkey.
20-24 September 1999	Training Assistant, International Engineering Education Symposium, Istanbul Technical University, Turkey.

SCHOLARSHIP

- 1997-2002 T.C. Prime ministry Scholarship
- 1998-2002 Istanbul Technical University Rectorate Scholarship

PROJECTS

- **Graduation Project:** Removal of Chromium from Aqueous solution using Activated Carbon
- **M.Sc. Project:** Mesophase Pitch Derived Graphitic Carbon Foam
- **Ph.D. Project**: Preparation And Characterization Of Carbon Nanofiber Added Mesophase Pitch Based Carbon Foam

PUBLICATIONS:

PAPERS in INTERNATIONAL JOURNALS

- Sipahi, M., **Gul, A.**, Sarac, A.S, Parlak, E.A., Ekinci, E., Yardım, M.F., *"**Electrochemical Impedance Study of Polyaniline Electrocoated Porous Carbon Foam",** Progress in Organic coatings*, **62**,1,96-104, 2008

- Kirca, M., **Gul, A**., Ekinci, E., Yardim, M. F., Mugan, A., ***Computational Modeling of Micro-Cellular Carbon Foam***, *Finite Elements in Analysis and Design*, **44**,1-2, p45-52,2007

PAPERS in NATIONAL JOURNALS

- **Gul, A**.,Yardim, M. F., *"**Düşük Basınçta Mezofaz Zift Bazlı Karbon Köpüğün Üretilmesi Ve Karkterizasyonu"**, ITU journal*,2012.

ORAL PRESENTATIONS in *CONFERENCES and SYMPOSIUMS*

- Sipahi,M., **Gul,A.**, Sarac,S., Alturk,P.E, Ekinci,E., Yardim,M.F., *"**Influence of Conductive Polymer Coating on the Properties of Carbon Foam**", International Carbon 2005 Conference,* Korea.

- **Gul,A.**, Dinçer,A., Yavuz,R., Karatepe,N., *"**Removal of Chromium from Aqueous solution using Activated Carbon**", International 5. Modern Management of Mine Producing, Geology and Environmental Protection Conference,* 2005, Bulgaria.

- Eksilioglu,A., Karadag, F., **Gul,A.**, Sipahi,M., Budinova,T., Petrov,N., Savova,D.,*"**Purification of Water from Metal Ions by Activated Carbons Obtained From Coals and Agricultural by-Products** ", 5P[tP]. International Modern Management of Mine Producing, Geology and Environmental Protection Conference,* 2005, Bulgaria.

- Gencay,N., Eksilioglu,A., **Gul,A.**, Karadag,F., Ekinci.E., Yardim,M.F., *"**Mesophase AR Pitch Derived Carbon Foam: Effect of Temperature, Pressure and Pressure Release Time**", International Carbon 2004 Conference*, Rhode Island, USA.

POSTERS in CONFERENCES and SYMPOSIUMS

- **Gul, A**., Ekinci, E., Yardim, M. F.,***"The Effect of HCNF Addition on the Cell Morphology of Mesophase Pitch Based Carbon Foam",*** 6th Chemical Engineering Conference For Collaborative Research In Eastern Mediterranean Countries, 2010, Turkey.

- **Gul, A**., Ekinci, E., Yardim, M. F., ***"The Effect of Carbon Nanofiber Addition on the Structure of Carbon Foam",*** Carbon Materials for Today and Future Symposium, 2010, Turkey.

- **Gul, A**., Ekinci, E., Yardim, M. F., *"**The Effect of Carbon Nanofiber on the Properties of Carbon Foam"**, 9th National Chemical Engineering Conferences*, 2010,Turkey.

- Eksilioglu,A., Gencay, N., **Gul, A.**, Yardım, M.F., Ekinci, E.,***"Influence of Carbon foam porosity as a bone implant"***, *6P[thP] National Chemical Engineering Conferences*, 2006, Turkey.

- **Gul,A.,***Yardım,M.F.,Ekinci,E.***, "Effect of pressure on carbon foam production",** *6P[thP] National Chemical Engineering Conference*, 2006, Turkey.